Development of Mockups and Instrumentation for Spent Fuel Drying Tests

Spent Fuel and Waste Disposition

Prepared for
US Department of Energy
Spent Fuel and Waste Science and Technology

A. Salazar
E.R. Lindgren
R.E. Fasano
R.J.M. Pulido
S.G. Durbin

Sandia National Laboratories
May 24, 2020
Milestone No. M2SF-20SN010203033
SAND2020-5431 R

Prepared by
Sandia National Laboratories
Albuquerque, New Mexico 87185 and Livermore, California 94550

Sandia National Laboratories is a multimission laboratory managed and operated by National Technology and Engineering Solutions of Sandia, LLC, a wholly owned subsidiary of Honeywell International, Inc., for the U.S. Department of Energy's National Nuclear Security Administration under contract DE-NA0003525.

Sandia National Laboratories

ABSTRACT

The purpose of this report is to provide updates on the experimental components, methodology, and instrumentation under development for use in advanced studies of realistic drying operations conducted on surrogate spent nuclear fuel.

Validation of the extent of water removal in a dry spent nuclear fuel storage system based on drying procedures used at nuclear power plants is needed to close existing technical gaps. Operational conditions leading to incomplete drying may have potential impacts on the fuel, cladding, and other components in the system. Water remaining in canisters upon completion of drying procedures can lead to cladding corrosion, embrittlement, and breaching, as well as fuel degradation. Additional information is needed on the drying process efficacy to help evaluate the potential impacts of water retention on extended long-term dry storage.

A general lack of data suitable for model validation of commercial nuclear canister drying processes necessitates additional, well-designed investigations. Smaller-scale tests that incorporate relevant physics and well-controlled boundary conditions are essential to provide insight and guidance to the simulation of prototypic systems undergoing drying processes.

This report describes the implementation of moisture monitoring equipment on a pressurized, submersible system employing a single waterproof, electrically heated spent fuel rod simulator as a demonstration of analytical capabilities during a drying process. A mass spectrometer with specially designed inlets was used to monitor moisture and other gases at 150 kPa to 800 kPa for a test simulating a forced helium dehydration procedure and below 1 torr for tests mimicking a vacuum drying process. The dew point data from the mass spectrometer was found to be in good agreement with a solid-state moisture probe. A distinct advantage of the mass spectrometer system was the capability to directly sample from the high-temperature (>200 °C) head space expected in a prototypic scale experiment where a solid-state moisture probe would suffer considerable loss of accuracy or fail altogether.

The operational and analytical experiences gained from this test series are poised to support an expansion to assembly-scale tests at prototypic length. These assemblies are designed to feature prototypic assembly hardware, advanced diagnostics for in situ internal rod pressure monitoring, and failed fuel rod simulators with engineered cladding defects to challenge the drying system with waterlogged fuel.

This page is intentionally left blank.

ACKNOWLEDGEMENTS

The authors would like to acknowledge the hard work and commitment of all contributors to the project. In particular, we would like to acknowledge the strong support and leadership of Ned Larson at the Department of Energy. Sylvia Saltzstein (SNL) and Geoff Freeze (SNL) are to be commended for their programmatic and technical guidance.

We would like to express our gratitude for the hard work and dedication of our technologists Greg Koenig, Ronald Williams III, Kyle Tsosie, and Adrian Perales that made the success of this project possible.

This page is intentionally left blank.

CONTENTS

This page is intentionally left blank.

LIST OF FIGURES

LIST OF TABLES

This page is intentionally left blank.

EXECUTIVE SUMMARY

Technical gaps exist in the understanding of the extent of water removal in a dry spent nuclear fuel storage system with commercial canister drying procedures. Operational conditions leading to residual water may have potential impacts on the fuel, cladding, and other components in the system, such as fuel degradation and cladding corrosion, embrittlement, and breaching. Additional information is needed on drying process efficacy to evaluate the potential impacts of water retention on long-term dry storage. Given the lack of data suitable for the model validation of drying processes, carefully designed investigations that incorporate relevant physics and well-controlled boundary conditions are needed to supplement existing field data. Experimental components, methodology, and instrumentation are therefore under development for use in advanced studies of realistic drying operations conducted on surrogate spent nuclear fuel.

A small-scale submersible pressure vessel was devised that incorporated a single waterproof, electrically heated spent fuel rod simulator to demonstrate analytical capabilities and the utilization of moisture monitoring equipment during drying processes. Vacuum drying and forced helium dehydration were two commercial procedures that were investigated to assess the removal of water introduced into the pressure vessel either in bulk or in small, controlled quantities in a copper ampoule. A mass spectrometer (MS) with specially designed inlets (“HPR-30”) was used to monitor moisture and gas composition at both high and low pressures, and a solid-state dew point sensor (“HX200”) was employed as an additional instrument. For energized tests, a power of 150 W was applied to the heater rod to investigate a peak cladding temperature of 400 °C, or the limit for normal storage operations.

A forced helium dehydration test, mimicking one type of commercial drying sequence, involved pressurizing the system to 800 kPa, holding the pressure for a period of time for thermal equilibration, and then venting to additional holds at 200 kPa and 150 kPa. A convection current induced by the heater rod was meant to bring residual water into vapor form for removal during the venting steps. Pressure, temperature, and gas composition were continuously monitored during several cycles of these hold periods.

In one iteration of the procedure, the pressure vessel was filled with deionized water to wet the internal volume below the electrical connections, drained, and then subjected to helium blowdown. Moisture content analysis by the HPR-30 was continuous, but the dew point data from the solid-state probe was only available during the pressure change steps which took place at the top of the pressure vessel. Results are shown in Figure E-1. The data from the HPR-30 and HX200 are in good agreement for the relevant points in time, although venting to lower pressures caused a transient downward dip in the dew point measurements. Because venting took place at the top of the PV, this may indicate that the dew point was lower elsewhere in the body of the PV than at the top where the measurements were made. During the high-pressure hold, the pressure dropped due to the higher sample rate of the MS at this high pressure. The sample to the MS appeared to be well-mixed when the PV was pressurized given the reproducibility of gaseous concentrations for each hold. While the exact quantity of water removed could not be determined, it was clear from the composition data that water content was not decreasing, indicating poor helium circulation in the pressure vessel.

Another iteration of the test used a controlled quantity of water in a copper ampoule with a 3.12 mm (0.123 in.) circular orifice. The location of the HX200 was modified to keep the sensor continuously exposed to the pressure vessel interior. Venting took place at the bottom of the pressure vessel. Figure E-2 shows large discrepancies in dew point measurements during the 800 kPa hold that may have been caused by the HPR-30 data being obtained with a flow rate of moist gas while the HX200 only measured stagnant gas. Upon isolation, the HPR-30 dew point steadily decreased, while conversely, the HX200 dew point increased. This indicates that the stagnation effect on the HX200 decreased as the volume of gas was heated and natural convection was established, allowing for better mixing. The HPR-30 dew points

were very close to the sample gas temperature, which is indicative of condensation in the sample line and were not observed in the other test. Upon the conclusion of testing, only a small fraction of water was measured to have been removed from the ampoule. Because the ampoule temperature was close to ambient, poor helium circulation was once again an inhibiting factor which is attributed to the small scale of the experimental apparatus.

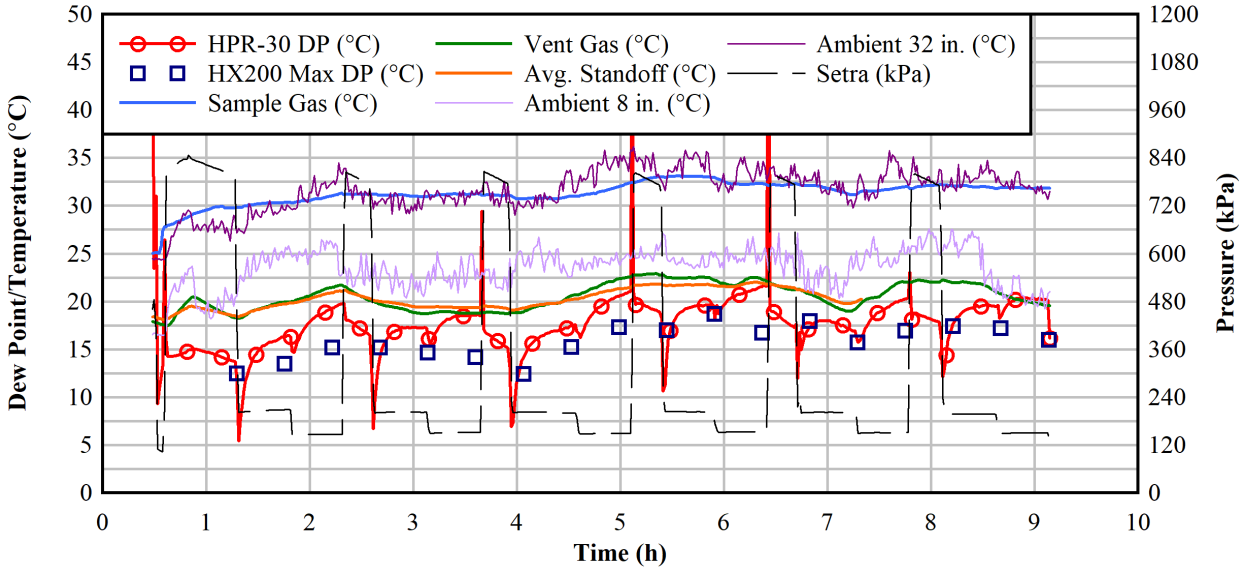

Figure E-1 Dew point and temperature data from the forced helium dehydration test with internal wetting of the pressure vessel.

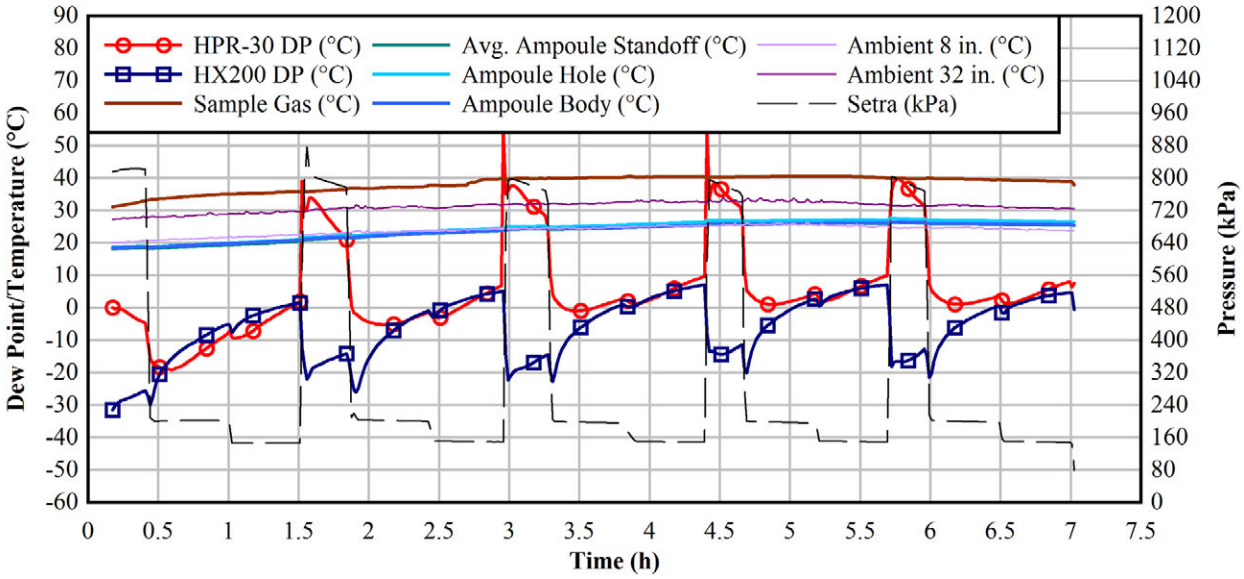

Figure E-2 Dew point and temperature data from the forced helium dehydration test with water contained in an ampoule with 0.123 in. orifice.

Both tests revealed the effects of systemic and procedural differences in applying mass spectrometer data. It is recommended that future tests be designed to ensure adequate convection and incorporate inline gas heaters to reduce the effects of cold zones within the internal void space and to more closely approach

prototypic storage systems. The instrumentation layout should also be considered with respect to stagnation effects and the sample flow rate of the mass spectrometer.

Vacuum drying was performed by implementing sequential hold points at increasingly lower pressures from 100 to 0.5 torr or less and monitoring the rise in pressure when the system was isolated from the turbo pump. The system was not to exceed 3 torr in the final hold as a dryness criterion. These tests were conducted under both ambient and heated conditions with water-filled ampoules of two different orifices: 0.53 mm (0.021 in.) and 3.12 mm (0.123 in.).

Figure E-3 shows the results of the heated vacuum drying test with the 3.12 mm (0.123 in.) orifice ampoule as an example. When the system was first evacuated to 100 torr, the dew point was at a minimal level below background. With sequential hold points, the dew point rose until it began to reach a peak level near the point in time when low pressures brought water into the vapor phase. At this point in time, the dew point and the temperature of the ampoule began to drop as the system was evacuated, and the rate of vaporization began to counteract the vacuum flow rate. Due to pressure rebound, several repetitions of the 3 torr hold were required before rebound was reduced. Solid deposition was observed during several of these evacuation stages, confirming that freezing can be assessed during the operation. However, the solid phase presence was very transient, even with considerable cold zones in the pressure vessel, and the vapor phase remained dominant throughout the test.

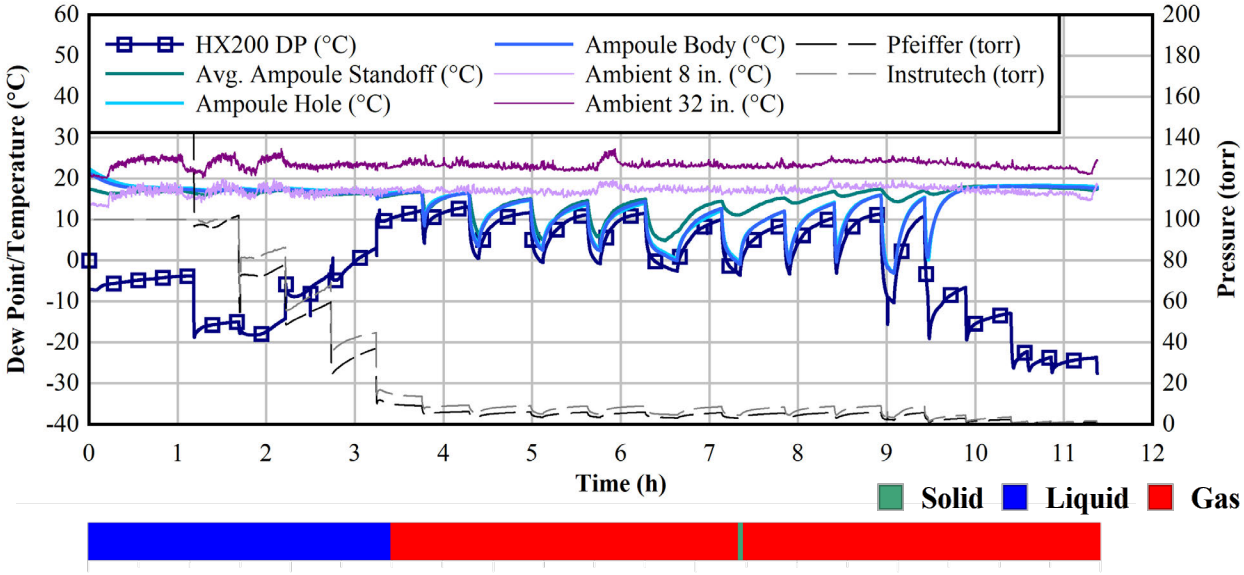

Figure E-3 Dew point and ampoule temperatures during the vacuum drying test at 150 W with a 0.123 in. orifice ampoule. The potential phase changes of water are also indicated.

The ampoule temperature did not realign with the pressure vessel (“standoff”) temperature until after the first hold at 1 torr. The mass spectrometer data aligned very well with the HX200 measurements for applicable pressures below 1 torr, although the calibration-based effects of water as the major gaseous species became apparent at the lowest pressures. Figure E-4 shows composition data during the final hold points of the test, which confirmed a reduction in water content over time. Indeed, the pressure rebounds became increasingly minimal and the drying criterion was met in the final hold. Water was observed to be completely removed in post-test examination of the ampoule, and an energy balance was used to confirm water removal using temperature data and the thermal mass of water.

The smaller orifice ampoule introduced transient pressure effects during evacuation stages and more pronounced pressure rebounds. This was caused by a combination of phase transition and a bottlenecking

effect. The ampoules were too far removed from the heater rod for differences between the unheated and heated tests to be significant. The main difference was the relative increase in pressure rebound for heated tests. Otherwise, similar moisture content behavior was observed in all vacuum drying tests. The peak cladding temperatures in the heated tests were observed to increase as the system became further evacuated of moist air. Therefore, while the commercial process can benefit from implementing low pressures in the procedure, there is a trade-off in elevating peak cladding temperatures to an extent that may impact cladding integrity.

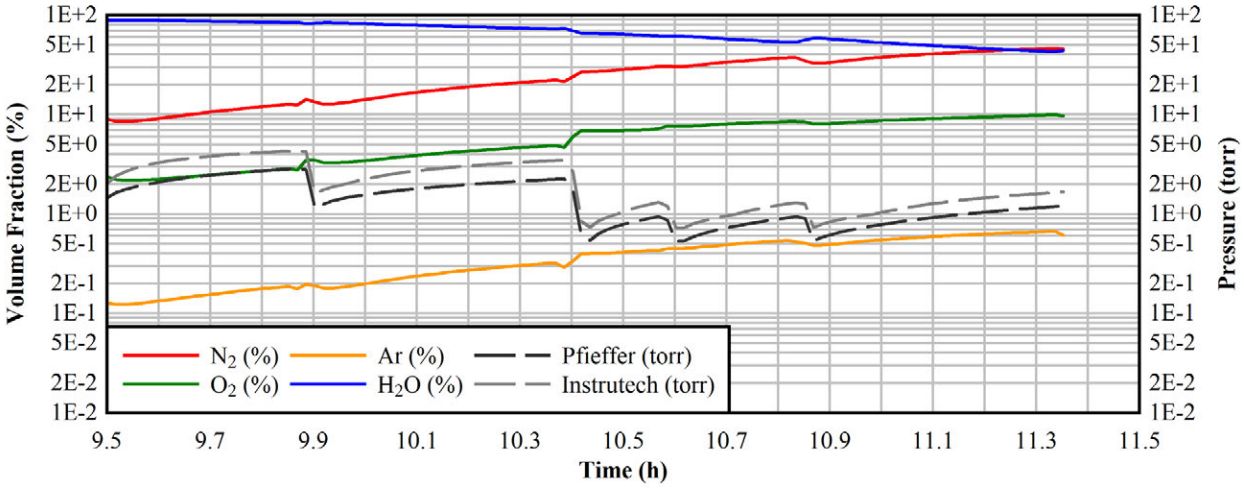

Figure E-4 Mass spectrometer composition data from the vacuum drying test at 150 W with a 0.123 in. orifice ampoule

Altogether, the vacuum drying tests were successful at removing water from ampoules with two different breach areas. This was confirmed with pressure rebound data, ampoule temperature data, and moisture content data for the final hold points. The mass spectrometer was found to be in excellent agreement with the solid-state moisture probe. It is recommended that the mass spectrometer be reconfigured to accommodate a higher subatmospheric pressure range. This will allow for moisture measurement during phase change and at elevated temperatures than those measured in the ampoule. The effect of implementing intermediate backfills of helium between hold points should also be investigated. For both vacuum drying and forced helium dehydration, it is clear that either test requires a tighter coupling of the implanted residual water to the temperature gradient of the fuel rod surrogate.

The data and operational experience from these tests will guide the next evolution of experiments on a prototypic-length scale with multiple surrogate rods in an assembly. These assemblies will feature partially submersible heater rods and specialized diagnostic rods to introduce cladding breach effects and internal rod pressure monitoring. The use of multiple heaters will provide more representative power profiles for PCT evaluations, and the breached rods will act as directly integrated water ampoules directly affected by the heat source. Altogether, the assembly components will provide a more representative array of water retention sites that would be expected in commercial operations with SNF, and drying effects will be observable in the water content of internal gas samples over a wide dynamic range of pressures.

Instrumentation and procedures were developed for this test series to verify their accuracy and resilience in quantifying conditions similar to commercial drying operations. These techniques and hardware provide the basic tools for more prototypic testing in the future including actual canister loadings if needed. The insight gained through these investigations is expected to support the technical basis for the continued safe storage of SNF into long term operations.

ACRONYMS / ABBREVIATIONS

BWR	boiling water reactor
DAQ	data acquisition system
DCC	dynamic contamination control
DL	detection limit
DOE	Department of Energy
EPRI	Electric Power Research Institute
FHD	forced helium dehydration
ID	inner diameter
IFBA	integral fuel burnable absorber
MS	mass spectrometer
NIST	National Institute of Standards and Technology
NPT	national pipe thread
OD	outer diameter
PCT	peak cladding temperature
ppmv	parts per million by volume
PTB	power test board
PV	pressure vessel
PWR	pressurized water reactor
RSF	relative sensitivity factor
SCR	silicon-controlled rectifier
SE	standard error
SNF	spent nuclear fuel
SNL	Sandia National Laboratories
SFWD	Spent Fuel and Waste Disposition
TC	thermocouple
TDL	tunable diode laser
VCR	vacuum coupling radiation
VT	vacuum test
WVP	water vapor pressure

This page is intentionally left blank.

DEVELOPMENT OF MOCKUPS AND INSTRUMENTATION FOR SPENT FUEL DRYING TESTS

This report fulfills milestone report M2SF-20SN010203033 in the Spent Fuel and Waste Science and Technology (SFWST) work package (SF-20SN01020303). This work was sponsored under the Department of Energy's (DOE) Office of Nuclear Energy (NE) Spent Fuel and Waste Disposition (SFWD) campaign.

1 INTRODUCTION

1.1 Objective

Numerous water retention sites exist within an internal volume of a multi-assembly dry storage system that require a specialized approach for the evacuation of water. While guidelines exist on ensuring sufficient evacuation of water from assembly cavities, there is a lack of time-dependent data on water removal from full-scale commercial drying procedures, which have been identified as a high-priority research topic to advance the technical basis for the long-term management of spent nuclear fuel (SNF) (Hanson and Alsaed, 2019). Previous studies have not provided transient moisture measurements during the vacuum drying procedure (Bryan *et al.*, 2019; Knight, 2019) and additional information is needed to evaluate the potential impacts of water retention on extended long-term dry storage.

The purpose of this report is to provide updates to vital experimental components, instrumentation, and procedures under development since the previous series of tests in Salazar *et al.*, 2019. This work is meant to support advanced studies of dry storage systems during vacuum drying and long-term storage operations. Direct measurement of residual water in a multi-assembly dry storage system based on the vacuum drying procedure used by industry is needed to advance current, technical understanding. Operational conditions leading to incomplete drying may have potential impacts on the fuel, cladding, and other components in the system.

Advanced fuel rod simulators are intended to populate a new thermal-hydraulic test apparatus with one or more fuel assemblies. This new dry storage system simulator will bridge the prototypic complexity of the DOE and Electric Power Research Institute (EPRI) High Burnup Demo (Montgomery *et al.*, 2018) and the controlled environment of a lab-fielded apparatus as well as allow for the replication of commercial drying cycles.

This report documents tests conducted on a small, single-rod scale that will demonstrate proof-of-concept for the utilization of an advanced fuel rod surrogate in drying procedures that can then be scaled to assembly-scale tests at prototypic length in the future. This chapter will discuss the motivating issues underlying the investigation and a summary of past tests that were designed to respond to some of these concerns. Chapter 2 will discuss development of the instrumentation, equipment, and procedures for the test series, while Chapter 3 will focus specifically on the moisture monitoring equipment and calibration procedures. Chapter 4 will discuss the results of the tests, while Chapters 5 and 6 will discuss future work and summarize the findings of the investigation.

1.2 Issues

1.2.1 Residual Water

Spent fuel assemblies are dried after interim storage in pools to ensure the removal of water in assembly cavities as a defense against issues related to pressurization and corrosion that might occur during the subsequent, potentially long-term, dry storage process. The evacuation of most water and oxidizing agents contained within the canister is recommended by NUREG-1536 (NRC, 2010). A pressure of 0.4 kPa (3 torr) is recommended to be held in the canister for at least 30 minutes while isolated from active vacuum

pumping as a measure of sufficient dryness in the canister. A similar drying method developed at Pacific Northwest National Laboratory (PNNL) is suggested (Knoll & Gilbert, 1987), where less than 0.25 volume percent of oxidizing gases are left in the canister (1 mole in 7 m^3 at 150 kPa and 300 K).

An industry standard guide was established for the drying of SNF after cooling in spent fuel pools (ASTM, 2016). The main purpose of the standard is to aid in the selection of a drying system and a means of ensuring that adequate dryness is attained. Examples of typical commercial processes are documented in the standard, where there is adherence to the aforementioned 0.4 kPa (3 torr) level when discussing the measurement of pressure rebounds. However, there are no substantial details on the utilization of moisture content measurements to ensure adequate water removal, and the establishment of related dryness metrics are deferred to regulatory agencies. There is only a broad recommendation to impose drying conditions that maximize moisture removal from the system.

Water remaining in canisters upon completion of vacuum drying can lead to corrosion of cladding and fuel, embrittlement, and breaching. There is also some risk of creating a flammable environment from free hydrogen and oxygen generated via the radiolysis of water. The remnant water may be chemically absorbed (chemisorbed), physically absorbed (physisorbed), frozen, or otherwise trapped in cavities, blocked vents, breached clads, damaged fuel, etc. Chemisorbed water is bound to components by forces equivalent to a chemical bond, such as the formation of hydroxides and hydrates on zirconium, or corrosion products on the fuel or cladding. Physisorbed water is bound to components by weaker forces (e.g. Van der Waals, capillary) as an adsorbate, and increased surface area provided by material defects enhances this effect.

The removal of unbound water is largely dependent on the geometry and tortuosity of the components and the speed of the drying process. Cladding breaches are notable cases in that water can become trapped between fuel pellets and absorbed in cracks and voids. Water vapor may continue to be diffusively released after vacuuming. Depending on the thermal profile, condensation may occur on the cooler surfaces of the canister and internal hardware, such as those lying at the lower extremes distant from heat-emitting SNF.

The pressure applied during vacuum drying lies below the water vapor pressure. Given the unique heat retention and phase change properties of water, when significant heat is removed during volatilization, some quantity of liquid may freeze (ASTM, 2016). It is therefore important to understand under what marginal conditions ice may form during the procedure. Careful control of the vacuum pumps may prevent ice formation by controlling suction near pressures liable to introduce phase transitions. Further mitigation may be achieved by implementing pressure reduction in stages that involve bringing the temperature to equilibrium with hot inert gases like helium prior to commencement of the next stage. In a general expansion of this concept, further research and development on forced helium dehydration (FHD) has been recommended to address recently identified technological gaps (Hanson & Alsaed, 2019).

If vacuum is employed to remove water from a canister, measurements in the pressure response to intermittent pump operation may serve as a good indicator of residual, unbound water (ASTM, 2016). Such an approach would involve analysis of the time-dependent pressure rebound when the vacuum is turned off. The system may be adequately dry if the 0.4 kPa (3 torr) pressure can be sustained for at least 30 minutes. Monitoring the moisture content in gas removed from the canister is also suggested as a means of evaluating adequate dryness. Dew point monitoring and spectroscopic techniques could be used to this end, although the exact utilization of these measurements to ensure dryness will have to be investigated.

1.2.2 Cladding Performance

Understanding cladding hoop stresses is critical for evaluating and predicting the mechanical integrity of the fuel rods. These hoop stresses have implications on corrosion, stress corrosion cracking, zirconium hydride reorientation, and creep. It is recommended to maintain pressure-induced hoop stresses in the

cladding below 90 MPa to reduce the probability of hydride reorientation (NRC, 2003; Billone *et al.*, 2013). During commercial reactor and drying operations, the internal rod pressure increases from the production of fission gases, the generation of gaseous decay products, and fuel pellet swelling, and overall these phenomena increase with burnup. The presence of axially reoriented hydrides increases the chance of cladding breaches. If a clad is breached during operation, fission gases are released, and water can penetrate the fuel through the gap. During vacuum drying, canister pressures are reduced to below 0.4 kPa (3 torr). Afterwards, they are pressurized with helium up to 800 kPa (6000 torr) during storage.

A technological gap exists in understanding the evolution of internal rod pressure during full-scale, drying operations. Direct measurements can provide valuable information on the state of stress in the fuel cladding as vacuum is applied during drying cycles.

1.2.3 Thermal Management

In the course of a typical vacuum drying cycle, the temperature of the fuel is predicted to increase due to reduced heat transfer from the evacuation of surrounding fluids. The peak cladding temperature (PCT) of the fuel should remain below 400 °C to minimize the potential for hydride reorientation in the cladding (NRC, 2003), which in turn results in alterations of mechanical cladding behavior. Temperature gradients should be analyzed to identify areas where condensation of water vapor may occur in the canister, as condensation can lead to long-term, localized corrosion issues. There may also be cold zones of the canister susceptible to being freezing sites for residual water during vacuum drying.

1.3 Expectations of Capabilities

Previous testing has provided a strong database and background from which to guide future test designs to meet remaining technical gaps (Hanson & Alsaed, 2019), and the desired capabilities are summarized below.

1.3.1 Transient Vacuum Drying Behavior

The test apparatus should be capable of replicating commercial drying cycles. These include both vacuum and FHD drying cycles. Simulated fuel assemblies should be capable of heated operation during drying, which will likely require a submersible heater design. These assemblies should have prototypic, geometric features capable of trapping bulk water such as dashpots from pressurized water reactor (PWR) assemblies and water rods of boiling water reactor (BWR) assemblies. Furthermore, the apparatus should accommodate the testing of damaged fuel surrogates.

A major knowledge gap exists in assessing the behavior of temperature and pressure in and surrounding a fuel rod during vacuum drying transients in a scaled test with surrogate materials. Time-dependent data with adequate breadth and versatility is needed to provide insight on internal rod pressures and cladding temperatures during drying and storage procedures. This, in turn, will have implications on the long-term behavior and integrity of fuel.

1.3.2 Prototypic Thermal-Hydraulics

The fuel assemblies should incorporate prototypic hardware and length scales to mimic the integral physics of dry storage systems. In lieu of a full-scale canister, a practical test approach is to employ prototypic length and reduced diameter to emulate the length of relevant canister components – namely, the siphon tube and the fuel assemblies (Miller *et al*., 2013). This approach would retain fuel assembly geometry and associated retention sites for residual water.

Figure 1-1 shows locations within a PWR fuel assembly that can serve as water retention sites, such as the mixing vanes and bulge joints of the grid spacers. The fuel assembly features guide thimble tubes for the insertion of control rods or burnable poison assemblies. The dashpots in the guide tubes are designed to drain water through a centrally located through-hole in the guide thimble bolt (i.e. vent hole). If the vent hole is fouled during reactor operations or pool storage, the dashpot could conceivably retain bulk water

during the initial draining operations preceding canister drying. However, the water would be free to communicate with the interior of the canister via the flow holes and the open top of the guide thimble during drying operations. Burnable poison rods are inserted and left in some fuel assemblies, which could restrict the flow area for any trapped water in the dashpot region if the vent hole is fouled.

Additional considerations include properly incorporating the influence of gravity on heat transfer (i.e. natural convection) along the longitudinal axis when determining PCTs, as well as including the effects of axially spread spacer disks as water entrapment points. The test apparatus should be configurable to allow a variety of storage configurations to be studied, and transportation configurations should be considered as well.

1.3.3 Monitoring of Cladding

The system should be capable of characterizing cladding behavior during drying and storage conditions. This characterization should include the measurement of cladding temperature and internal rod pressure. In order to achieve a realistic peak cladding temperature, the test fuel assembly needs to be populated with as many individually heated fuel rod simulators as is practical. The impact of cladding failures from pinhole to gross breaches should be considered, as the internal free volume of a fuel rod expands the number of water retention sites.

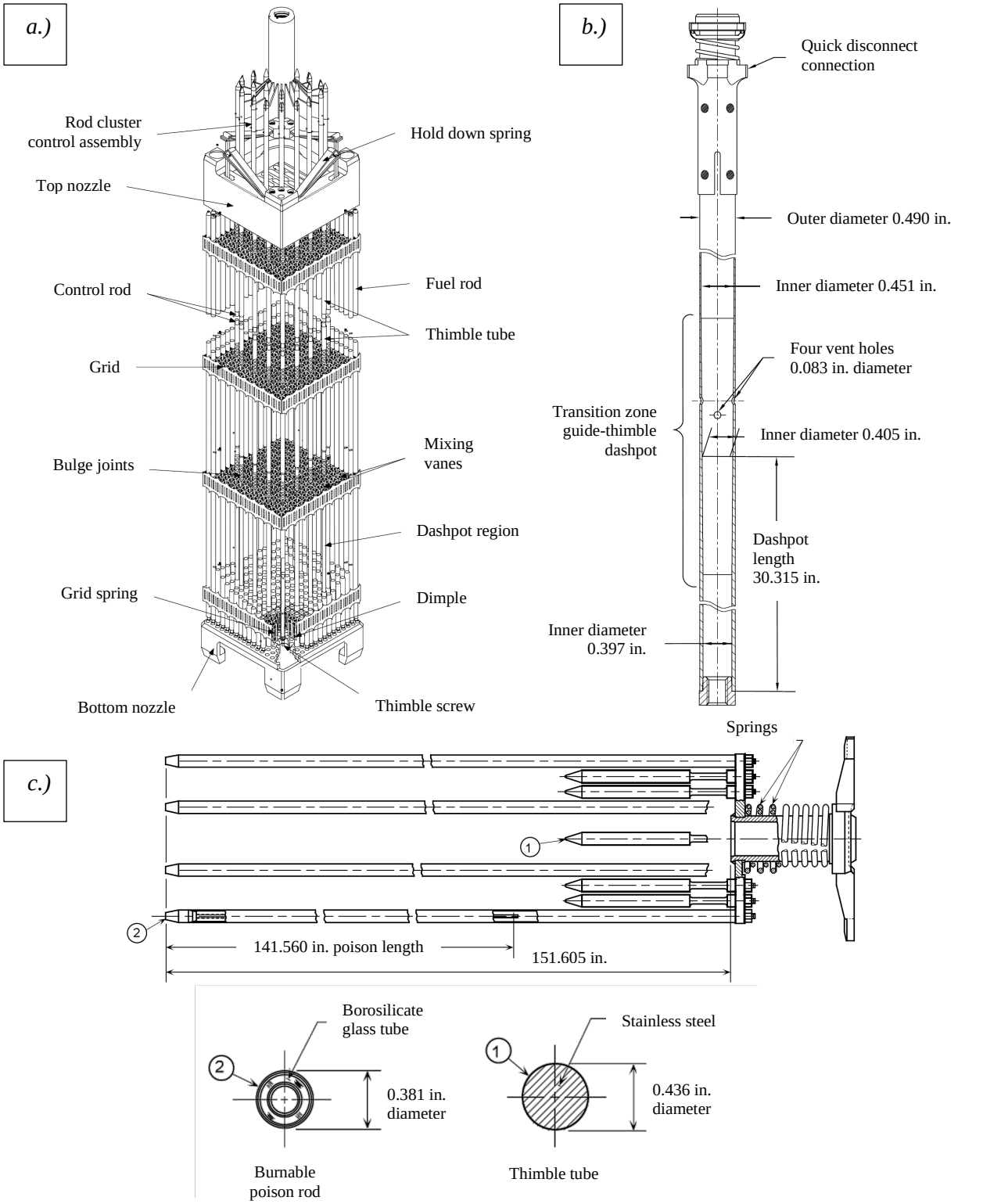

Figure 1-1 Water retention sites exhibited in *a.)* a typical 17×17 PWR fuel assembly construction, *b.)* a typical PWR guide thimble tube, and *c.)* a burnable poison rod assembly (Figures 3.1-16, 4.2-8, and 3.1-26 in NRC, 2002).

This page is intentionally left blank.

2 DEVELOPMENT AND TESTING

This chapter will discuss the testing setup and methodology that aims to address gaps in the current understanding of vacuum drying and residual water analysis that were previously covered in SAND2019-11281 R, "Advanced Concepts for Dry Storage Cask Thermal-Hydraulic Testing" (Salazar *et al.*, 2019). The updates in this report primarily focus on the progress made on equipment, procedures, and water content measurement instrumentation for tests utilizing a submersible heater rod. The procedures presented in this report can be employed in assemblies of prototypic-length fuel rod surrogates for advanced water retention studies. Ultimately, many such assemblies may be employed in a versatile dry cask simulator for thermal-hydraulic experiments.

2.1 Test Objectives

Tests were conducted to verify the removal of residual water in a stainless-steel pressure vessel with an electrically heated, partially submersible fuel rod surrogate. The heater accommodates complete submersion in water below the upper electrical connection points. This allows for thermal hydraulic investigations of vacuum drying efficiency in water removal, along with the effects of backfilling with inert gas as an additional dehydration measure.

The main objectives of the test include the following:

1. Demonstrate that a sequenced vacuum drying procedure can be implemented to remove water retained in the pressure vessel, where pressure measurements can confirm minimal rebound pressures after the application of several hold points
2. Demonstrate that inert gas can be implemented to remove residual water using pressurization cycles in a forced dehydration procedure
3. Refine procedures and provide diagnostics for system equipment and moisture monitoring instrumentation that can be used in a larger scale test, in particular the use of mass spectrometry

In addition, work is being conducted on devising a means of monitoring internal rod pressure during drying operations to address knowledge gaps from the High Burnup Demo. Therefore, another stated objective is as follows:

4. Demonstrate that a pressure tube simulating a fuel rod plenum can be used to investigate internal pressure fluctuations during drying procedures

Performance verification in this small-scale, single heater test series will allow more advanced drying tests to proceed that can employ several of these rods in assemblies, which in turn can provide data scalable to commercial dry cask storage and transportation applications.

2.2 Submersible Heater Rod

A waterproof heater rod designed to simulate spent fuel was proposed in Lindgren, Salazar, and Durbin, 2019. It was demonstrated to fully perform while partially submerged under water as well as under pressurized, evacuated, and moist conditions, and is discussed in Salazar *et al.*, 2019. It was also observed to be unaffected by boiling water at atmospheric pressure, indicating that the electrically insulating material was not compromised by steam production or condensation reflux. These results have confirmed the rod's candidacy for use in tests meant to assess thermal phenomena in a dynamic, wet environment expected during drying operations.

The heater is comprised of magnesium oxide (MgO) compacted around a spirally-wound Nichrome wire with cold pins on either end, as shown in Figure 2-1 (a schematic with as-built dimensions is shown in Figure A-1). The coil is wound in a helix that is approximately the radius of the cold pin. MgO ceramic

was selected as a surrogate fuel material due to similar thermal mass (ρC_p) behavior with increasing temperature relative to SNF (Lindgren & Durbin, 2007).

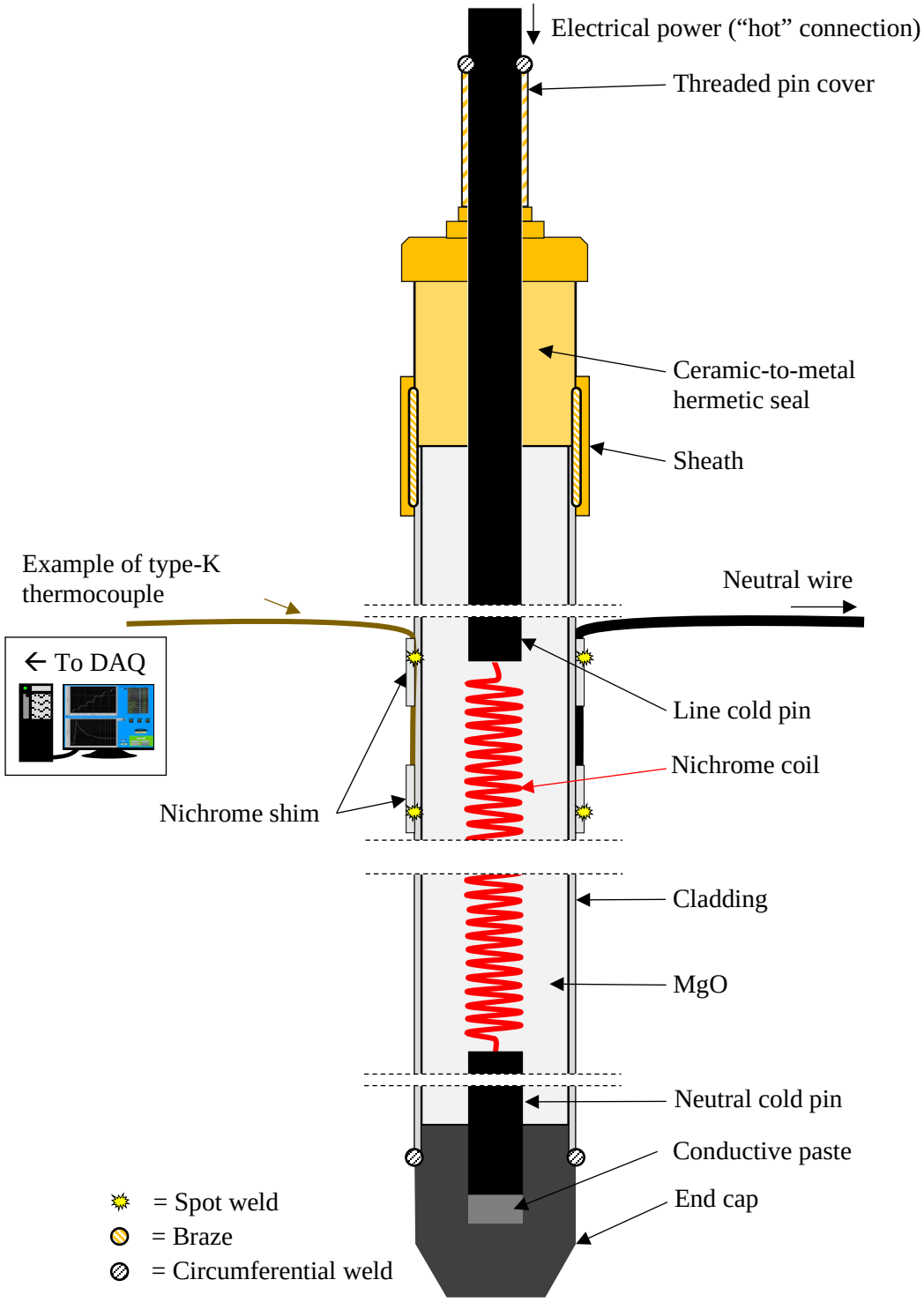

Figure 2-1 Heater rod diagram.

Each heater features a top fitting with a hermetic ceramic-to-metal bond (Figure 2-2) that allows connection to the power source while electrically isolating the cladding and protecting the MgO from moisture. The top fitting is welded to the pin at the upper extreme of the threaded pin cover, along with brazing between the sheath at the clad/seal interface. The bottom fitting has similar geometry to a bottom fuel plug, with an internal blind hole containing high-temperature electrical grease to receive the neutral cold pin. This bottom plug is circumferentially welded to the cladding, effectively bonding the cladding to the electrical neutral (see Figure 2-3). The cladding is therefore electrically isolated from the hot connection via the top hermetic seal. In lieu of an electrically connected bottom fitting, the neutral is drawn from a wire attached near the upper portion of the cladding.

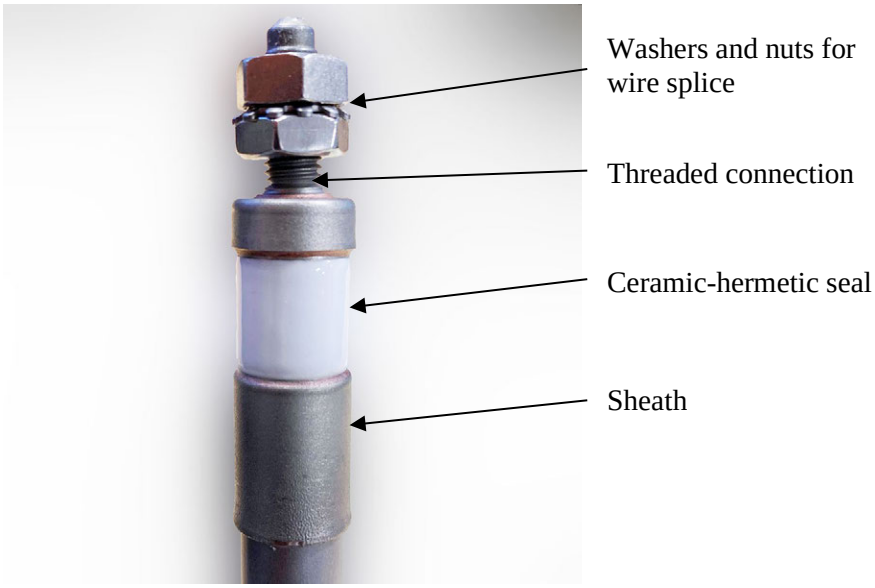

Figure 2-2 View of threaded connection, hermetic seal, and heater sheath on waterproof heater rod.

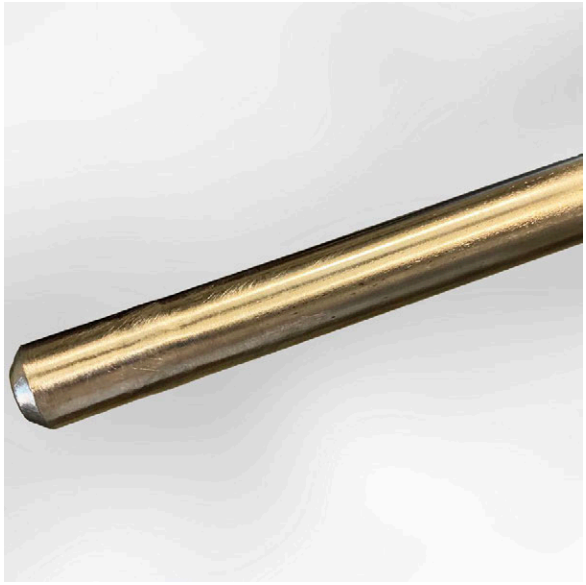

Figure 2-3 View of welded end cap on waterproof heater rod.

2.3 Pressure Monitoring Tube

To assess the viability of the pressure monitoring tube design, a scaled, proof-of-concept pressure rod was built and tested externally of the drying pressure vessel in a tube furnace (Thermo Scientific Lindberg/Blue M HTF55342C with CC58114PC-1 control console). A 304 stainless-steel pressure tube with an outer diameter (OD) of 3.18 mm (0.125 in.) was constructed as shown in Figure 2-4. This tube had four distinct cross-sections: 1) the bottom standoff made of solid stainless steel with an OD of 3.18 mm (0.125 in.), 2) the “fuel” region made of a thick-walled 3.18 mm (0.125 in.) tubing with an internal diameter (ID) of 0.69 mm (0.027 in.) and a solid wire of 0.46 mm (0.018 in.) inserted throughout the length of this section, 3) the “plenum” region made of thin-walled 3.18 mm (0.125 in.) tubing with an ID of 2.67 mm (0.108 in.), and 4) the pressure tap made of thick-walled tubing with an OD of 1.59 mm (0.0625 in.) and ID of 0.15 mm (0.006 in.). A transition collar was fabricated to join the plenum section ID of 2.67 mm (0.108 in.) to the pressure tap OD of 1.59 mm (0.0625 in.).

The design geometry was carefully selected to closely scale to the relative volumes of gas in the fuel and plenum regions of SNF. The pressure tap was chosen to minimize the amount of gas outside of the region of interest in the pressure monitoring rod. For these initial efforts, no effort was made to minimize the volume of “cold” gas in the external pressure fittings and Setra ASM pressure transducer. The authors recognize that this cold gas region needs to be minimized for a final design to maximize the response of the pressure tube to the thermal transients in the fuel and plenum regions. The estimated volumes for the pressure tap, plenum, and fuel region are 5.04, 0.71, and 0.18 mL, respectively. The ratio of the plenum to fuel regions is 79.9%, which is similar to SNF (NRC, 2001).

Six type-K thermocouples (TCs) were attached to the outer diameter of the tube by spot welding nichrome shim stock around the TC tip. The TCs were further secured with strain relief to the tube using the same method of attachment. Four TCs were placed to measure the tube temperature in the fuel region and were located at z = 0.203, 0.406, 0.610, and 0.813 m (8.00, 16.0, 24.0, and 32.0 in.) where the z-coordinate has its origin at the lower extreme of the tube, as shown in Figure 2-4. The pressure tube pipe fittings, furnace, and TCs are shown in Figure 2-5.

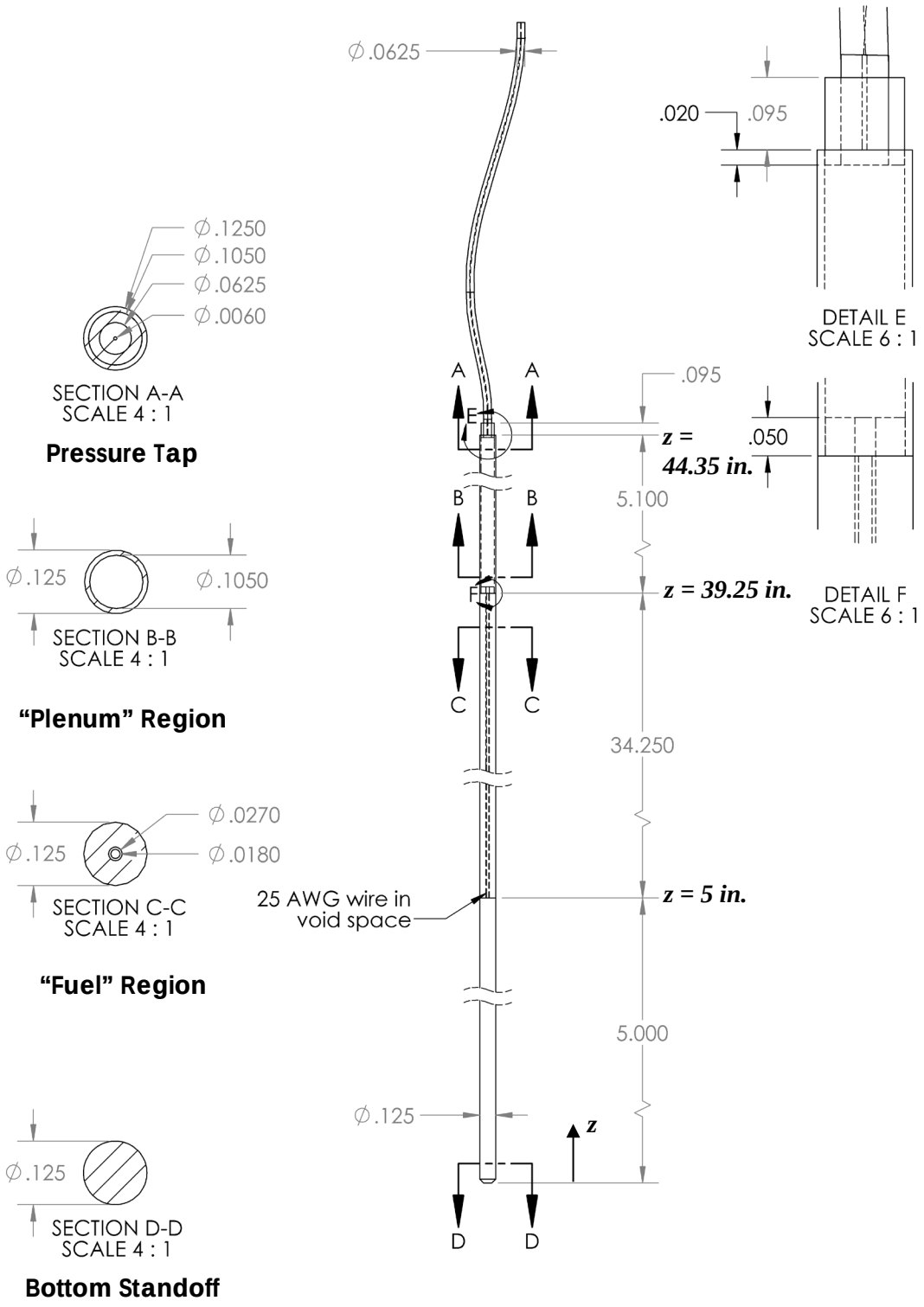

Figure 2-4 Schematic of the scaled pressure monitoring rod.

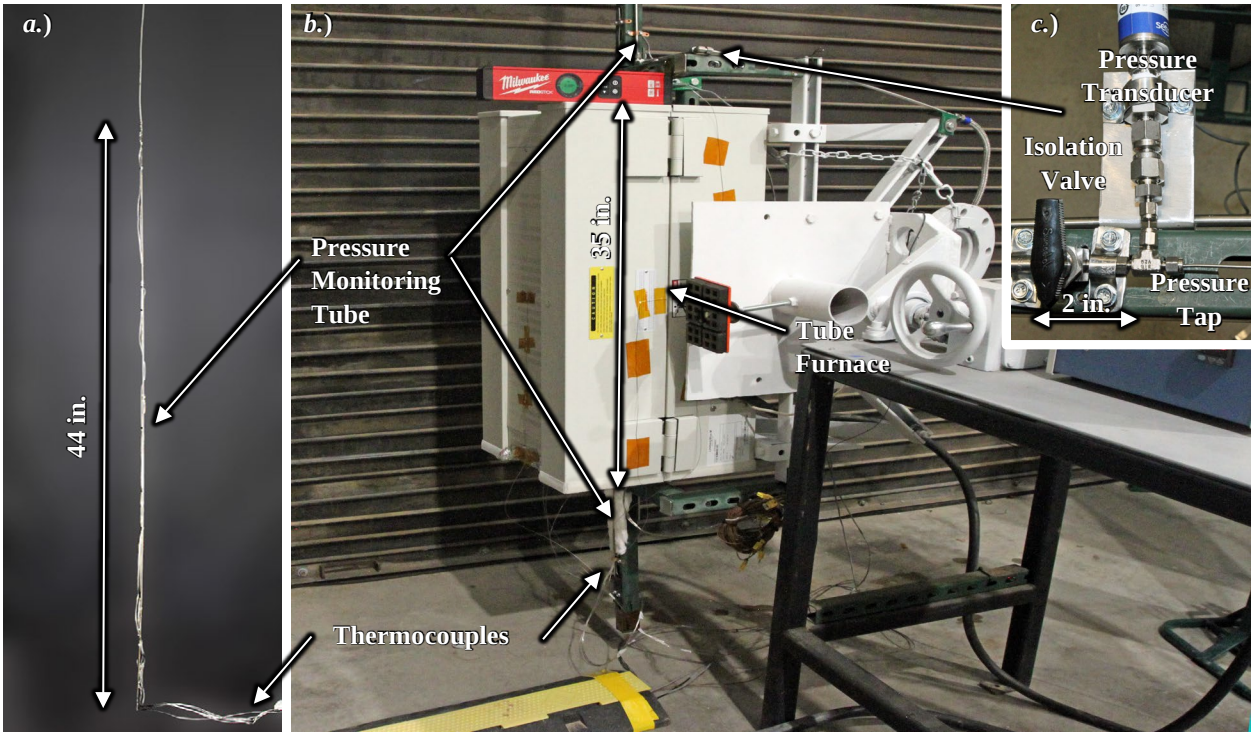

Figure 2-5 Photographs of *a.*) pressure monitoring rod with thermocouples attached, *b.*) heated pressure monitoring rod test setup and *c.*) pressure fittings and pressure transducer.

2.4 Pressure Vessel

A pressure vessel (PV) was constructed of 316 stainless-steel pipe fittings with vacuum coupling radiation (VCR) face seal connections as well as stainless-steel tubing with welded VCR glands. A schematic is shown in Figure 2-6 with additional details shown in Figure A-2 and a system layout shown in Figure B-2. From bottom to top, its main components are a 1 in. tee, a long section of 1 in. stainless-steel tube, a middle 1 in. cross, and an upper 1 in. cross. The bottom tee serves as the base for the heater rod and provides penetrants for the thermocouples and the water filling line, along with the venting of fluids in general. The middle cross provides penetrants for the neutral line and overflow of water. The top cross allows penetrants for the electrical power connection, pressure and vacuum pump systems, pressure gauges, and moisture monitoring equipment.

All VCR connections are sealed with unplated, non-retaining stainless-steel gaskets. Non-VCR connections within the PV include the compression-type tube fittings used to mount the Omega HX200 dew point transmitter and the Setra ASM pressure transducer. There are also NW25 flanged connections on the vacuum transducers, which feature Viton centering rings.

Bellows-sealed valves form the boundaries to the main internal volume of the PV, which amounts to approximately 1.0 liter of net void space. The upper left valve is the inlet for either the vacuum pump (see Figure B-3) or an inert gas cylinder (see Figure B-4). This valve is used to control the internal pressure of the PV through pressurization, venting, or evacuation. The upper right valve serves as the isolation valve for the 1/16 in. tube leading to the mass spectrometer ample inlet. This isolation valve allows for the MS to sample only when the PV is evacuated to the MS's operational pressure range. The valve at the middle cross allows for the overflow of water, while the valve at the lower right standoff is used for the filling and draining of water or venting of pressurized gas. Low-pressure and high-pressure gauges are placed on their own separate trees that are separated from the PV with valves.

Altogether, this revamped, vacuum-tight design reduces leakage and allows for finer control of both sub-atmospheric pressures and high pressures up to 1000 kPa. As a further improvement from the early PV design in Salazar *et al.*, 2019, the pressure vessel has been designed to allow for the temperature safety margin to be extended to investigate a peak cladding temperature of 400 °C. The temperature limits imposed by feedthrough packing sets have been mitigated through 10 in. long standoffs that reduce heat transfer to these materials. However, as a trade-off, these standoffs also introduce many cold zones in the PV that may influence fluid behavior when the heater rod is energized.

The heater rod is installed within the main axial length of the pressure vessel and rests on the bottom 1 in. tee. It is centered with winglets of nichrome shim (see Figure A-4 in the appendix) which also function as water retention sites. Prior to installation on the heater rod, thermocouples are fed through a Teflon Conax fitting on the lower left standoff as well as all other gaskets and pipe fittings leading up to the upper cross. This method of installation was permanent and prevented the replacement of gaskets or faulty TCs. The 14-gauge wire for the electrical power connection is fed through a grafoil Conax fitting at the top of the upper standoff and fastened to the heater using a spade on the threaded connection. The welded endcap makes the cladding beneath the ceramic hermetic seal function as the electrical neutral. Therefore, an 18-gauge wire is attached to the cladding above the middle cross (the water line) with nichrome shim and fed through a grafoil Conax fitting on the middle left standoff to complete the electrical circuit outside of the PV.

The pressure vessel was mounted to a wooden board that was fastened to a Unistrut frame. The lower 1 in. tee rested on a pedestal outcrop while the top 1 in. cross was secured to the frame using L-brackets and hose clamps. This mount also supported peripheral plumbing lines and a convenient location for the mass spectrometer controller to minimize the length of the sample line tubing. The power supply and related equipment were located nearby on a separate, similar mount within an electrical enclosure.

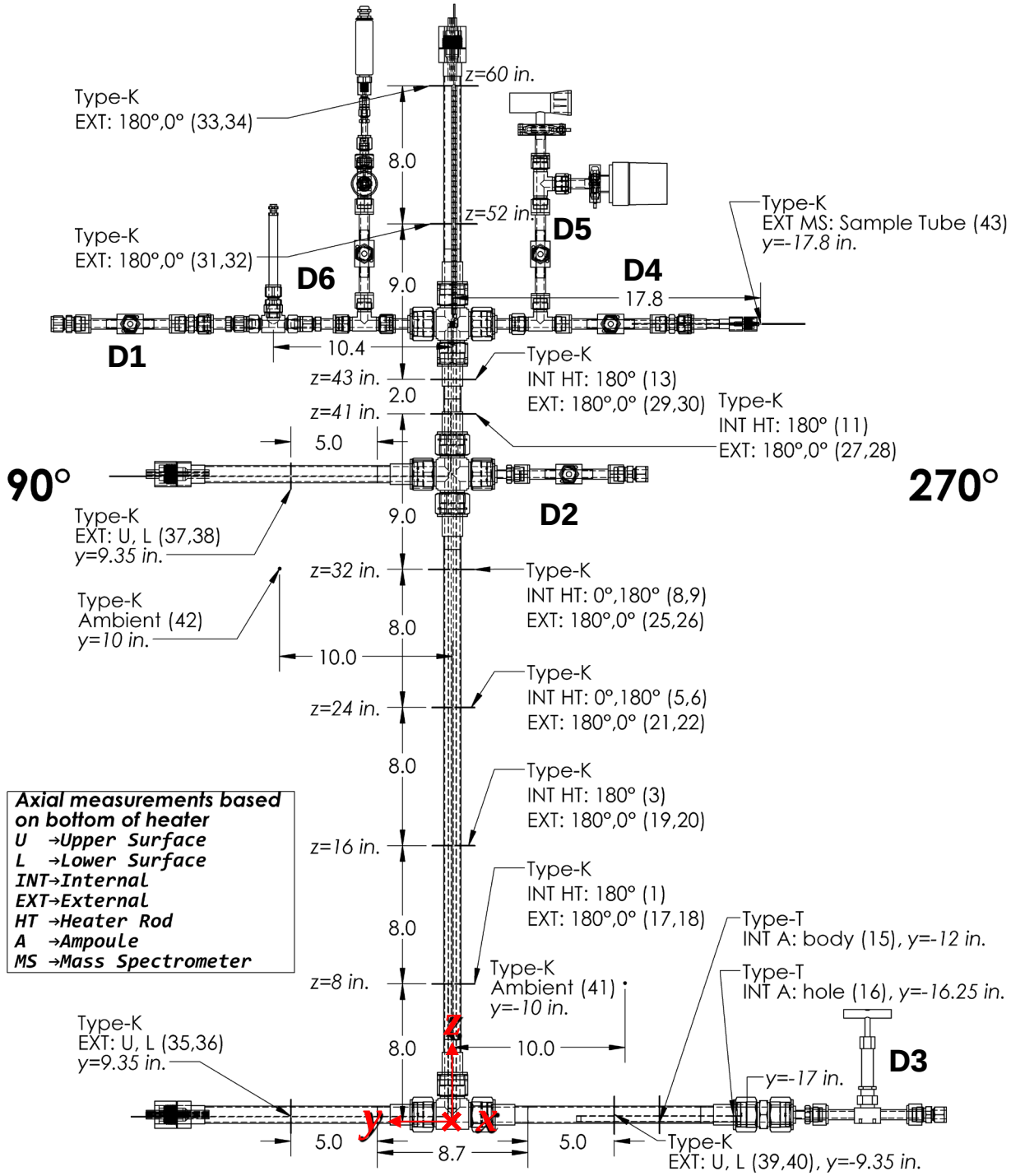

Figure 2-6 Diagram of thermocouples in pressure vessel along with valve nomenclature. (TC #44 on the vent is not shown.)

2.5 Introduction of Water

2.5.1 Water Ampoule

To allow for the installation of a pre-determined quantity of water into the PV, ampoules were created out of 9.5 in.-long/ 3/8 in. OD/0.311 in. ID copper tubing. A photograph of the 0.123 in. diameter ampoule is shown in Figure 2-7 with a corresponding schematic in Figure A-3. The ampoule is plugged with 0.25 in.-long copper rods to accommodate a total wetted length of 9 in. and an internal volume of 11.2 cm^3. Deionized water was injected via a nozzled wash bottle.

Another ampoule with a 0.021 in. drill hole diameter was also tested. This allowed for a comparison of a pinhole breach with the 0.123 in. orifice as a "gross breach" (i.e. not a pinhole or hairline crack) as defined in the ASTM standard (ASTM, 2016). The 0.021 in. hole size required water injection via a syringe. The mass of injected water was verified using a scale with milligram resolution. The dry weights of each ampoule are listed in Table 2-1, including those noted after vacuum drying tests for which the vacuum pump was run overnight. It is shown that the initial masses included some quantity of oil or debris that was later evacuated during the vacuum tests (VTs). The actual masses of water will be shown in the test matrix.

Wire was wrapped around the ampoules to keep the drill hole facing upwards when installed inside of the lower right standoff. The hole was oriented away from the heater rod for the vacuum drying tests and towards the heater rod for the applicable FHD test. This configuration for FHD was chosen because heated tests indicated minimal impact on the ampoule temperature. This was due to the combined effects of the cold pin length and standoff length, so the orifice needed to be as close as possible to the warm gas during FHS tests.

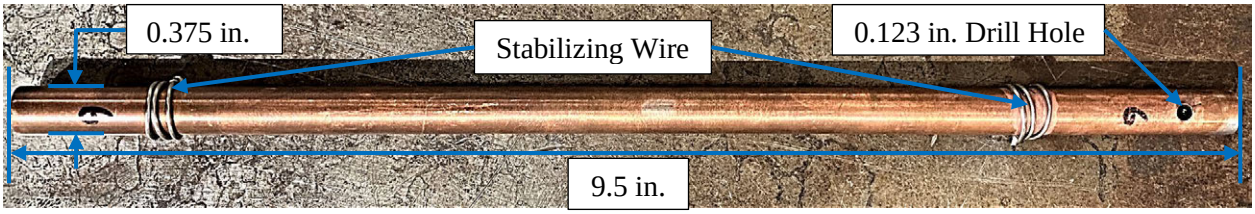

Figure 2-7 View of a 9.5 in. copper tube ampoule with 0.123 in. diameter drill hole.

Table 2-1 Dry weights of ampoules.

Hole ID (in.)	Initial Dry Weight (g)	Dry Weight Post-VT (g)	Dry Weight Post-VT (g)
0.021	56.396	56.365 (VT #5)	56.366 (VT #7)
0.123	56.650	56.612 (VT #6)	56.610 (VT #8)

2.5.2 Bulk Filling and Draining

The pressure vessel is capable of being filled with deionized water up to the middle cross (D5 in Figure B-2) where it overflows before reaching the electrical connections on the heater rod. It can be drained via the valve in the lower right standoff (valves D2 and D3), with further draining possible through a pressurized blowdown. This approach would allow for the thorough wetting of internal surfaces to maximize water retention sites, including the heater cladding, neutral wire, thermocouples, centering winglets, welding slag and pipe fitting junctions.

The water filling line components are diagrammed in Figure B-5. No mass flow controllers were used to restrict the flow of water from the pump, limiting the water balance to measurements of source water and water released to the drainage basin. A needle valve and rotameter (C3 and C4) were installed to control the flow rate of the transfer pump but fine control was not realistically possible for the small volume of the PV.

2.6 Instrumentation

This section will describe the instrumentation used to measure temperature and pressure during this test series. Instrumentation specific to moisture/water content measurement will be described separately in Chapter 3.

2.6.1 Thermocouples

Temperatures were measured using type-K or type-T thermocouples using the standard ASTM calibration specifications (ASTM, 2017) and no additional calibrations were performed. The thermocouples installed along the surfaces of the heater rod and ampoule are shown in Table 2-2 with their data acquisition (DAQ) labels, while ambient TCs and those installed on the surface of the pressure vessel are listed in Table 2-3. A coordinate system was defined with an origin at the center of the bottom end plug of the heater rod, where the rectilinear *z* coordinate runs along the axial length towards the upper standoff, the *y* coordinate runs towards the neutral feedthrough, and the *x* coordinate runs towards the pressure vessel mounting board (see Figure 2-6).

The 0° angular direction is defined as the negative *x* direction, such that 90° points towards the neutral feedthrough and 270° towards the lower standoff with the ampoule (see Figure A-4). In Table 2-2, internal thermocouples on the heater rod are installed at 0° and 180° angles to provide enough space for the combined mass of TC feedthroughs at 90°. These TCs are type-K for an upper measurement limit of 1090°C, which allow for an investigation of PCTs at or above 400°C. Several internal thermocouples not listed in the table were intended to be attached to a pressure monitoring tube placed at 0°. However, these TCs were never used since the pressure tube was never integrated into the pressure vessel due to a failed laser weld (see Section 5.4).

Table 2-2 List of internal (Int) thermocouples.

#	Type	Position (in.)			Direction (Degrees)	Surface	DAQ Label
		x	*y*	*z*			
1	K	0.24	0	8.0	180	Int	08.00_180_Heater_Rod
3	K	0.24	0	16.0	180	Int	16.00_180_Heater_Rod
5	K	-0.24	0	24.0	0	Int	24.00_000_Heater_Rod
6	K	0.24	0	24.0	180	Int	24.00_180_Heater_Rod
8	K	-0.24	0	32.0	0	Int	32.00_000_Heater_Rod
9	K	0.24	0	32.0	180	Int	32.00_180_Heater_Rod
11	K	0.24	0	41.0	180	Int	41.00_180_Heater_Rod
13	K	0.24	0	43.0	180	Int	43.00_180_Heater_Rod
15	T	0	-12.0	0.00	270	Int	00.00_270_Water_Tube_Body*
16	T	0	-16.25	0.375	270	Int	00.25_270_Water_Tube_Hole*
*Used to determine minimum ampoule temperature.							

The internal TCs on the water ampoule are type-T and mounted on the body of the ampoule and near the drill hole. They are meant to detect temperatures that may be indicative of freezing during the vacuum drying procedure, as their measurement range runs from -270°C to 400°C. Under vacuum, the vapor pressure of the water inside the tube will decrease and allow water to evaporate and escape through the hole. As the rate of evaporation increases with decreasing pressures, the liquid temperature drops through evaporative cooling. At some point, freezing will occur when the enthalpy of fusion is exceeded, and it will occur near the drill hole as it serves as the flow orifice of water vapor and the main point of heat transfer for the main body of water. At the lowest hold points, freezing will most likely assume the form of solid deposition directly from vapor.

Table 2-3 List of external (Ext) and ambient (Amb) thermocouples.

#	Type	Position (in.)			Direction (Degrees)	Surface	DAQ Label
		x	*y*	*z*			
17	K	0.50	0	8.0	180	Ext	08.00_180_Pressure_Vessel
18	K	-0.50	0	8.0	0	Ext	08.00_000_Pressure_Vessel
19	K	0.50	0	16.0	180	Ext	16.00_180_Pressure_Vessel
20	K	-0.50	0	16.0	0	Ext	16.00_000_Pressure_Vessel
21	K	0.50	0	24.0	180	Ext	24.00_180_Pressure_Vessel
22	K	-0.50	0	24.0	0	Ext	24.00_000_Pressure_Vessel
25	K	0.50	0	32.0	180	Ext	32.00_180_Pressure_Vessel
26	K	-0.50	0	32.0	0	Ext	32.00_000_Pressure_Vessel
27	K	0.50	0	41.0	180	Ext	41.00_180_Pressure_Vessel
28	K	-0.50	0	41.0	0	Ext	41.00_000_Pressure_Vessel
29	K	0.50	0	43.0	180	Ext	43.00_180_Pressure_Vessel
30	K	-0.50	0	43.0	0	Ext	43.00_000_Pressure_Vessel
31	K	0.50	0	52.0	180	Ext	52.00_180_Pressure_Vessel
32	K	-0.50	0	52.0	0	Ext	52.00_000_Pressure_Vessel
33	K	0.50	0	60.0	180	Ext	60.00_180_Pressure_Vessel
35	K	0	9.35	1.0	90	Ext	01.00_090_Standoff
36	K	0	9.35	0.0	90	Ext	00.00_090_Standoff
37	K	0	9.35	38.3	90	Ext	38.30_090_Standoff
38	K	0	9.35	37.3	90	Ext	37.30_090_Standoff
39	K	0	-9.35	1.0	270	Ext	01.00_270_Standoff
40	K	0	-9.35	0.0	270	Ext	00.00_270_Standoff
41	K	-1.0	-10.0	8.0	270	Amb	08.00_270_Ambient
42	K	-1.0	10.0	32.0	90	Amb	32.00_090_Ambient
43	K	0	-17.8	46.5	270	Ext	Mass_spec_gas_temp
44	K	0	23.1	42.5	90	Ext	Chilled_mirror_gas_temp*

* This thermocouple was mounted downstream of the needle valve vent (B5 in Figure B-3) and remained after the chilled mirror was removed from the system.

The external TCs in Table 2-3 are type-K and installed along the axial length of the pressure vessel in a collinear manner with those installed on the heater rod per given axial level at both 0° and 180° (see Figure A-4). Three additional TCs were also placed at z = 52 in. and z = 60 in. for the upper standoff. Each standoff oriented along the y axis also features TCs at the midpoint of length for the lower and upper surfaces (-z and +z directions). These are also meant to assess whether the temperature safety margin of the feedthrough packing sets is not exceeded (limited to 232 °C for the Teflon thermocouple-feedthrough packing)

A type-K TC was placed on the surface of the 1/16 in. OD tube leading to the mass spectrometer sample inlet to determine whether moist gas samples from the PV are susceptible to condensation relative to the dew point. Such a phase change was expected to interfere with the quality of measurements. A type-K TC was also installed in a tee downstream of the needle valve used for venting the vacuum line and pressure vessel (see B5 in Figure B-3).

2.6.2 Pressure Measurement

A Setra Model ASM high-accuracy pressure transducer is used to monitor pressure during the FHD tests. It has an accuracy of ±0.05% over a 300 psia full-scale range, or ±1.5 psia (±0.010 kPa), and was

calibrated to a primary standard traceable to the National Institute of Standards and Technology (NIST). The instrument directly interfaces with the pressure vessel via a peripheral branch lying between the main axial extent of the pressure vessel and the inlet for the gas cylinder and the vacuum pump (D9 in Figure B-2). This branch includes a 125 psig (862 kPa) pressure relief valve, and it is isolated during vacuum drying tests to reduce leakage. Linear voltage output from the Setra pressure transducer was directly converted to psia in the DAQ output and then converted to kPa in the post process.

Two vacuum gauges are employed to provide redundant sets of sub-atmospheric pressure data. They are mounted on a common tee in a branch lying between the main axial length of the pressure vessel and the mass spectrometer sample line (D13 in Figure B-2). This branch is valved-off for tests at high pressure due to the overpressure limits on the instruments.

A Pfeiffer PKR 251 full-range gauge is mounted horizontally on the middle of the branch and employs a combination of a Pirani gauge and a cold cathode system for measurement (although only the former system is active for the range of pressures in this report). A Pfeiffer TPG-362 dual-channel measurement and control unit is used for both direct pressure readout and providing logarithmic analog output to the DAQ. Since the DAQ is limited to processing voltage with polynomials, only the voltage was recorded, which was later post-processed into units of torr. While the gauge is calibrated for air, corrections to the indicated pressure would be needed for pure gases, i.e. if a pump-and-purge with helium preceded the vacuum drying test. Measurements on the Pfeiffer vacuum gauge are reproducible to ±5% of reading according to manufacturer specifications.

An InstruTech CVG101 Worker Bee convection Pirani gauge is mounted horizontally on the upper part of the branch. It was connected to an InstruTech VGC-301 vacuum gauge controller that provided direct millitorr readout and a linear analog output to the DAQ. To preserve fidelity in the linear 0 to 10 VDC output, the full-scale range was defined from 10 millitorr to 100 torr. (It should be noted that this convention exceeded the three-decade limit recommended by the manufacturer for linear analog output.) The gauge is calibrated for nitrogen, and pressure corrections for other gases must be made based on the relative difference in thermal conductivity. Since air resides in the pressure vessel prior to evacuation, corrections are not needed. Measurements on the InstruTech are reproducible to ±2% of reading according to manufacturer specifications.

The Pfeiffer gauge was used to determine the hold point during vacuum drying, but it should be noted that it underestimated pressures compared to the InstruTech. This caused the InstruTech to be saturated during the 100 torr target hold. For this reason, InstruTech measurements for the 100 torr hold point are omitted. This limitation was considered the best tradeoff to have two reliable measurements at the lowest hold pressures. Both gauges were locally calibrated to the onsite barometric pressure of 838 mbar (629 torr), although a low-pressure calibration under vacuum was not feasible due to turbo pump limitations.

2.7 Power Control

The electrical voltage and current delivered to the heater rod were controlled to maintain a constant power level by a digital silicon-controlled rectifier (SCR). The device software provided a digital power setpoint to the SCR that was controlled based on external power feedback from a calibrated Ohio Semitronics multifunction power test board (PTB). To have an additional calibrated reference, manual measurements of the current and voltage were taken intermittently with calibrated, handheld Fluke multimeters.

Table 2-4 lists the instruments used for power control and measurement, and Figure 2-8 shows the power control setup. Given the 1000 W rating of the heater rod, 10-amp fuses were installed in the circuit in the event that the heater rod shorted during the tests. The full-scale settings for SCR control were defined as 1,000 W, 120 V, and 8.333 A. The SCR, PTB, and pressure vessel shared the same ground as the power source.

The analog power feedback setup on the SCR was found to conflict with calibrated power measurements. The LabVIEW program on the DAQ therefore utilized a power stabilization module that automatically

adjusted the SCR fieldbus setpoint to the intended power setting using power output measurements from the PTB in a manner similar to a proportional-integral-derivative controller. A power conditioner was also used to stabilize the power signal to the SCR itself. These measures imparted more predictable power fluctuations during the test and resulted in an overall reduced margin of error in the actual power imparted to the heater rod (±2 W compared to ±5 W).

Table 2-4 List of power control equipment.

Description	Manufacturer	Model
Digital SCR AC Power Controller	Control Concepts	uF1HXLGI-130-P1RSZ
PTB – Measures voltage, current, and power	Ohio Semitronics	PTB-112D1PCY48
24 VDC Power Supply	Black Box	MDR-60-24
Voltmeter	Fluke	789 ProcessMeter
AC/DC Clamp Meter	Fluke	381 Remote Display TRMS
Power Conditioner	Eaton	PowerSure 800

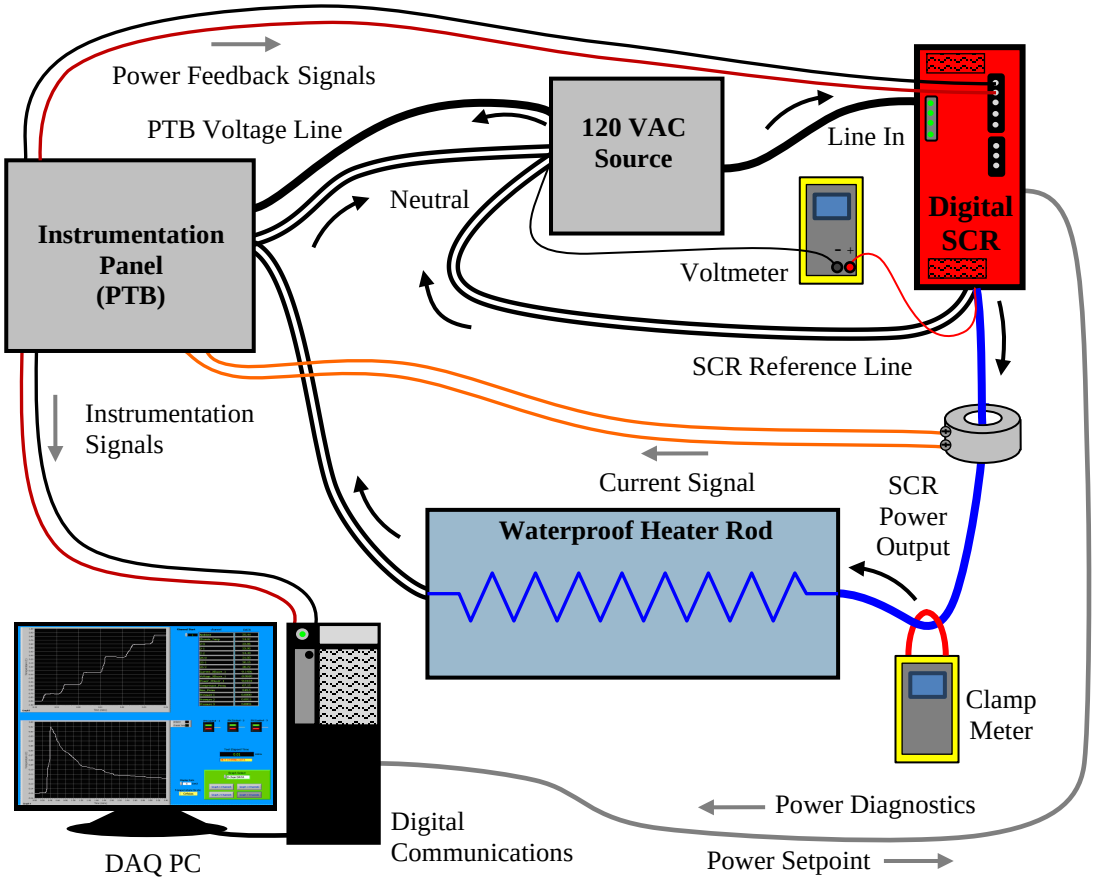

Figure 2-8 Power control setup with optional handheld meters.

2.8 Test Series

2.8.1 Forced Helium Dehydration

The forced helium dehydration test evaluated the effectiveness of employing a pressurized backfill in the PV in removing water. Helium is used because its thermal properties impart adequate heat transfer during

extended storage and because it provides an inert atmosphere pursuant to long-term SNF integrity. It also provides a means of leak testing the system.

Water was introduced as either the residual water from a bulk filling and draining of the PV, or contained in a fixed quantity within a copper ampoule. With the heater rod energized, the approach relies on the generation of a natural convection current in the PV based on the heater and external surface temperature profiles. Heated helium would be driven into various retention sites within the internal volume and bring liquid water into the vapor phase. This vapor phase water would then be removed when venting the pressurized helium. In the prototypic process, the procedure does not rely solely upon natural convection and employs a recirculation pump to impart the forced convection of helium. Furthermore, inline gas heaters and gas dryers are employed to keep the helium at elevated temperature and enhance water removal. In this small-scale test, no second heater or recirculating pump were available to imitate the commercial nuclear power plant process. Furthermore, water was designed to be removed in solution with helium rather than physically (as with steam dryers or drying silica).

The test employed five pressures to ascertain their efficiency at removing water from the system: 800, 520, 200, 150, and 100 kPa. (Prototypically, a pressure of about 520 kPa is used.) These pressures allow for continuous mass spectrometer measurements that can provide information on the evolving water content over time. With a heater power optimized to achieve a PCT of 400 °C, it should be possible to bring water into vapor form, as shown in Figure 2-9. The pressure step-down procedure was employed to maximize convection at high pressure and then maximize vapor phase transition at lower pressures. This approach was limited by the total heat transferred to the helium in the annulus between the heater and pressure vessel, the density differences in helium from top to bottom, and the subsequent buoyancy-driven flow of helium.

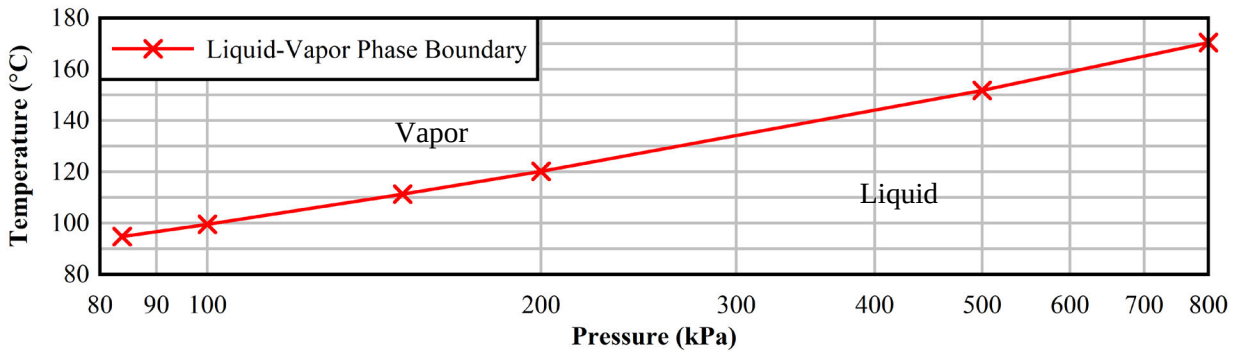

Figure 2-9 Phase boundaries relevant to the FHD tests.

2.8.2 Vacuum Drying

A vacuum drying procedure was devised where the pressure vessel would be isolated and held at incrementally decreasing pressure levels, which are shown in Table 2-5 and plotted in Figure 2-10. A convention was employed to hold pressures for 30 minutes before proceeding to the next pressure level. If a rebound pressure threshold was exceeded during that time period, the hold was repeated either immediately or at the end of the 30-minute time interval. If sampling was underway with the mass spectrometer, the hold was terminated if the pressure approached the 3.75 torr limit on the low-pressure sample line to avoid tripping the MS solenoid valve. The rebound criteria in this test series was the throttle pressure of the previous hold.

A given drying test was considered successful if the pressure during the final hold does not exceed 3 torr after 30 minutes, as inspired by NUREG-1536 (NRC, 2010). The use of a 0.25 torr hold is representative of commercial practice by applying a lower vacuum level to ensure that this criterion is met.

The pressure vessel is initially at atmospheric pressure and is filled with the surrounding air. Air can be removed from the PV using a pump-and-purge procedure with helium or inert gas, but this was not done for the vacuum drying tests in this report. In such a procedure, the PV would begin at a pressure slightly above atmospheric to prevent the influx of air.

Table 2-5 Hold points for vacuum drying procedure.

#	Period (min)	Throttle Pressure (torr)	Rebound Threshold (torr)	Throttle Pressure (kPa)	Rebound Threshold (kPa)
1	30	100	150	13.332	19.998
2	30	75	100	9.999	13.332
3	30	50	75	6.666	9.999
4	30	25	50	3.333	6.666
5	30	10	25	1.333	3.333
6	30	5	10	0.667	1.333
7	30	3	5	0.400	0.667
8	30	1	3	0.133	0.400
9	30	0.5	1	0.067	0.133
10	30	0.25	0.5	0.033	0.067

The vacuum line is devised such that the pump runs continuously while isolated from the PV. The isolation valve (D1 in Figure B-3) is carefully opened by the operator until a gauge indicator reads the hold pressure, upon which the PV is isolated. In this report, the Pfeiffer gauge controller was used to determine hold points, which were typically higher than the readouts on the InstruTech controller.

When the pressure stabilized within the low-pressure MS sampling regime (0.375-3.75 torr), the MS isolation valve (D4 in Figure B-2) was opened while D1 was still open to the vacuum stream, then D1 was isolated upon reaching the specified hold point. The quantity of air retained in the sample line tube between D4 and the MS sample block is not exposed to vacuum until this low-pressure regime, but the effects of this air pocket on water content are considered negligible.

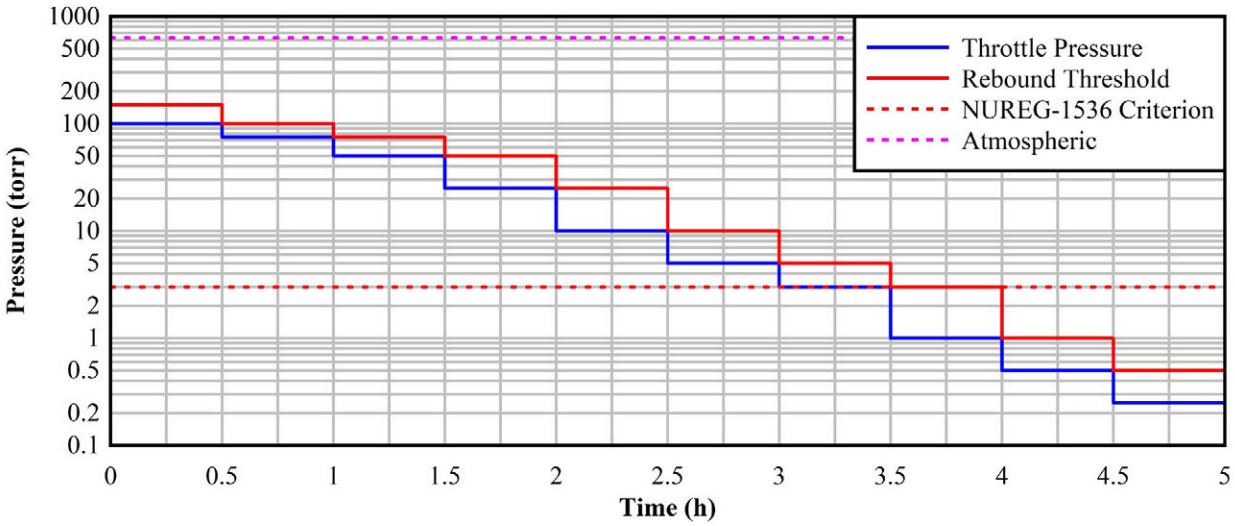

Figure 2-10 Vacuum drying hold points idealized over time.

Among the hold pressures listed in Table 2-5, there are certain pressures that are liable to result in phase changes. Figure 2-9 shows the phase diagram of water for the applicable range of pressures in the VTs. At temperatures near ambient, boiling of liquid water in the ampoule is liable to occur during the 25, 10, and

5 torr holds. When progressing to the 3 torr hold point, the PV falls below the triple point of 4.59 torr, which can result in complex phase transitions during the evacuation and pressure rebound. In this regime, the liquid water in the ampoule is most likely to enter the solid phase as the pressure vessel is exposed to the full vacuum flow rate. This phase transition may actually hinder the low pressure achieved by the pump and require a repeat of the hold. For 1 torr and below, liquid water remaining in the ampoule and PV, if any, may undergo solid phase deposition during the evacuation and then immediately vaporize. Otherwise, water is in a vaporized form from this point onward.

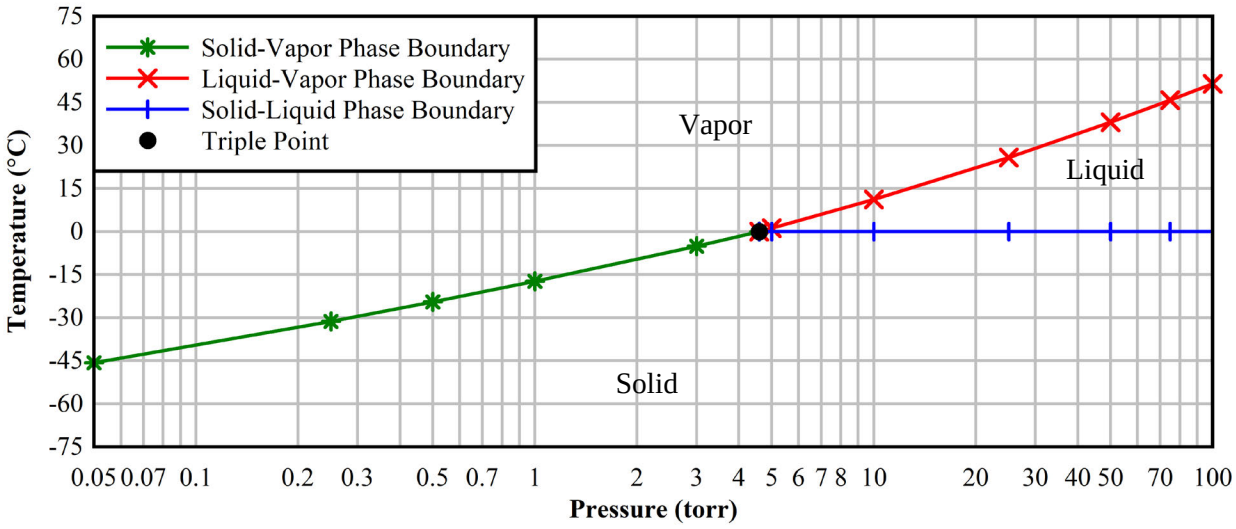

Figure 2-11 Phase boundaries relevant to the vacuum drying tests.

2.9 Test Matrix

The series of tests conducted with the pressure vessel are shown in Table 2-6 parameterized by the fluids, pressures, water masses, and heater rod power levels involved.

An early phase of unheated vacuum drying was completed without penetrations for electrical connections to the heater and the HX200 dew point transmitter (described in Section 3.4) installed outside of the bellows valve on the pressure vessel. This resulted in dew point data being measured discreetly in the gas evacuated after each hold point, rather than continuously. The water ampoule was of a preliminary design and there was also no accurate means available for measuring water mass at a milligram resolution. Furthermore, there were no penetrations for internal thermocouples so the ampoule temperature could not be measured. For these reasons, only the baseline unheated results (VT #3) from this early phase are referenced in this report. Nonetheless, these tests provided initial isothermal pressure data corresponding to the removal of water from an ampoule, and results are documented in Salazar *et al.*, 2020.

The heated phase of vacuum drying testing (VT #4 through 8) began with an assessment of the background vacuum leak rate with the heater energized. The vacuum tightness of the pressure vessel gradually improved from that point forward because it was standard practice to leave the pump running overnight after every test. For this reason, the 250 millitorr hold point was achievable in VT #5 through 7 (VT #8 was halted at 500 millitorr due to time constraints and because the drying criterion was satisfied).

The first forced helium dehydration test (FHD #1) was conducted with bulk filling and draining of water as opposed to a more controlled quantity in an ampoule. This was meant to purposefully maximize water retention in the PV. Since the HX200 was installed outside of the pressure vessel, no continuous dew point data was available and the venting after each hold had to be made at the top of the vessel against gravity to obtain dew point data (see Figure 4-1).

A preliminary FHD test was conducted with a maximum pressure of 520 kPa, which is closer to the prototypic pressure used for dehydration. While the water mass balance was logged, it became clear that the relatively large quantity of water was not being removed through the procedure. In a subsequent test, the maximum pressure was increased to 800 kPa and a blowdown was implemented after gravity drainage in an effort to remove larger pockets of water in the standoffs. However, only one initial blowdown was performed, which was not sufficient to remove residual air in the free volume of the pressure vessel, as was confirmed in analyses of the MS data.

In FHD #1, the minimum pressure was elevated to 150 kPa to remain above the sampling threshold of the sample inlet, and the measuring periods were lengthened for the lower pressures. As opposed to a single blowdown, this test introduced a full pump-and-purge procedure to remove air pockets.

In FHD #2, the HX200 directly interfaced with the pressure vessel to provide continuous data that could be directly matched with mass spectrometer data. An ampoule with a set quantity of water was used as opposed to a bulk filling and draining of water. The peripheral standoffs were also insulated to augment heat transfer to the ampoule, whose hole was oriented towards the heater as opposed to the outer boundary. Venting to the required hold points was performed on the bottom of the pressure vessel to be aligned with gravity. In this report, results for FHD #1-2 will be presented to highlight differences in the procedures and setup.

Table 2-6 Test matrix.

Test Series	#	Internal Fluid	Vessel Pressure (kPa)	Power (W)	Hold Period (min)	Ampoule Hole OD (in.)	Initial Mass H_2O (g)	Residual Mass H_2O (g)
FHD	1	He + H_2O	800-200-150	150	15-30-30	n.a.	n.m.	n.m.
	2	He + H_2O	800-200-150	150	15-30-30	0.123	10.706	10.608
Vacuum Drying	3	Air	13-0.07	0	10	n.a.	n.a.	n.a.
	4	Air	13-0.07	150	30	n.a.	n.a.	n.a.
	5	Air + H_2O	13-0.03	0	30	0.021	5.174	0
	6	Air + H_2O	13-0.03	0	30	0.123	10.774	0
	7	Air + H_2O	13-0.03	150	30	0.021	6.327	0
	8	Air + H_2O	13-0.07	150	30	0.123	10.737	0

n.a.: not applicable
n.m.: not sufficiently measurable

This page is intentionally left blank.

3 METHODOLOGY FOR WATER CONTENT MEASUREMENT

3.1 Overview

Vacuum drying tests present a challenging set of conditions for moisture monitoring due to the large swing in pressures (0.5 to 6000 torr) at elevated temperatures up to 400 °C (Salazar *et al*., 2019). A number of technologies have previously been used for monitoring moisture in the gas phase that provide an absolute moisture concentration measurement. The most common are solid-state capacity humidity sensors, chilled mirror hygrometers and to a lesser degree, tunable diode laser (TDL) absorption spectroscopy. However, neither the solid-state sensors nor chilled mirror probes can operate at the elevated temperatures required for *in situ* measurements in the head space of the pressure vessel due to high temperature or low pressure. The TDL cannot operate at pressures below 10 torr so the system cannot be used throughout the entire vacuum drying process.

Solid-state capacitance humidity sensors and chilled mirror hygrometers can be used to monitor the moisture in the vacuum extraction flow during the vacuum drying step since the temperature of the extracted sample stream can be lowered. However, as the extractive flow rate drops with increasing vacuum, the representativeness of the measurements to the environment inside the pressure vessel diminishes. After the vacuum extraction step, monitoring the moisture during the pressure rebound and after backfilling with helium is problematic. Extracting a representative sample during these steps may perturb the system in ways that may be difficult to quantify unless the sample flow is small.

Mass spectroscopy is a nontraditional method for measuring the relative moisture concentration in gas (i.e. parts per million by volume, ppmv). In MS, a small sample stream (1 to 20 scm^3/min, where an scm^3 is a cubic centimeter of gas referenced at a standard temperature and pressure, depending on sample pressure) is ionized and drawn into a vacuum chamber through a quadrupole filter that influences how ionized species interact with the ion detector. Because MS draws such a small sample flow, no perturbation of the system is expected. However, adsorption and desorption of water on the small-bore stainless steel or glass capillary sample tubes can be an issue especially as the sample flow rate drops with falling sample pressure. Heating the sample lines and quadrupole minimizes the problem, but it will still take several minutes of sample flow for equilibrium to be reached. For slowly changing transient operations expected in drying operation, the anticipated lags are expected to be manageable. With a properly designed inlet, the high temperature and the wide range of pressures inside the pressure vessel can be accommodated.

3.2 Mass Spectrometer

The Hiden Analytical HPR-30 is a 6 mm quadrupole mass spectrometer with a Faraday cup detector employed to analyze transient gas concentrations in gas samples from the pressure vessel obtained via a stainless-steel capillary tube with 0.173 in. (0.439 cm) inner diameter at two pressure ranges. A high-pressure range of 100 to 1000 kPa (14.5 to 145 psia) was used for forced helium dehydration tests and a low-pressure range of 0.05 to 0.5 kPa (0.375 to 3.75 torr) was used for vacuum drying tests. The mass spectrometer, shown in Figure 3-1, uses a scroll pump in combination with a turbo molecular pump to evacuate the internal volume and reduce the pressure within the spectrometer. This allows sample gases to flow into an ion source, which ionizes the molecular components of the sample gas.

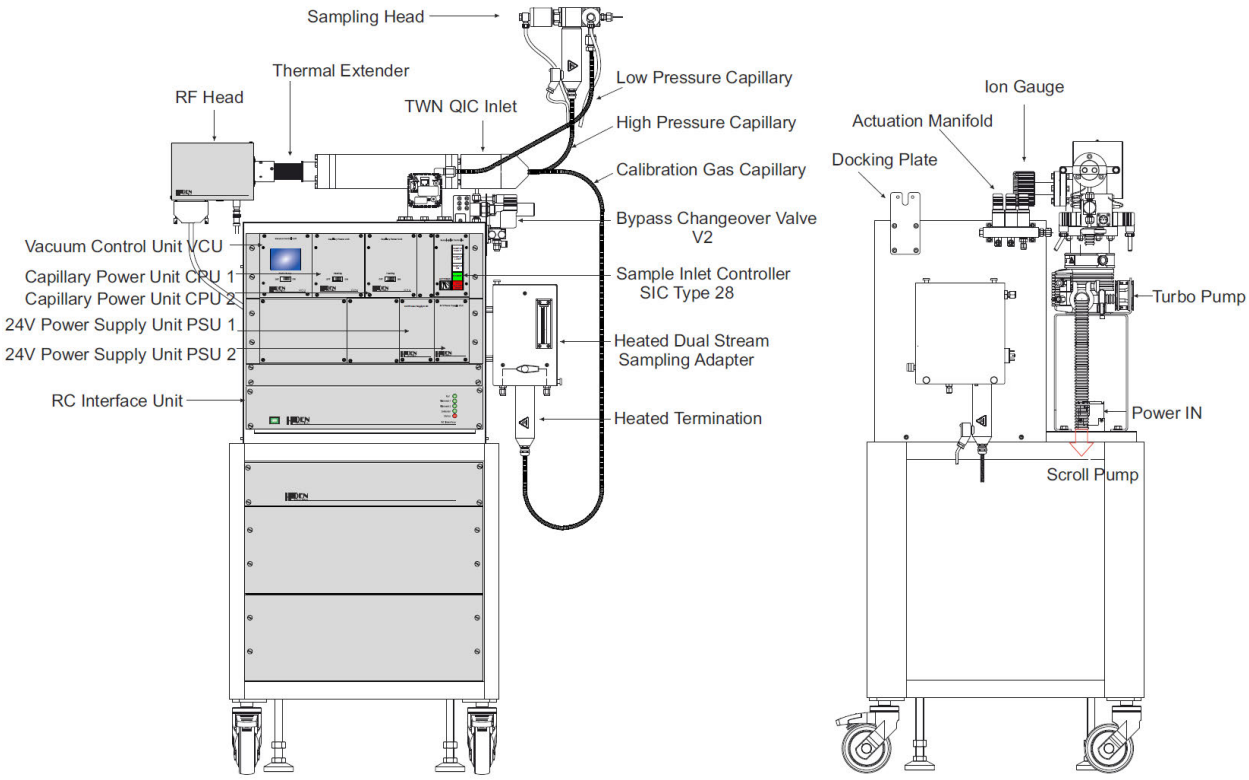

Figure 3-1 Hiden Analytical HPR-30 mass spectrometer system with a QIC dual-stage sampling head for measuring water content from the waterproof heater rod pressure vessel (Hiden Analytical Limited, 2018).

The ionized molecules are guided by a potential gradient between the ion source and ground to a quadrupole, which filters the molecules based on their mass-to-charge ratio m/z (amu/Coulomb). The quadrupole influences how the charged molecules are detected by the Faraday cup – the mass spectrometer outputs the number of counts of ion-detector collisions based on m/z. The relative concentrations of each molecular component can thus be calculated from the ion detector collision count peaks at each m/z value.

A given gas sample will have multiple peaks based on how the molecules are ionized (singly- or doubly-charged) and the presence of molecular isotopes. For each molecule, determining a relative concentration amounts to accounting for the major peak of that molecule, which is associated with the molecule's most common ionic species. For example, as shown in Figure 3-2, the three peaks associated with nitrogen come from singly-charged $^{28}N_2$ (28 amu/1 C = 28 amu/C), doubly-charged $^{28}N_2$ (28 amu/2 C = 14 amu/C), and singly-charged $^{29}N_2$ (29 amu/1 C = 29 amu/C). The 28 amu/C peak is the largest peak in the mass spectrum of nitrogen, so it is the peak used for quantification. A method could have been developed using all three peaks but the analysis would take longer to complete. Since the drying process is transient, a rapid method was needed to resolve temporal changes and only the major peak for water, helium, nitrogen, oxygen and argon were analyzed. The resulting analysis time for the method developed was about 45 seconds.

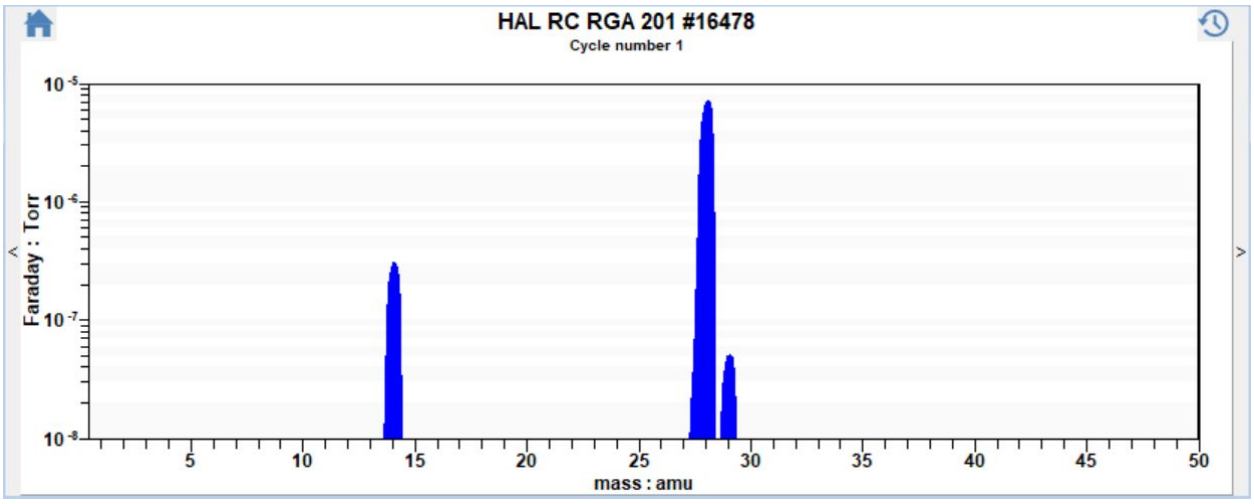

Figure 3-2 Mass spectrum of air showing the major peaks for nitrogen.

The amount of residual water detected will help define the effectiveness of the drying procedures implemented. An advantage of using an MS is that all other gaseous species are analyzed. For vacuum drying, the amount of air components can be used to evaluate the air leakage into the system. If used to monitor a commercial dry cask, an MS can also detect hydrogen generation that would indicate radiolysis or noble gas fission products (e.g. Kr-85 or Xe-137) that would indicate a leaking fuel rod.

3.3 Calibration with Dew Point Generator and Chilled Mirror Hygrometer

The mass spectrometer was calibrated to detect water content using a Michell DG2 two-stage dew point (DP) generator (-40 °C to +20 °C dew points). The generator uses a dry gas source such as ultra-high purity helium or air and generates a split stream that is mixed with moisture at a controlled temperature to generate a gas with a known dew point between -40 °C to +20 °C. The dew point of the calibration gas was verified by passing through a Michell S8000 chilled mirror hygrometer that can provide precision measurements to -65 °C dew point. The mass spectrometer was calibrated for moisture concentrations between zero and 25,000 ppmv using either helium or air as the background gas.

3.3.1 Calibration Procedure

Using the experimental setup in Figure B-6, the mass spectrometer is calibrated to accurately measure the water content in the waterproof heater rod pressure vessel during forced helium dehydration and vacuum drying tests. To calibrate the HPR-30, a chilled mirror hydrometer (Michell S8000) was used to determine the dew point of the calibration gas. The S8000 was selected due to its low measurement uncertainty of ±0.1 °C DP (±0.18 °F DP) and large measurement range of –60 to +40 °C DP (–76 to +104 °F DP) (Michell Instruments, 2019). The S8000 was calibrated using reference instruments with United Kingdom Accreditation Service certificates.

Calibration of quadrupole mass spectrometers is important due to the complex dependence the response has on several relative sensitivity factors (RSFs). Based on a report detailing RSFs by Hiden Analytical, it is best practice to continuously measure the total RSF for a given experimental setup (Hiden Analytical Limited, 2008). Given that it may not be feasible to directly measure the RSF, Hiden Analytical uses the source sensitivity (R_S), fragmentation (R_F), and quadrupole transmission (R_Q) factors, as reported by (Leck, 1989; Mass Spectrometry Data Centre, 1991; Hiden Analytical Limited, 2008) to estimate the overall RSF factor for a variety of common gases normalized to nitrogen. Hiden Analytical's default RSFs neglect the inlet sensitivity (R_I) and detection efficiency (R_D), which are a function of specific experimental conditions, by setting these factors equal to one (Eq. 1).

$$RSF = R_I R_S R_F R_Q R_D \quad (1)$$

The following procedure was used to calibrate the HPR-30 MS:

1. A dry gas (typically research purity) that is the desired background gas was used to dry out the experimental setup (Figure B-6) and purge all other residual gases.
    a. A flow controller was used to establish a constant flow rate.
    b. It was confirmed that the S8000 DP sensor and HPR-30 MS were receiving a sample within the flow rate specifications of the instruments.
2. The pressure and temperature of the sample gas were measured.
    a. Pressure was used to correct the measured ppmv value reported by the S8000. It is common that DP sensors use atmospheric pressure at sea level by default.
    b. The temperature of the sample gas was required, along with the DP measurement converted to water vapor pressure (WVP), to calculate the absolute humidity.
3. A constant DP in the experimental setup was established using a DP generator.
    a. Real-time measurement of the DP aided in achieving a constant DP since precise control of a DP generator can be difficult, especially for gases that are not atmospheric air.
    b. The DP was first measured at full dry and was systematically increased to cover the range from full dry to near the saturation temperature of the experimental setup.
4. Once a steady state was established at a known DP, the system was held at that DP until at least thirty data points had been collected by the HPR-30 MS and the S8000 DP sensor.
    a. A maximum DP measurement was determined by the experimental setup temperature to avoid water condensing within the experimental setup.

Subsequently, the overall RSF for water was determined using the following approach:

1. The MS and S8000 sample gas data were collected for post-processing.
    a. Data was synced in time. For this calibration, the HPR-30 MS collected data approximately every forty seconds while the S8000 chilled mirror hygrometer collected data every two seconds.
2. The DP measured by the S8000 was converted to ppmv and the raw counts of the HPR-30 MS were converted to ppmv for water.
    a. ppmv (wet) from the S8000 was calculated using the pressure of the sample gas. In this case, a saturation vapor pressure correlation, based on the well-known Goff-Gratch equation developed by Parish and Putnam from the NASA Dryden Flight Research Center, was used to convert DP to WVP and ultimately to ppmv at the sample gas pressure (List, 1951; Parish & Putnam, 1977).
    b. ppmv (wet) was calculated from the MS by dividing the measured, partial pressure of water by the total partial pressure of the major peaks of all present gases: water and the background gas – either helium or air (Eq. 2 & 3).
    c. If a gas with a single component, such as research grade helium, was used, an RSF of one was used for both the background gas and water initially (i.e. the sample gas) to obtain ppmv for water from the MS raw data (Eq. 2). Once the RSF factor for water is determined it can be applied to Eq. 2.

$$ppmv = \frac{\frac{C_{sample}}{RSF_{sample}}}{\frac{C_{background}}{RSF_{background}} + \frac{C_{sample}}{RSF_{sample}}} = \frac{C_{sample}}{C_{background} + C_{sample}} \quad (2)$$

d. If a gas that had several components was used, such as atmospheric air, RSFs for the major peaks of the gas (e.g. nitrogen, oxygen, and argon) were used to yield the known concentrations of the components of the background gas. Furthermore, an RSF of one was used for the major peak of water (i.e. the sample gas) to obtain ppmv from the MS raw data (Eq. 3).

$$ppmv = \frac{\frac{C_{sample}}{RSF_{sample}}}{\sum_{i=1}^{n} \frac{C^i_{background}}{RSF^i_{background}} + \frac{C_{sample}}{RSF_{sample}}} \quad (3)$$

3. The ppmv of water measured by the HPR-30 MS was plotted as a function of the ppmv of water measured by the S8000 DP sensor. A linear regression was used to find the overall RSF of the sample and the detection limit (DL).

   a. The relationship between the S8000 and HPR-30 ppmv values is linear, the slope is the RSF of the sample gas, and the intercept is the detection limit of the sample gas for a given background gas (Eq. 4).

$$(MS\ ppmv) = RSF \cdot (Known\ ppmv) + DL \quad (4)$$

   b. A key assumption of determining the RSF for a sample gas was that the concentration of the sample is much less than the concentration of the background gas (Eq. 5).

$$C_{background} \gg C_{sample} \therefore ppmv \approx \frac{\frac{C_{sample}}{RSF_{sample}}}{\sum_{i=1}^{n} \frac{C^i_{background}}{RSF^i_{background}}} \quad (5)$$

4. The calibration was checked by comparing the corrected HPR-30 MS ppmv values to the ppmv values measured by the S8000 DP sensor. HPR-30 ppmv values were corrected using the calculated RSF and detection limit for water. (Eq. 4 solved for MS ppmv)

   a. To determine the uncertainty of the calibration the measurement uncertainty of the S8000 DP sensor [±0.1 °C DP (±0.18 °F DP)] and the error between the corrected HPR-30 and S8000 ppmv values was considered. Furthermore, in subsequent sections of this report the corrected HPR-30 ppmv values were converted to DP. The error introduced by the correlation to convert ppmv to DP is less than one percent and was accounted for in the given uncertainty of the calibration (Parish & Putnam, 1977) (Eqs. 7 & 8).

   b. To obtain the DP from the MS measurement the ppmv values are first corrected using the relevant calibration. The second step is to convert the ppmv values to WVP, Eq. 6, and lastly Eqs. 7-8 are numerically solved to obtain the DP. Eq. 7 is used when the DP is greater than 0 °C and Eq. 8 when the DP is less than 0 °C, to find the frost point. The subscript w for Eq. 7 indicates a WVP over water, while the subscript I for Eq. 8 indicates a WVP over ice.

$$WVP = \frac{ppmv}{10^6} \cdot P \quad (6)$$

$$WVP_w = 10^{23.5518 - \frac{2937.40}{DP + 273.15}} (DP + 273.15)^{-4.9283} \quad (7)$$

$$WVP_I = 10^{11.4816-\frac{2705.21}{DP+273.15}}(DP+273.15)^{-0.3228} \quad (8)$$

3.4 Calibration Results

Two background gases were used to calibrate the Hiden Analytical HPR-30 MS: compressed dry atmospheric air and research purity helium. During the vacuum drying and FHD tests, either air or helium were present as the background gas with water vapor as the intended sample. In this section, the calibration results for air and helium following the procedure outlined in the previous section are presented.

3.4.1 Water Content Calibration using Atmospheric Air

Atmospheric air contains three main components – namely nitrogen, oxygen, and argon gases; all other gases present in air have concentrations much less than one percent (Mackenzie F.T. & Mackenzie J.A, 1995). To properly calibrate the HPR-30 MS, the RSFs for nitrogen, oxygen, and argon must also be known. Experimentally, it was determined that using the default Hiden Analytical RSFs with the HPR-30 MS for nitrogen, oxygen, and argon provide the concentrations of air to within less than one percent of the known atmospheric composition of air (Table 3-1). When the concentration of water was above sixty percent, however, there was significant deviation from the known composition of air (Table 3-2). The assumption used by Eq. (5) becomes invalid and the RSFs for both the background and the sample gases must be considered simultaneously.

Table 3-1 Experimental measurements of the atmospheric composition of air using the HPR-30 with water content less than sixty percent; data collected on 01/24/2020 (Salazar *et al.*, 2020).

Time	N_2 Dry	O_2 Dry	Ar Dry	Water Content
1/24/2020 16:33	78.16%	20.73%	1.12%	53.02%
1/24/2020 16:35	78.68%	20.22%	1.10%	45.63%
1/24/2020 16:37	79.13%	19.78%	1.09%	44.10%
1/24/2020 16:38	79.06%	19.85%	1.09%	45.05%
1/24/2020 16:40	79.02%	19.89%	1.09%	45.80%
1/24/2020 16:41	78.98%	19.92%	1.09%	46.38%
1/24/2020 16:43	78.94%	19.97%	1.09%	46.81%
1/24/2020 16:45	78.92%	19.98%	1.10%	47.22%
1/24/2020 16:46	78.96%	19.95%	1.09%	47.58%
Measurement Average	78.87%	20.03%	1.10%	46.84%
Known Gaseous Composition of Dry Air	78.08%	20.95%	0.93%	N/A

It is well known that when using electron spray ionization, the relative concentration of the sample affects the detection efficiency (R_D) of the mass spectrometer (Hoffmann & Stroobant, 2007). As mentioned previously, the default RSFs provided by Hiden Analytical neglect R_D and R_I. For water concentrations less than sixty percent, the experimental results suggest that R_I for the vacuum drying test setup does not significantly impact the accuracy of the measurement (Table 3-2). Overall, the results suggest that using the default Hiden Analytical RSFs is justified for air with water concentrations less than sixty percent assuming the performance of the HPR-30 does not change significantly over time. Furthermore, for the purposes of vacuum drying and FHD, the RSF for water is independent of the RSFs used for air when the RSFs for air are constant (Eq. 3). Using the default Hiden Analytical RSFs only for air has the added benefit of yielding the approximate known concentrations of air to be used as a baseline measurement and to ensure consistency with the default RSFs given by the manufacturer of the HPR-30 MS.

Table 3-2 Experimental measurements of the atmospheric composition of air using the HPR-30 with water content greater than sixty percent; data collected on 01/24/2020 (Salazar *et al.*, 2020).

Time	N_2 Dry	O_2 Dry	Ar Dry	Water Content
1/24/2020 15:55	75.89%	23.32%	0.79%	97.31%
1/24/2020 15:58	70.74%	28.25%	1.01%	97.67%
1/24/2020 15:59	70.74%	28.24%	1.01%	97.73%
1/24/2020 16:01	71.06%	27.92%	1.02%	97.75%
1/24/2020 16:02	70.95%	28.02%	1.02%	97.80%
1/24/2020 16:04	70.57%	28.40%	1.03%	97.85%
1/24/2020 16:05	67.79%	31.25%	0.96%	97.19%
1/24/2020 16:07	70.65%	28.32%	1.03%	96.99%
1/24/2020 16:09	70.87%	28.09%	1.04%	97.22%
Measurement Average	71.03%	27.98%	0.99%	97.50%
Known Gaseous Composition of Dry Air	78.08%	20.95%	0.93%	N/A

3.4.1.1 Air Calibration Procedure Steps 1 & 2

The first step of calibrating the HPR-30 MS for water in air involved collecting the data and converting the output of the HPR-30 MS and S8000 DP sensor to ppmv of water. Figure 3-3 shows the raw data for the HPR-30 and S8000. Since the ppmv of water measured by the S8000 is a function of pressure, the pressure data in Figure 3-4a is also considered using Eq. 6, where P is pressure:

$$ppmv = \frac{WVP}{P} 10^6 \tag{6}$$

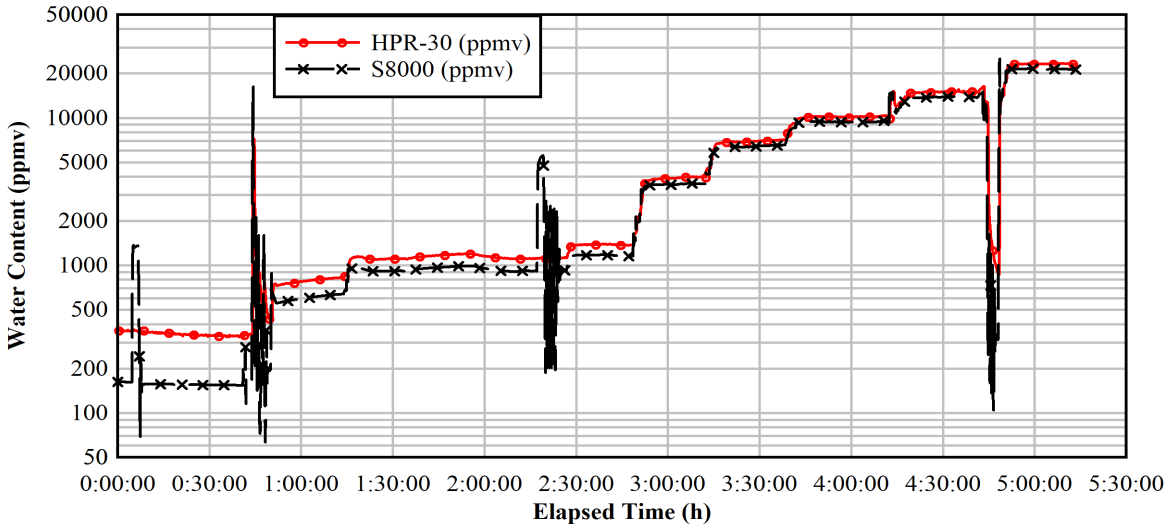

Figure 3-3 Raw HPR-30 and S8000 ppmv data with air as the background gas. Dynamic contamination control on the S8000 causes regular spikes in the calibration data.

By default, the S8000 outputs ppmv but uses atmospheric pressure at sea level in its internal calculations. Additionally, to determine the absolute humidity, the temperature of the sample gas is also measured as shown in Figure 3-4b. Absolute humidity is not used in the calibration procedure but is an additional parameter that can be determined for completeness.

As can be seen in Figure 3-3, the data includes several transitions to different hold points. Furthermore, the HPR-30 and S8000 are sampling at different rates. The S8000 collects data every two seconds while

the HPR-30 collects data approximately every forty seconds. In order to easily compare the measured output of the HPR-30 and S8000 at steady state, the data was filtered and synced in time to the nearest minute using averaging. The result of filtering and syncing the data can be seen in Figure 3-5.

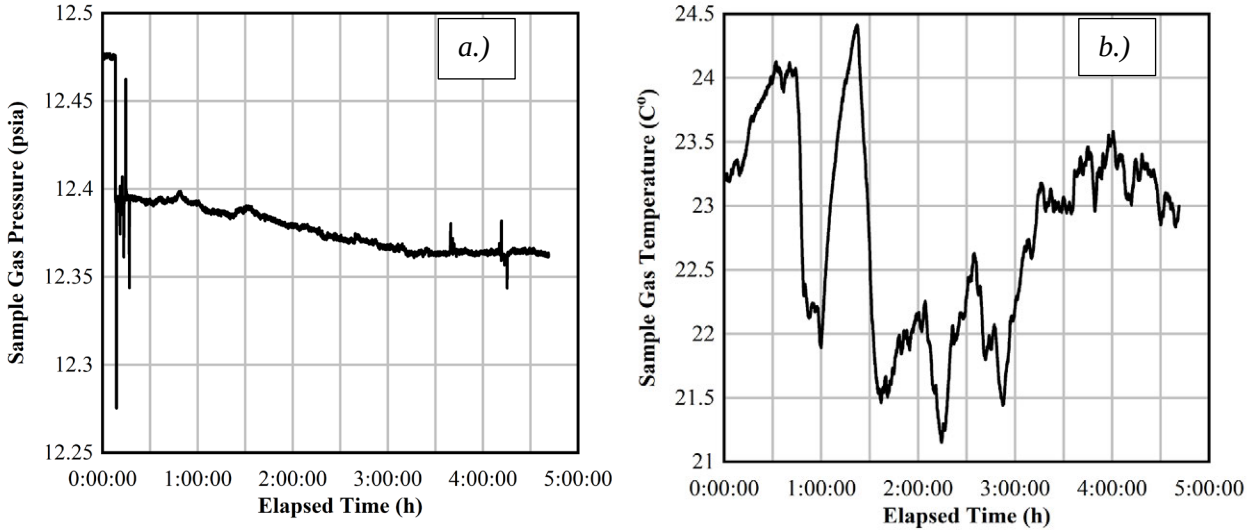

Figure 3-4 *a.)* Inlet pressure and *b.)* outlet temperature of the sample gas measured at the S8000 with air as the background gas.

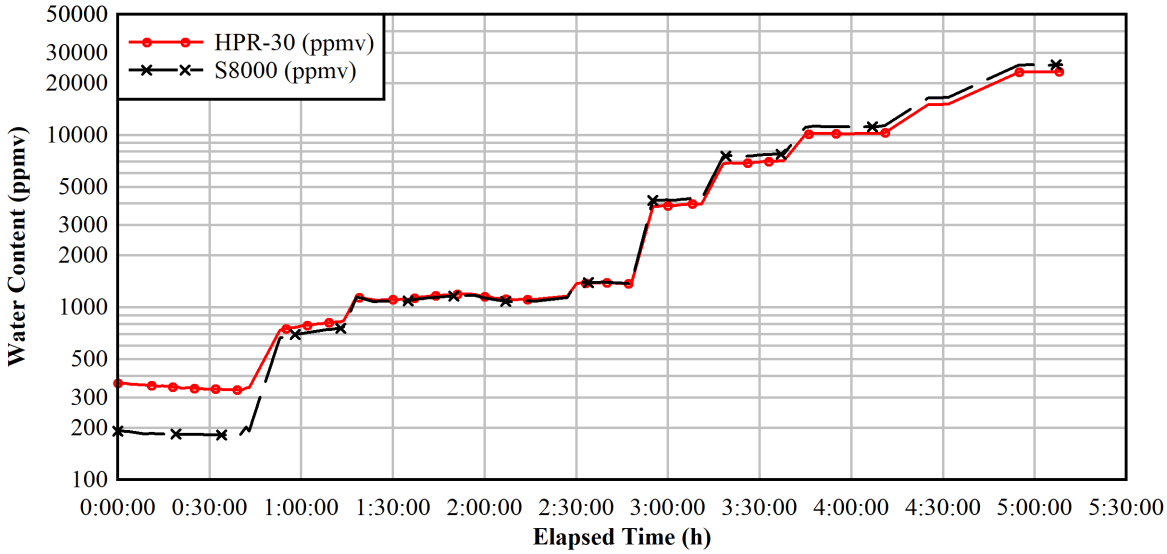

Figure 3-5 HPR-30 and S8000 ppmv data filtered and synced in time with air as the background gas.

It is important to note that all dynamic contamination control (DCC) spikes in the S8000 data and temporally corresponding HPR-30 data were filtered out. DCC is used to remove contaminants from the chilled mirror in the S8000 by heating up the surface of the mirror, causing a spike in ppmv.

3.4.1.2 Air Calibration Procedure Step 3

From Figure 3-5, it is apparent that the HPR-30 and S8000 gave conflicting measurements of the water content in an air background. To calibrate the HPR-30 with respect to the S8000, a relationship was found

between the HPR-30 and S8000 using a linear regression analysis, shown in Figure 3-6. The RSF for water is the slope of the linear regression and the intercept is the detection limit. The RSF for water is 0.9038 and the detection limit is 132.84 ppmv; the linear regression gave a coefficient of determination of $R^2 = 0.9999$ and a standard error (SE) of the regression of 41 ppmv. The 95% confidence interval for the regression based on the *t*-statistic = 1.975 and the standard error gives ±81 ppmv. The standard deviation of the difference between the corrected HPR-30 and S8000 data was ±45.68 ppmv and ±1.679 °C DP. The DP standard deviation includes the S8000 measurement uncertainty (±0.1 °C DP) and ppmv to DP correlation uncertainty of ±1%.

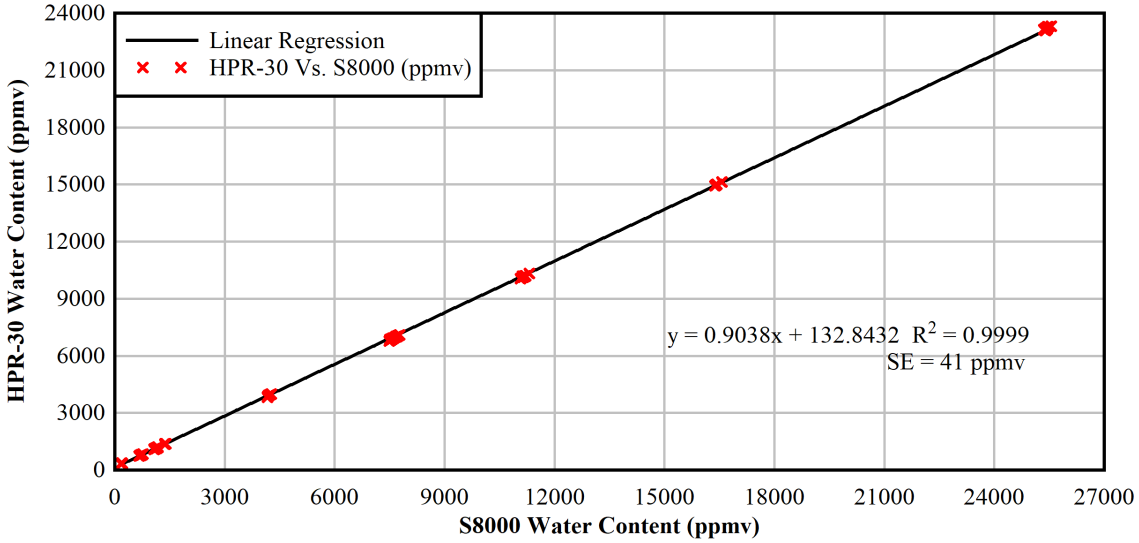

Figure 3-6 Linear regression of the ppmv of water measured by the HPR-30 as a function of the ppmv of water measured by the S8000 with air as the background gas.

3.4.1.3 Air Calibration Procedure Step 4

Using the detection limit and RSF determined in step 3 of the air calibration procedure, the ppmv measured by the HPR-30 was corrected as shown in Figure 3-7. The concentration of the sample (water) is assumed to be much less than the concentration of the background gas. The concentration of water never exceeds 3% (30,000 ppmv) of the total concentration of the sample gas.

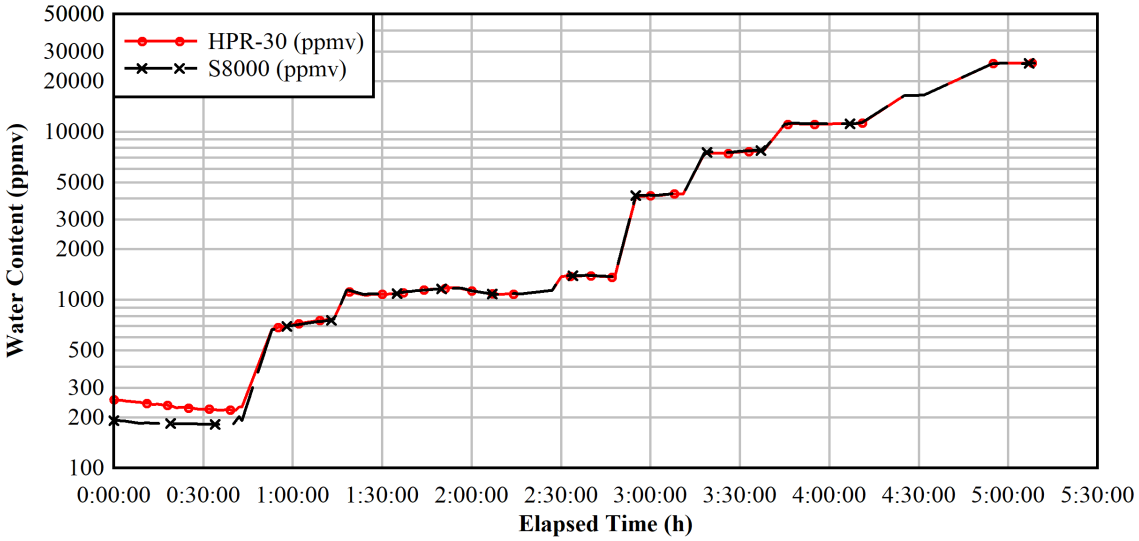

Figure 3-7 Comparison of corrected S8000 and HPR-30 ppmv data using the RSF and detection limit calculated for water with air as the background gas.

3.4.2 Water Content Calibration using Helium

3.4.2.1 Helium Calibration Procedure Steps 1 & 2

Calibration of the HPR-30 MS using research purity helium (> 99% purity) as the background gas to measure water content was completed in the same way using the same experimental setup as the calibration with atmospheric air. The RSF used for helium is one, and the raw ppmv data is shown in Figure 3-8 while the associated pressure and temperature of the sample gas are shown in Figure 3-9. Again, water content never exceeds 3% of the total concentration of the sample gas to satisfy the assumption made in Eq. 5 and to avoid water condensation in the experimental setup.

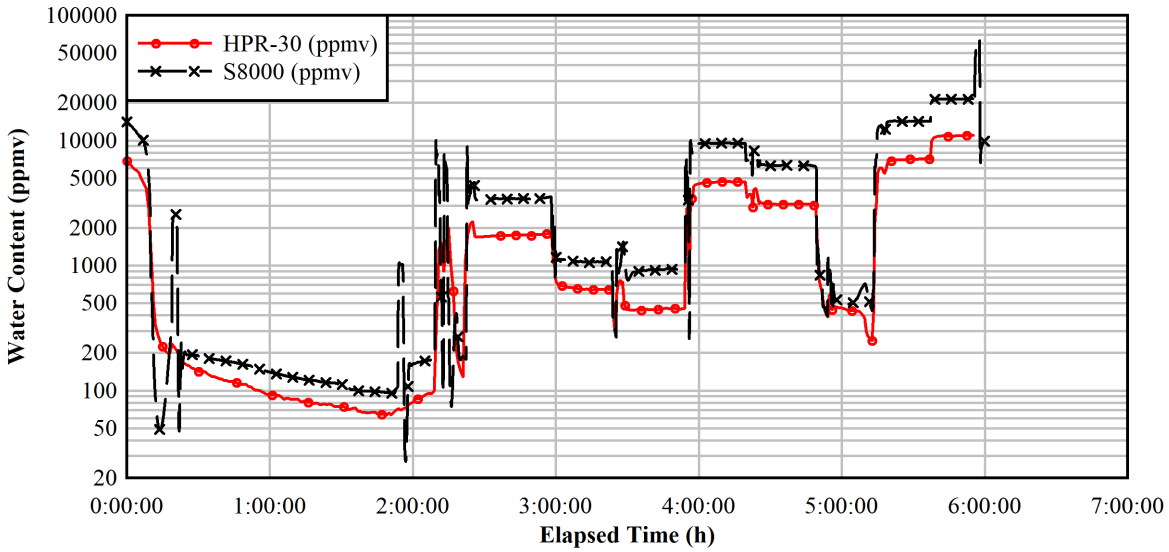

Figure 3-8 Raw HPR-30 and S8000 ppmv data with helium as the background gas. Dynamic contamination control on the S8000 causes regular spikes in the calibration data.

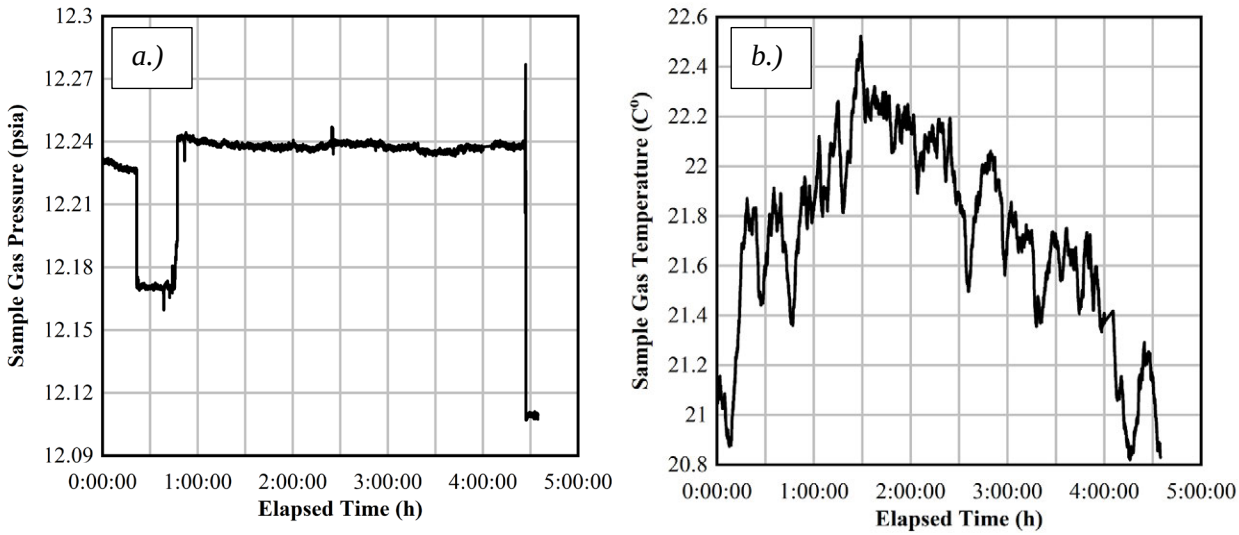

Figure 3-9 *a.)* Inlet pressure and *b.)* outlet temperature of the sample gas measured at the S8000 with helium as the background gas.

Again, it is necessary to synchronize and filter the data in time to obtain the steady state holds of the S8000 and HPR-30, as shown in Figure 3-10.

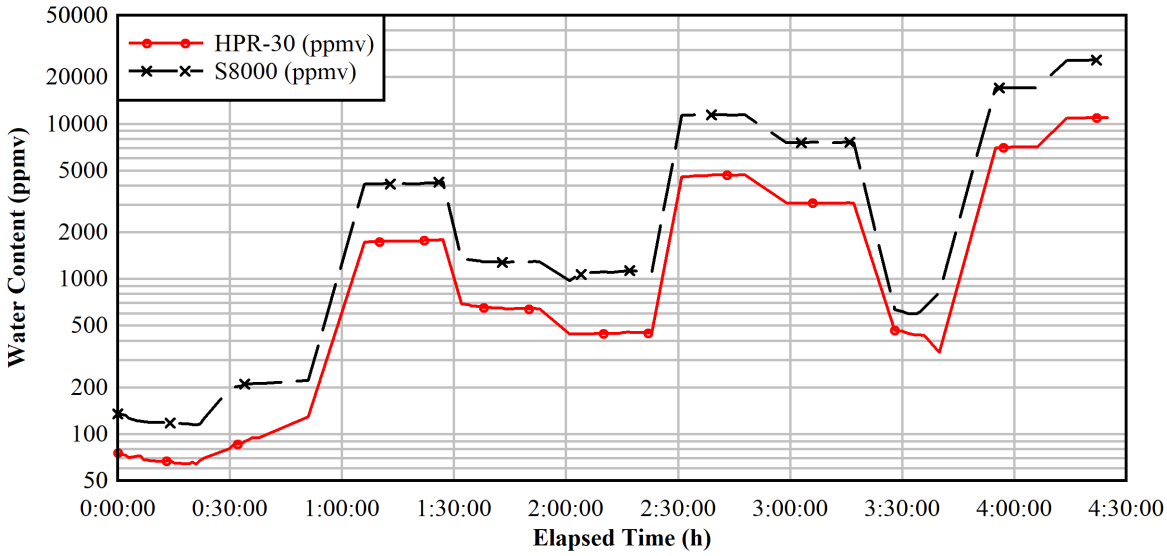

Figure 3-10 HPR-30 and S8000 ppmv data filtered and synced in time with helium as the background gas.

3.4.2.2 Helium Calibration Procedure Step 3

The RSF for water is the slope of the linear regression and the intercept is the detection limit. In this case, as shown in Figure 3-11, the RSF for water using helium as the background gas is 0.418 and the detection limit is 19.0 ppmv; the linear regression has a coefficient of determination of $R^2 = 0.999$ and an SE of 90 ppmv. This equates to a 95% confidence interval of ±178 ppmv on the regression.

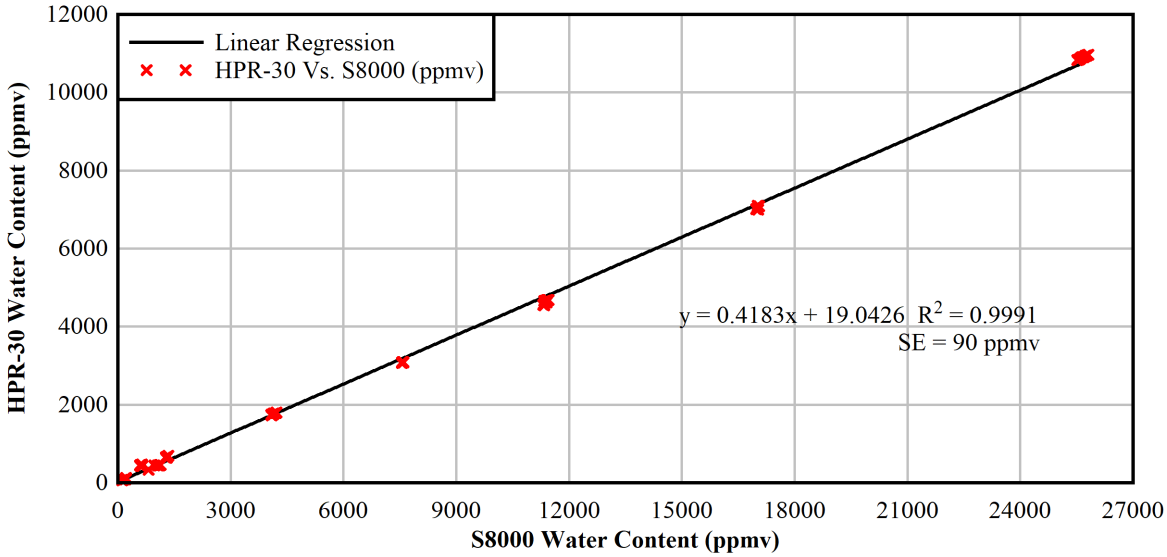

Figure 3-11 Linear regression of the ppmv of water measured by the HPR-30 as a function of the ppmv of water measured by the S8000 with helium as the background gas.

The standard deviation of the difference between the corrected HPR-30 and S8000 data is ±215.8 ppmv and ±1.5 °C DP.

3.4.2.3 Helium Calibration Procedure Step 4

Using the detection limit and RSF for water determined in step 3 of the calibration procedure, the ppmv measured by the HPR-30 can be corrected as shown in Figure 3-12.

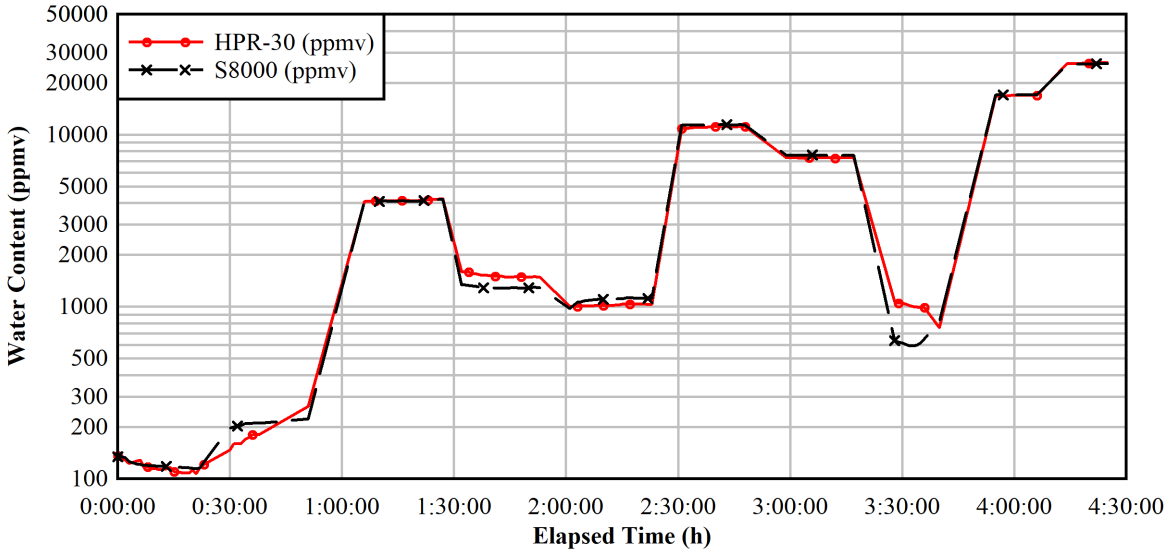

Figure 3-12 Comparison of corrected S8000 and HPR-30 ppmv data using the RSF and detection limit calculated for water with helium as the background gas.

From these results, it was demonstrated that the HPR-30 MS had successfully been calibrated to measure water content with respect to the S8000 DP sensor by determining the RSF and detection limit for water with either atmospheric air or helium as the background gases. This calibration is used in subsequent sections to compare the DP measurements in vacuum drying and FHD experiments with the measurement obtained by the MS. As stated in the previous section the ppmv values measured by the MS are converted to DPs using the relevant water calibration depending on the background gas and Eqs. 6-8.

3.5 Auxiliary Instrumentation

An Omega HX200 DP solid-state capacitance humidity sensor was used as an auxiliary instrument to monitor the dew point in the pressure vessel. (For VT #1 through 3 and FHD #11, it monitored the flow extracted from the pressure vessel.) This instrument features an enhanced calibration procedure with NIST-traceable Roscid Technologies standards that allows for the measurement of dew points down to -60 °C. The operating temperature of the sensor is 0 °C to 200 °C, with a pressure rating of 750 psi. The sensor was sensitive to bulk water and had to be installed at the top of the pressure vessel either before or after the main inlet valve for vacuum and pressure. Because its fittings were non-VCR, a vacuum sealing compound was used externally to ensure leak-tightness. While the sensor featured a display of dew point and temperature, only DP was available for milliamp output to the DAQ. However, given its position at y = -10.4 in., z = 46.4 in., an average of the temperatures at the upper and middle left standoffs would serve as a reasonable approximation.

4 TEST RESULTS

4.1 Forced Helium Dehydration

This section will describe results of the forced dehydration test with helium. As mentioned in Section 2.9, the first set of FHD tests were run with the bulk filling and gravity drainage of water, while the last test was performed with a small, fixed quantity of water in a copper ampoule with insulated standoffs. The first test had the HX200 transmitter outside of the pressure vessel, which allowed for discrete measurements when venting from the top left bellows-sealed valve (D1 in Figure 4-1). In the last test, the transmitter was inside the PV and venting was performed on the bellows-sealed valve in the lower right (D3 in Figure 4-1).

The results shown in this section otherwise have procedural commonality in terms of the hold periods, preliminary pump-and-purge, and no MS sampling until after the pump-and-purge. It is also worth noting that neither test features the HX200 directly in line with the MS sample gas stream. The results of these two tests are therefore considered a demonstration of procedural nuances.

4.1.1 Bulk Water (FHD #1)

The test was run at 150 W with water introduced via a bulk filling and drainage procedure. The PV was observed to have a 0.4° tilt to the left (nominal 90°, $+y$ direction), resulting in a bias towards flooding the neutral and thermocouple standoffs.

Water was pumped into the pressure vessel via the lower right valve (D3 in Figure 4-1) until water was observed to overflow from the valve at the middle cross (D2 in Figure 4-1) into the drainage basin, upon which pumping was ceased. This amounted to 420 g H_2O introduced into the pressure vessel, drainage basin, and filling line. The water filling line (Figure B-5) was emptied into the drainage basin, then the pressure vessel was drained via gravity from the lower valve, resulting in a total of 80 g H_2O in the drainage basin. After the pump and purge procedure with helium, an additional 278 g H_2O was driven into the drainage basin, leading to a total of 358 g of water that was removed. This left a maximum of 62 g of source water left unaccounted for in the system. The rotameter and plumbing line were liable to have retained 46 g of water, so a lower-bound estimate of retained water before the test is 16 g.

The pressure holds employed during the test are shown in Figure 4-2 along with the initial pump-and-purge, and tabulated data per hold are shown in Table C-1. Helium pressures were held in cycles from 800 kPa, 200 kPa, and 150 kPa for 15, 30, and 30-minute periods, respectively. This allowed for continuous moisture monitoring with the mass spectrometer while having positive pressure above the lower limit of the high-pressure sample line (100 kPa) to prevent tripping the solenoid, and above atmospheric pressure (84 kPa) to prevent the influx of air. The helium used for pressurizations to 800 kPa was not heated, and the lower pressure levels are achieved through controlled venting to ambient through the top left of the pressure vessel (D1 and B5 from Figure B-4).

The first hold cycle includes large temperature error margins due to unsteady temperature effects (see Figure C-1 in Section C.2.1.) Afterwards, temperature fluctuations in the heater and pressure vessel are stable. The helium in the annulus reduces the margin between the heater and pressure vessel temperature relative to the delta for an evacuated system that will be shown for vacuum drying in Section 4.2.

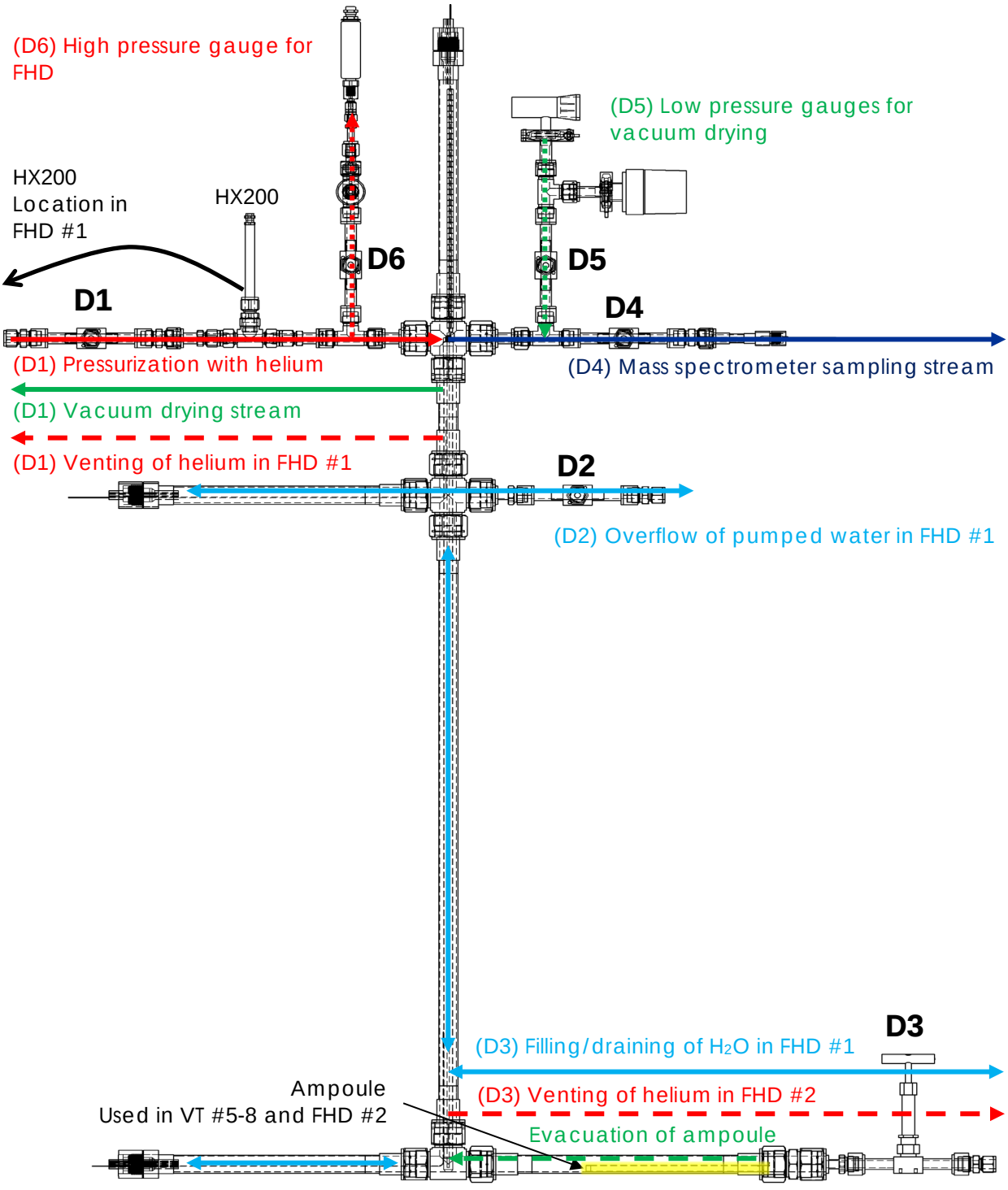

Figure 4-1 Diagram of flow paths and valves in pressure vessel for various tests.

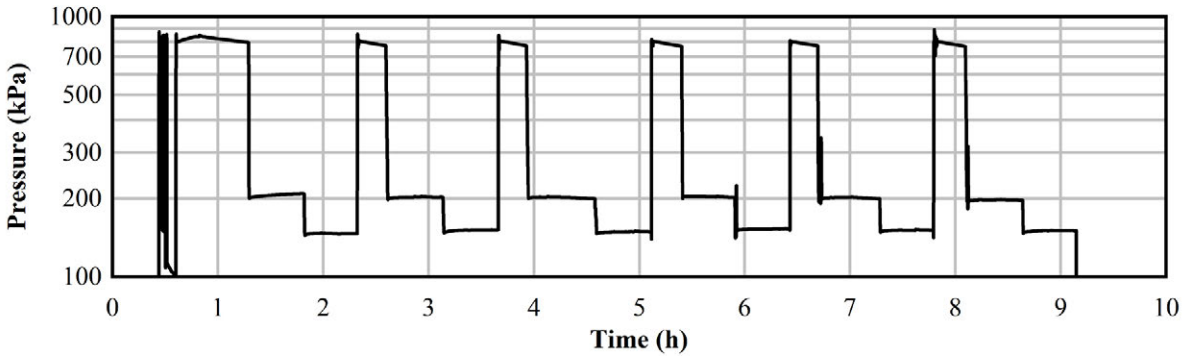

Figure 4-2 Pressure during FHD #1 at 150 W after bulk filling and drainage of water, including the initial pump-and-purge cycles.

The dew point transitions are only shown for the venting steps when they could be measured by the HX200. Figure 4-3 shows these discrete measurements along with the dew points sampled continuously from the HPR-30 mass spectrometer. The data from the two instruments are in good agreement for the relevant points in time. However, venting to lower pressures causes a transient downward dip in the dew point measurements. Since venting takes place at the top of the PV, this may indicate that the dew point is lower elsewhere in the body of the PV than at the top where the measurements are made. During the lower pressure holds, the dew point trends higher with a dip at the release between the middle and low-pressure hold. During the high-pressure hold, the dew point drops with total pressure. The pressure is dropping due to the 15 scm^3/min sample rate of the mass spectrometer at this high pressure.

The temperatures in the lower standoffs and vent appear to be coupled to the lower ambient and dew point temperatures. At times the surface temperature hits the dew point, which is a reliable indicator of condensation. The MS sample line temperature seems coupled to the upper ambient temperature and exhibits no water condensation. The differences between the two ambient temperature measurements (despite the 24 in. gap) may have been caused by exhaust from the operation of the rotary vane pump of the main turbo system and the scroll pump of the MS system, which were located on the floor of the test facility. The heating and ventilation system of the facility was also liable to have affected ambient temperatures, which is likely the case for FHD #1.

The concentration data in Figure 4-4 shows similar trends to the dew point. During the lower pressure holds, the N_2 and O_2 concentrations trend upwards with the H_2O concentration and there is a discontinuity after each pressure release. The discontinuities may be caused by a small amount of air getting introduced by the operation of the valves. The decrease in concentrations going from the low pressure to the high pressure can be explained by simple dilution (assuming good mixing in the PV). In this test, the sample to the MS appears to be well-mixed when the PV is pressurized given the reproducibility of concentrations for each hold.

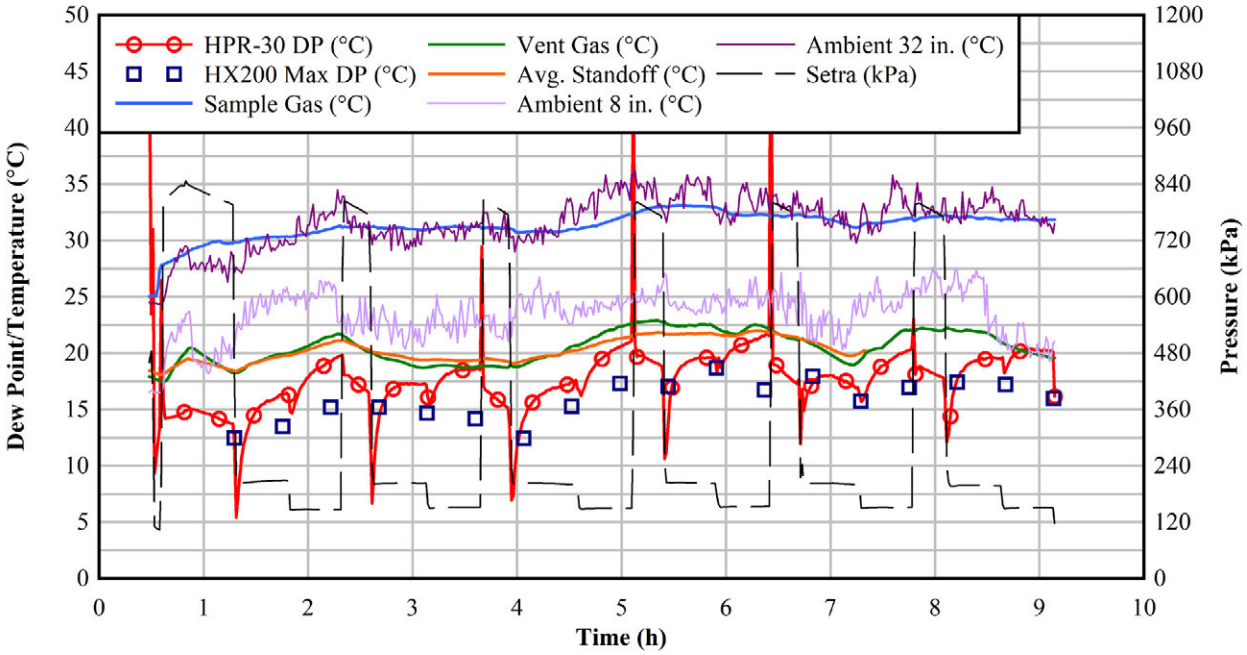

Figure 4-3 Dew point and pressure during FHD #1 at 150 W with bulk filling and draining of water. Peak dew point data from the HX200 is shown during venting of the PV.

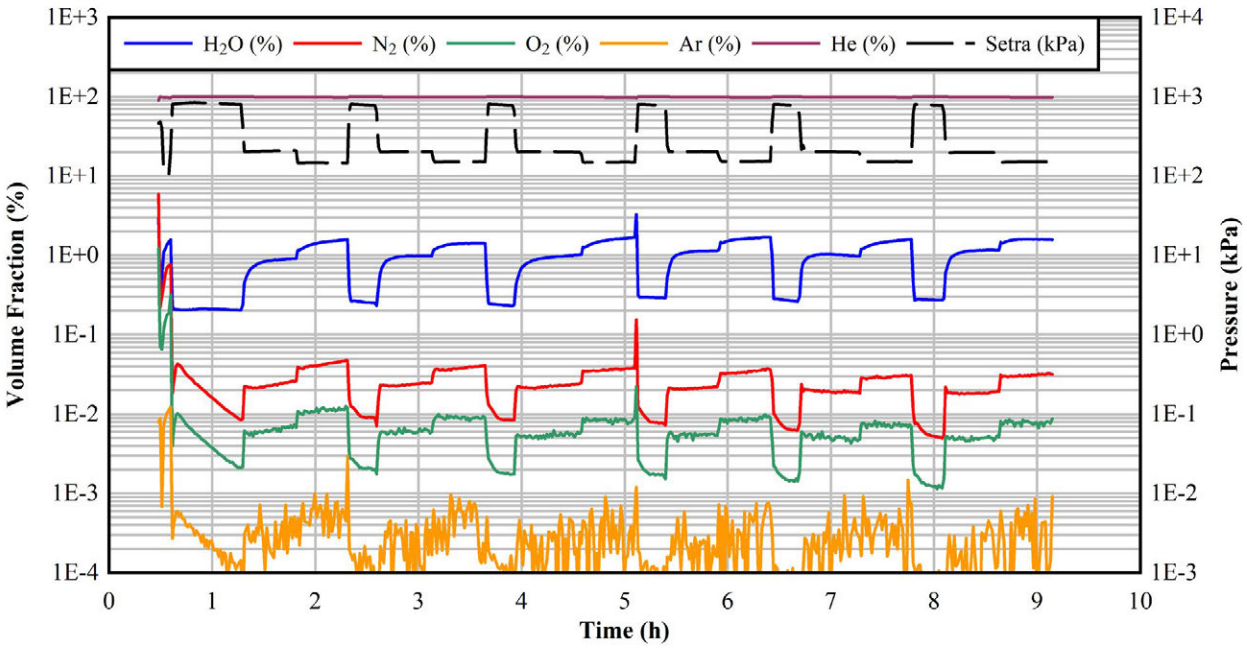

Figure 4-4 Mass spectrometer composition data from FHD #1 at 150 W with bulk filling and draining of water.

4.1.2 Ampoule (FHD #2)

The test was run at 150 W with a 10.7 g source of water contained in a copper ampoule with a 0.123 in. OD drill hole. The ampoule was installed with the drill hole near the heater in the lower standoff at nominal 270°. After installation of the ampoule and the adjoining blowdown line in the standoff, the

heater was energized, and a pump-and-purge process was employed to remove ambient air before beginning the hold procedure. The first hold cycle therefore includes unsteady temperature effects (see Figure C-2 in Section C.2.1).

Helium pressures were held in cycles from 800 kPa, 200 kPa, and 150 kPa for 15, 30, and 30-minute periods, respectively, as plotted in Figure 4-5, along with tabulated data for each holding period in Table C-2. Similar to before, the gas used for initial pressurizations to 800 kPa was not heated; however, while the lower pressure levels are achieved through controlled venting to ambient, this venting takes place through the valve at the bottom right of the pressure vessel (D3 from Figure 4-1) rather than through the valve at the top left of the pressure vessel (D1 from Figure 4-1).

There is an instance at t = 1.5 h where the 800 kPa target was overshot and had to be corrected by venting using a combination of valves D1 and B5 from Figure B-4. Because the regulator (A3) was also adjusted to correct the maximum pressure on the outlet, the cylinder-side vent (A7) was also used for some duration of time. This may have introduced a small amount of air into the otherwise helium-filled pressure vessel.

Like before in FHD #1, the high thermal conductivity of the helium results in a small temperature difference between the average heater rod measurement and the maximal pressure vessel measurements. The ampoule temperature is shown to climb with ambient but does not exceed it. This indicates poor circulation of hot gas in the lower right standoff, which runs counter to bringing water in the ampoule into the vapor phase. The maximal changes in ampoule temperature are thus a mirror of changes in ambient temperature. The minimal axial pressure vessel temperatures (most likely the TCs on the upper standoff) are close to the average temperatures measured on external surfaces of the lateral standoffs, as plotted in Figure C-2. Therefore, conductive heat transfer in the radial direction substantially outweighs natural convection in the axial direction.

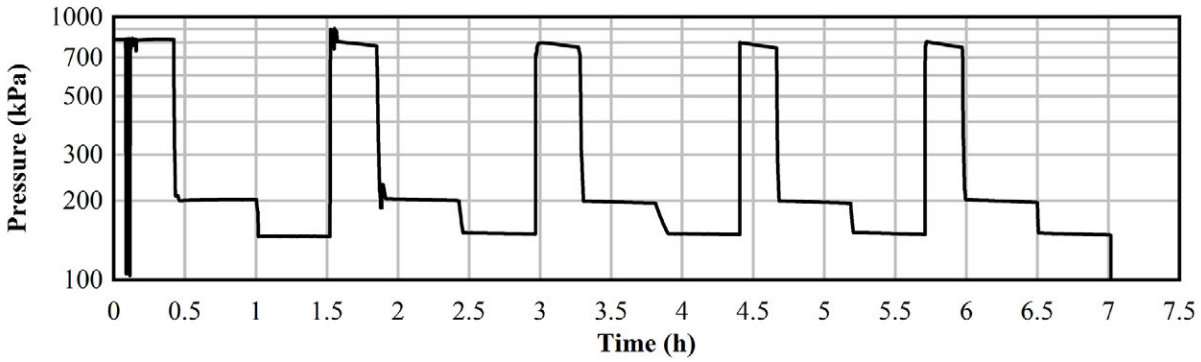

Figure 4-5 Pressure during FHD #2 at 150 W with the 0.123 in. OD ampoule including the initial pump-and-purge cycles.

The high-pressure sample line on the mass spectrometer was active for all pressures during the test, and the dew point results from the HPR-30 and the Omega HX200 are shown in Figure 4-6 continuously over time. For the first 800 kPa hold at steady temperature, the HPR-30 data shows the dew point approaching the temperature of the sample inlet and exceeding that of the ampoule and its surrounding standoff. This would indicate condensation of moisture in the system; however, the dew points registered by the HX200 on the other side of the pressure vessel are about 50 °C less. The large discrepancy may be caused by the HPR-30 data being obtained with a flow rate of moist gas while the HX200 only measures stagnant gas. Upon isolation, the HPR-30 dew point steadily decreases, while conversely, the HX200 dew point increases. This would indicate that the stagnation effect on the HX200 decreases as the volume of gas is heated and natural convection takes place, allowing for better mixing. For the HPR-30, the dew point

appears to decrease in accordance with the reduction in pressure from sampling. Because fresh, cold gas is used for further pressurizations to 800 kPa, these effects are seen throughout the test at 800 kPa.

Upon pressurization to 800 kPa, the dew point indicated by the HX200 drops 20 °C due to the flow of dry helium past the sensor. The dew point indicated by the HPR-30, on the other hand, increases 30 °C. Notably, the HPR-30 dew points are very close to the sample gas temperature, which would be indicative of condensation in the sample line; this was not observed previously in FHD #1. During the high-pressure hold, the HPR-30 dew point drops with total pressure due to the 15 scm^3/min sample rate of the mass spectrometer at this high pressure, while the HX200 dew point rises. The dew point measurements for the HPR-30 and HX200 begin to align at 200 kPa, and at 150 kPa, the dew point measurements behave more closely in unison and are nearly convergent. This may be caused by reduced effects of stagnation in the gas by the HX200 with a reduced sample flow rate to the HPR-30. From this observation, it is recommended to have a second, redundant HX200 directly before the sample inlet in future tests. Significantly, both the HPR-30 and the HX200 sensor show a similar step change in dew point temperature at the 200 to 150 kPa pressure transition.

The water content data is shown in Figure 4-7. The water concentration essentially remained constant just after compression to 800 kPa and was not decreased by dilution as was seen in FHD #1. This may indicate condensation in the MS sample leg not seen by the HX200 because of the inflow of dry helium. During the high-pressure hold, the moisture concentration drops as the MS brings in ~15 scm^3/min of sample. In the first pressurization cycle, the N_2 and O_2 concentrations jump higher, while in the next two cycles they drop lower (like in FHD #1, but not quite as drastically) and in the final cycle they jump higher again. The discontinuities are likely caused by a small amount of air getting introduced by the operation of the valves. The discontinuities were larger for the first and fourth cycle because an additional vent valve was operated.

By the end of the test, only 100 milligrams of water were actually removed from the ampoule. This is two orders or magnitude less than the original filled mass. While it is helpful to have a known water quantity in an ampoule, the minimization of wetted surface area combined with the small orifice has drawbacks in severely limiting the effect of the helium backfill compared to a fully wetted internal volume.

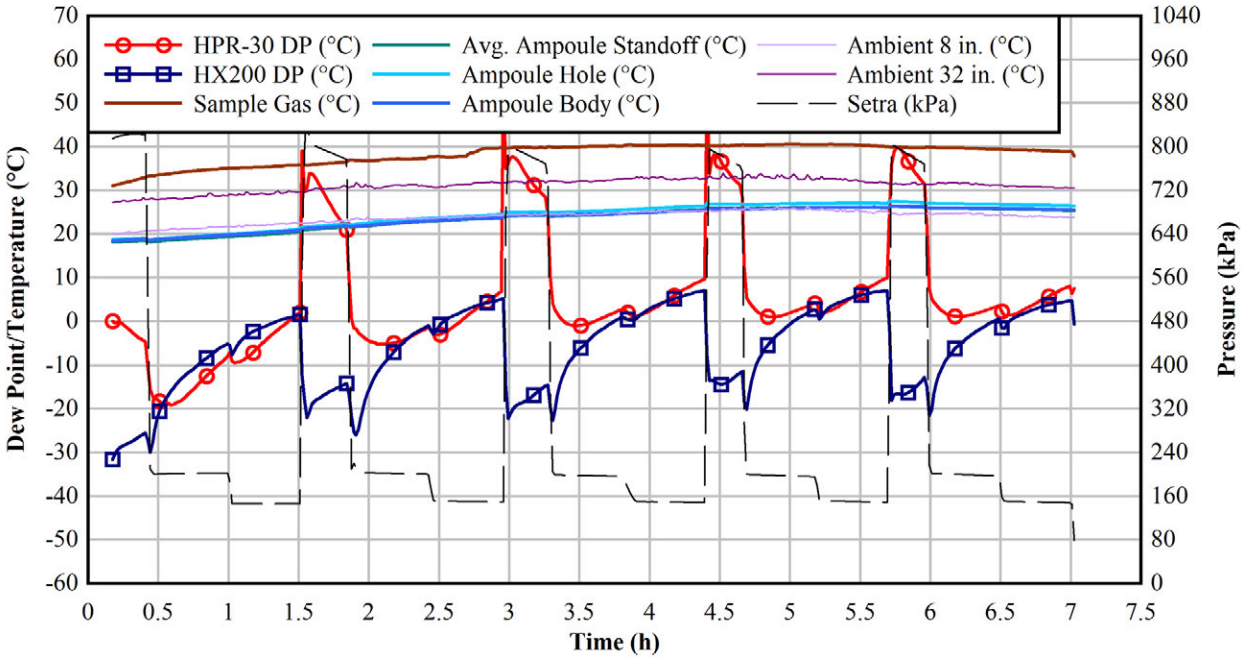

Figure 4-6 Dew point and pressure during FHD #2 at 150 W with the 0.123 in. OD ampoule.

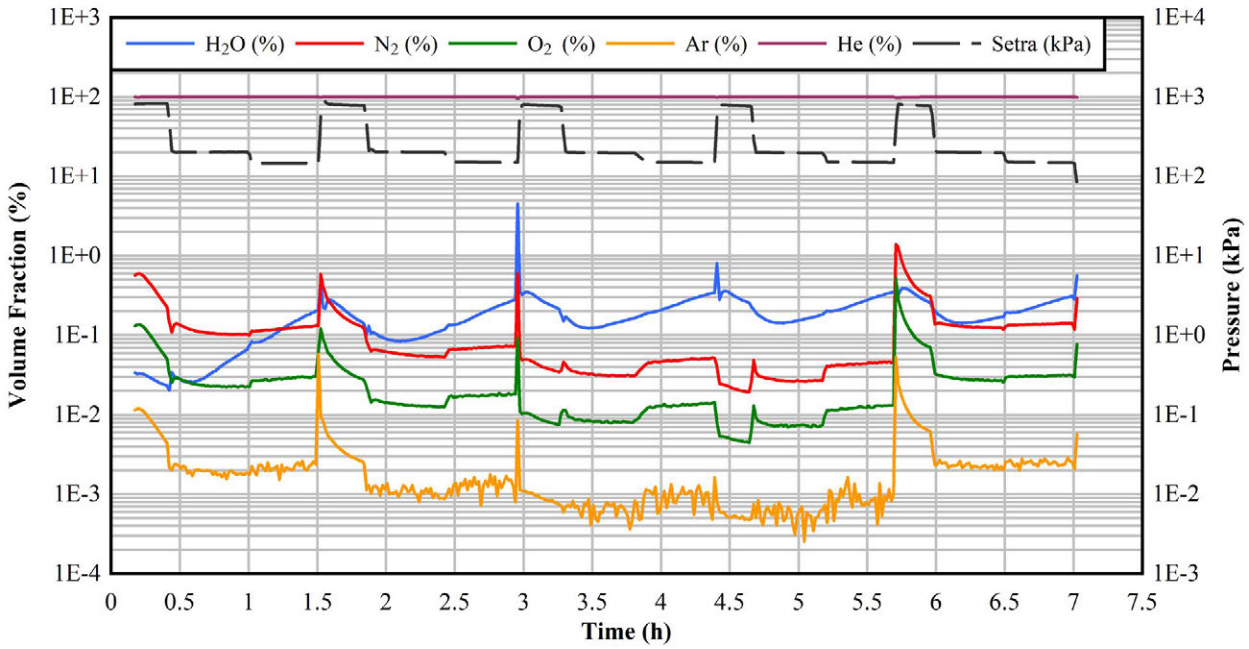

Figure 4-7 Mass spectrometer composition data from FHD #2 at 150 W with the 0.123 in. OD ampoule.

4.1.3 Temperature Profiles

The hold time average temperature profiles of the heater rod and pressure vessel from the bulk filling test (FHD #1) are shown in Figure 4-8 at the midpoint of each hold point. For forced helium dehydration, this axial variation in temperature between the top and bottom of the pressure vessel is expected to drive a convection current in the annular void space around the heater. However, the peak temperatures between the heater rod and the PV indicate strong conductive heat transfer in the annulus, which may reduce the effects of natural convection. Furthermore, given the unheated lengths of the heater rod, appreciable convection of helium was unlikely in the cold lateral standoffs where most, if not all, of the residual water in the system was located.

As discussed previously, the first hold in FHD #1 is unsteady due to the heater rod warming up; therefore, the average profile is suppressed in temperature. The time-averaged heater temperature peaks at 296 °C, while the PCT (not shown) is 303 °C, both at z = 32 in. and t = 3.4 h (150 kPa hold). The average PV temperature is maximal at 232 °C, with a maximum recorded PV temperature of 235 °C, both of which occur at z = 16 in. and t = 3.8 h (800 kPa hold). The time lag between the two peaks is due to the thermal diffusivity of the helium in the annulus. The difference in axial level is likely due to differences in conductive heat transfer to the non-insulated pipe fittings.

The profiles for the test with the ampoule (FHD #2) are shown in Figure 4-9 per given hold point. The average heater temperature peaks at 302 °C at z = 24 in. and t = 1.3 h (150 kPa hold). The PCT (not shown) is only slightly higher at 304 °C and occurs later at z = 24 in. and t = 2.7 h (150 kPa hold). The average PV temperature peaks at 251 °C at z =16 in. and t = 1.7 h (800 kPa hold). The maximum recorded PV temperature is only slightly higher at 252 °C, which occurs later at z = 24 in. and t = 2.7 h. These temperature statistics indicate that in this test, the heater and PV are in better thermal equilibrium. The PV temperatures are higher than those in FHD #1 due to the use of insulation on the standoffs, which reduces their fin effects.

Compared to FHD #1, the profiles in FHD #2 are spaced more closely together at long times. This may be an effect of minimal water entry from the ampoule into the void space, which leads to consistent heat

transfer in the annulus and steadier profiles. The bulk filling test had water more thoroughly dispersed throughout the PV cavity, which is liable to have caused variation in the annulus water content as liquid water was removed from cavities and vaporized. This likely resulted in more diffused temperature profiles from effects on the thermal conductivity of the annulus. However, given the ambient temperature fluctuations in FHD #1 (likely due to climate control in the test facility) these findings are not conclusive.

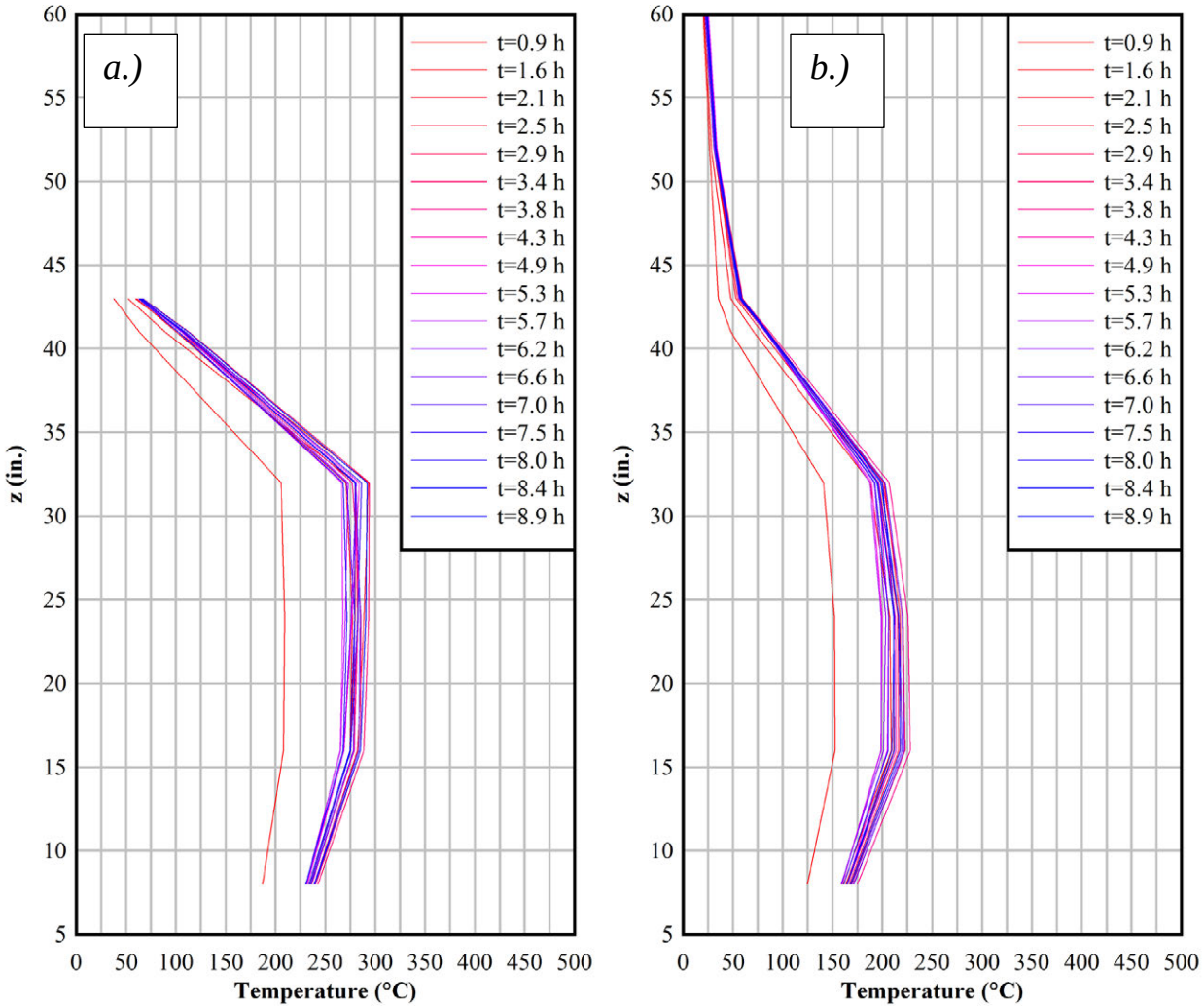

Figure 4-8 Average temperature profiles for the *a.)* heater and *b.)* pressure vessel for holds during FHD #1 at 150 W with bulk filling/drainage of water. The reported times indicate the midpoint of the hold.

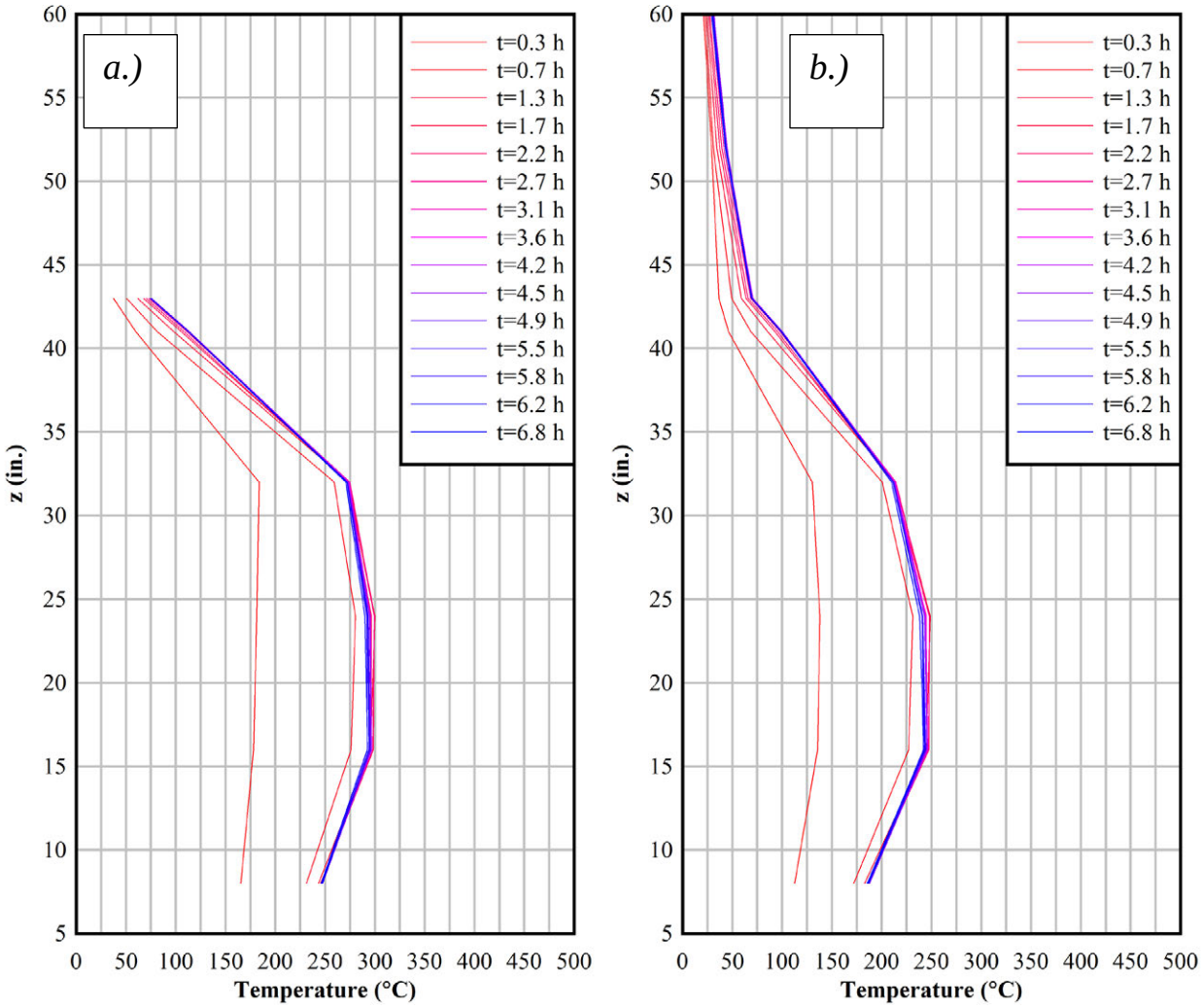

Figure 4-9 Average temperature profiles of the *a.)* heater and *b.)* pressure vessel for holds during FHD #2 at 150 W with the 0.123 in. hole ampoule. Reported times indicate midpoint of the hold.

4.2 Vacuum Drying

The vacuum drying tests were parameterized based on the mass of water in the ampoule, the diameter of the orifice on the ampoule (0.021 in. and 0.123 in.), and the power level imparted to the heater (0 or 150 W). The water content results from the mass spectrometer are presented using the Hiden Analytical relative sensitivity factors (RSFs) for helium. The partial pressures of air (nitrogen, oxygen, and argon gas), water, and helium are corrected using these RSFs and included in the post-processed data set. This processed dataset is then synchronized with the normal DAQ data obtained separately in parallel.

The turbo/rotary vane pump system was nominally rated to 1 mtorr and reached a minimum pressure of 16 mtorr in post-test measurements. However, for the test results presented in this report, the minimum pressure observed was around 45 mtorr. As will be shown later, water in the pressure vessel prevented this minimum pressure from being attained upon reaching certain hold points, as the rate of evaporation counteracted suction capacity.

4.2.1 Dry Tests

Preliminary vacuum hold tests were conducted to determine the pressure rebound under unheated, dry conditions. These measurements essentially serve as background leakage rates that serve as the primary control group for comparison to tests that are wetted and heated. A similar test was then conducted with the heater energized.

4.2.1.1 Unheated Dry Test (VT #3)

The unheated baseline pressure rebound results are shown in Table 4-1 in terms of the initial pressure upon isolation (P_0) and the change in pressure during the hold (ΔP), along with average ambient (T_A) and pressure vessel (T_{PV}) temperatures. The 100 torr measurements for the InstruTech are not shown because the instrument became saturated. Due to time constraints, the measurement period was shortened to ten minutes. While it is clear that the readings from the two vacuum gauges are shifted (due to different means of calibration to atmospheric pressure), the changes in pressure upon isolation are considered to be comparable values. Therefore, average rebounds are presented that are linearly extrapolated to a 30-minute period. The pressure error is propagated from random error and instrument error from either gauge reading during the hold, and it is then adjusted by a constant for the extrapolated period.

Measurements between the two gauges appear to reach a point of alignment at 50 torr. Rebounds are generally shown to decrease with the exception of the 10 and 25 torr measurements on the InstruTech gauge, which showed larger increases in pressure upon isolation. The lowest pressure achieved by the turbo pump in this dry test was 410 mtorr, although lower pressures were attainable in the post-test period after cumulative leak tightness measures had been instituted (e.g. applying vacuum sealing compound on joints, new ferrules and gaskets). Measurements were therefore repeated at 250 and 500 mtorr. Because these measurements took place at higher ambient temperature, the 30-minute rebounds are higher. Nonetheless, they provide a reasonable metric for comparison to the wetted tests, as the final pressures of the ultimate holds do not exceed 3 torr and allow the criterion to be investigated during the wet test.

Table 4-1 Pressure changes upon isolation for hold points in VT #1 (dry, unheated).

Hold (torr)	Period (min)	Pfeiffer (torr)		Instrutech (torr)		30 min ΔP (torr)	T_A (°C)	T_{PV} (°C)
		P_0	ΔP	P_0	ΔP			
100	11.36	99.94	22.92	-	-	-	17.6	19.9
75	11.04	74.51	1.22	74.43	1.63	3.87±4.34	18.1	19.7
50	9.36	49.56	0.12	49.38	0.18	0.48±3.36	18.3	19.5
25	9.38	24.86	0.06	33.90	0.22	0.44±20.62	18.2	19.3
10	9.50	9.95	0.06	13.93	0.55	0.95±9.42	18.3	19.1
5	9.30	4.97	0.03	7.19	0.09	0.19±5.10	17.9	18.9
3	9.26	2.98	0.03	4.28	0.04	0.11±2.98	17.6	18.7
1	8.96	1.00	0.02	1.35	0.04	0.11±0.84	17.5	18.5
Full	10.00	0.41	0.003	0.52	0.01	0.01±0.24	17.0	18.2
0.5†	29.62	0.49	0.25	0.67	0.32	0.29±0.16	24.9	29.6
0.25†	28.95	0.24	0.17	0.34	0.23	0.21±0.09	24.6	29.2
† Baseline measurements repeated in warmer weather after original tests.								

4.2.1.2 Heated Dry Test (VT #4)

The baseline pressure rebound results with the heater energized to 150 W are shown in Table 4-2 along with the average heater rod temperature (T_H). The 100 torr rebound data was considered spurious due to leak-sealing effects from reconstruction and it is excluded from the table. The 250 millitorr hold point was not measured in this test but rebound from a minimum pressure of 70 millitorr was assessed. The baseline data indicate a reduction of pressure rebounds with increasingly low hold points. The final hold

at 0.5 torr does not exceed 3 torr, allowing for the NUREG-1536 criterion to be reasonably assessed in the heated tests with water (NRC, 2010).

Table 4-2 Pressure changes upon isolation for hold points in VT #4 (dry test at 150 W). The data at 100 torr was considered anomalous and is excluded from the table.

Hold (torr)	Period (min)	Pfeiffer (torr)		Instrutech (torr)		30 min ΔP (torr)	T_A (°C)	T_{PV} (°C)	T_H (°C)
		P_0	ΔP	P_0	ΔP				
75	29.96	72.69	0.32	83.33	4.84	2.58±9.13	24.9	129.5	324.9
50	30.42	48.64	3.15	58.90	4.28	3.66±7.55	25.2	129.6	324.0
25	30.64	24.33	2.66	36.23	3.15	2.84±8.41	25.5	131.4	324.7
10	31.92	9.71	1.55	14.38	1.99	1.67±3.25	26.0	132.3	325.5
5	30.15	4.86	1.06	7.31	1.33	1.19±1.82	26.5	133.0	325.6
3	30.00	2.92	0.89	4.30	1.08	0.98±1.04	27.7	133.4	325.3
1	30.48	0.97	0.64	1.35	0.92	0.77±0.36	28.6	133.7	329.8
0.5	30.06	0.49	0.67	0.65	0.94	0.80±0.21	28.6	133.7	331.9
Full	20.00	0.07	0.36	0.09	0.50	0.43±0.05	28.8	124.9	365.1

4.2.2 Unheated Tests at Ambient Temperature

The wet vacuum drying tests were conducted with water-filled ampoules, as evacuation after a bulk filling and draining of water was thought to negatively impact the turbo pump. Two ampoules were used with drill holes of either 0.021 in. OD or 0.123 in. OD. A scale was used to monitor water mass after the initial filling and after the drying procedure. These tests constituted the secondary control group with the heater deenergized (zero watts) and PV at ambient temperature to isolate the effects of pressure without heat.

4.2.2.1 Ampoule with 0.021 in. OD Hole, Unheated (VT #5)

The pressure holds during the unheated vacuum drying test with the 0.021 in. OD ampoule are shown in Figure 4-10 on a log-linear scale. The Pfeiffer gauge controller was used to determine the hold points and the InstruTech data is considered supplementary to this primary dataset, although this does not imply the veracity of one over the other. The plot shows how measurements from the two instruments differ per given pressure range, although overall, both appear to act in unison during pressure rebounds. Either instrument indicates that the magnitude of the pressure rebound decreases over time (see Table C-3).

The 10 torr target hold at 2.3 hours exhibits a transient rise in pressure to 11.6 torr (16.2 torr on the InstruTech) followed by a steady approach to a lower pressure of 8.6 torr (12.2 torr on the InstruTech). From Figure 2-11, the boiling point of water at 10 torr is 11.13 °C, while the triple point of water lies at 0 °C and 4.59 torr. The minimum ampoule temperature measured during this hold was 14.9 °C while the average temperature was 15.7 °C, so the liquid-vapor phase-transition would therefore occur at 12.8 torr (13.5 torr on the InstruTech). Therefore, it is clear that phase change activity is taking place during the rebound of this hold, as results indicate an initial vaporization of water followed by extensive condensation. This is corroborated by the substantial rise in dew point observed in Figure 4-11. For reference, Figure C-7 shows an overlay of pressure and temperature data on the water phase diagram, where vapor phase transition around 10 torr is readily apparent.

The 10 torr target hold marks the approach of maximal dew points during the pressure rebound due to substantial vaporization of water. Beginning with the 5 torr hold, the temperature of the ampoule significantly decreases upon evacuation and then increases when the PV is isolated. Upon approaching the first 3 torr target hold, increases in evaporative heat transfer cause the minimum ampoule temperature to markedly decrease. The 3 torr evacuation steps exhibit staggered, sawtooth-like spurts in pressure likely due to a streaming effect of water through such a small orifice, although these are not visible in Figure 4-10. Some 3 torr holds have to be truncated due to strong rebound.

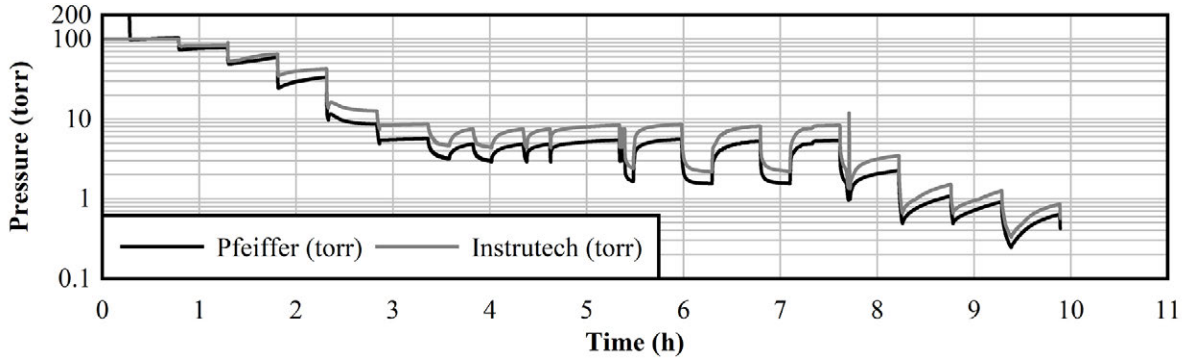

Figure 4-10 Pressure rebounds during VT #5 (unheated, 0.021 in. OD ampoule).

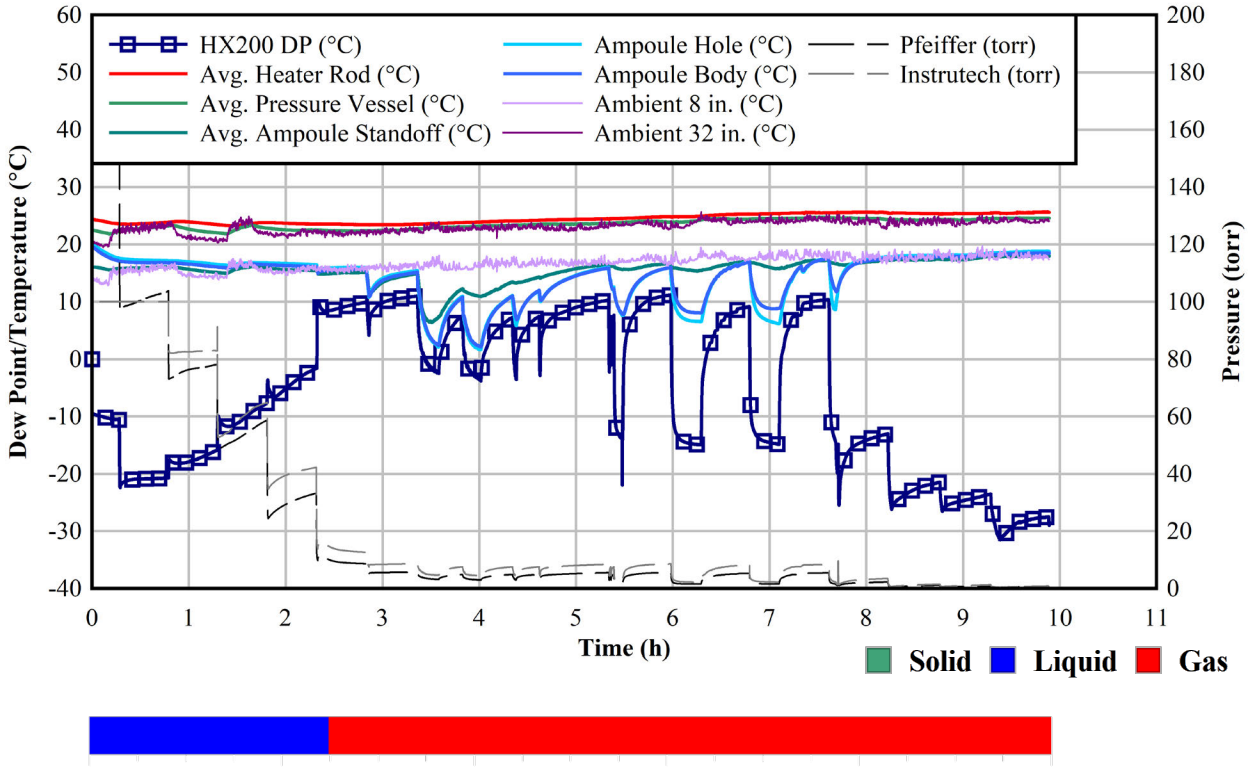

Figure 4-11 Dew point and ampoule temperatures during VT #5 (unheated, 0.021 in. OD ampoule). Indicator shows when water may enter gas phase based on minimum ampoule temperatures.

When evacuating to 1 torr, the turbo pump is unable to reach its full capacity as suction and evaporation counteract each other. On the third attempt to hold at 1 torr, the changes in both ampoule temperature and dew point upon isolation are strongest. Only on the fourth attempt is the rebound threshold satisfied, maximum dew point finally begins to decrease, and the ampoule temperature is brought back closer to ambient. The dew point behavior for subsequent holds at 0.5 and 0.25 torr appears to indicate that water has been substantially evacuated.

The mass spectrometer data collected for the last four holds is shown in Figure 4-12 along with the HX200 dew point data shown previously. The two dew point measurements align well, although

eventually, the discrepancies increase due to water becoming the background gas. The dew point rises to a steady level during the pressure rebound, but the maximum steady DP decreases per hold.

Figure 4-13 shows composition data from the mass spectrometer. Over time, the proportion of water in the PV sample decreases relative to the components of air. Despite the high water content of 50 vol% in the MS sample, given that the corresponding pressure is so low, the data still confirm that most of the water has been removed from the PV. It should be noted that no vacuum drying test in this report was able to reduce water content below the 0.25 vol% criterion from Knoll & Gilbert, 1987. However, given the 1.0 L internal pressure vessel volume and ≤ 0.5 torr pressures in this test series, the scaled quantity of water is substantially lower. For example, if additional dry air were added to the PV sample at the end of VT #7 to reach the 7 m^3 canister gas volume and 0.15 MPa pressure in the cited study, the total water content would lie at $2*10^{-7}$ vol% (assuming ideal gas behavior).

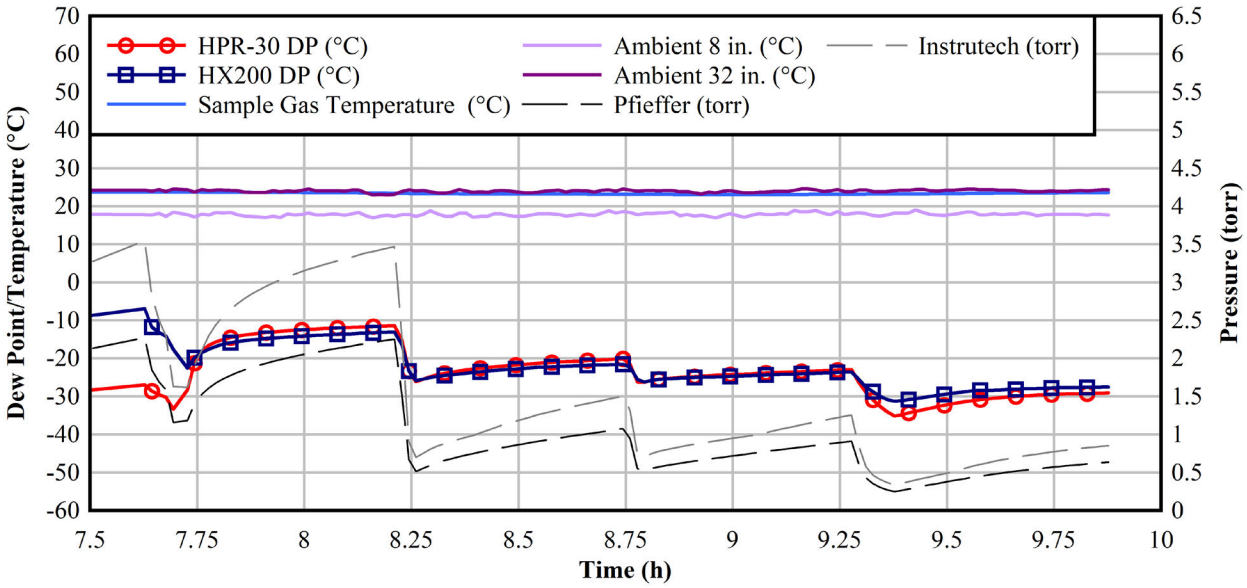

Figure 4-12 Mass spectrometer dew point data during VT #5 (unheated, 0.021 in. hole ampoule).

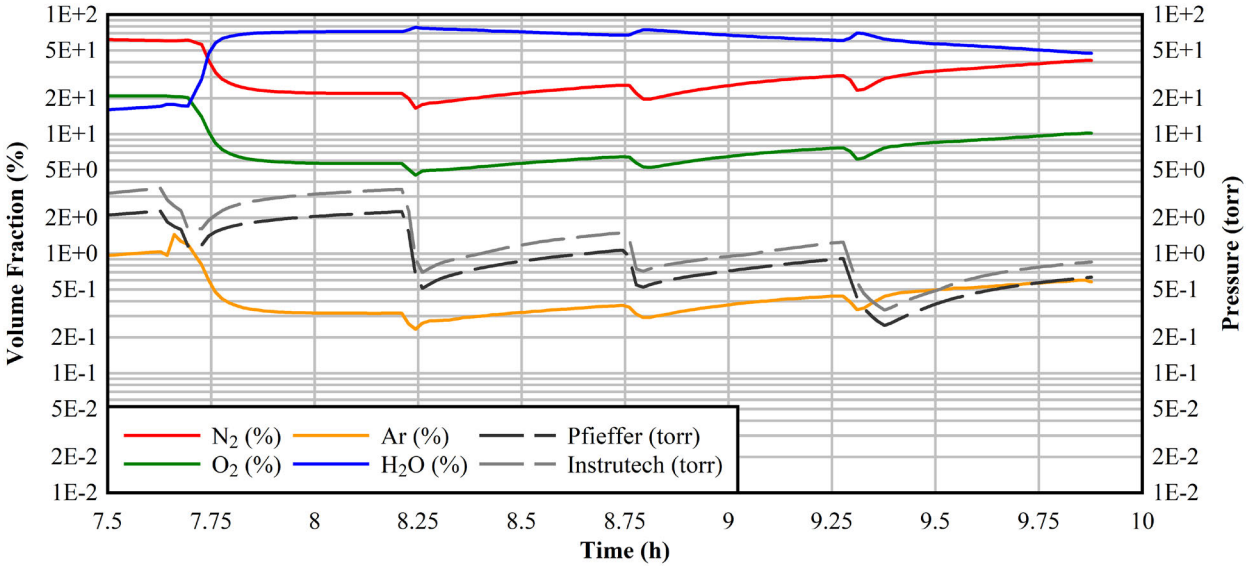

Figure 4-13 Mass spectrometer composition data from VT #5 (unheated, 0.021 in. OD ampoule).

4.2.2.2 Ampoule with 0.123 in. OD Hole, Unheated (VT #6)

The pressure holds during the unheated vacuum drying test with the 0.123 in. OD ampoule are shown in Figure 4-14 while tabulated data is shown in Table C-4. Pressure rebounds result in multiple attempts to hold at 3 torr to remain below the threshold pressure. Nonetheless, the rebounds eventually decrease over time and do not exceed the 3 torr criterion in the final hold. The dew point data is plotted in Figure 4-15, along with additional MS data points for a subset of pressures in Figure 4-16. The strongest rises in dew point are observed in the final two holds at 3 torr. This is also the target hold during which the ampoule temperatures drop slightly below 0 °C (which still corresponds to vapor phase). The final hold at this level marks the point where the ampoule temperature begins to increase towards ambient and maximum dew points decrease. The composition data in Figure 4-17 confirm that water content is reduced by the end of the drying operation.

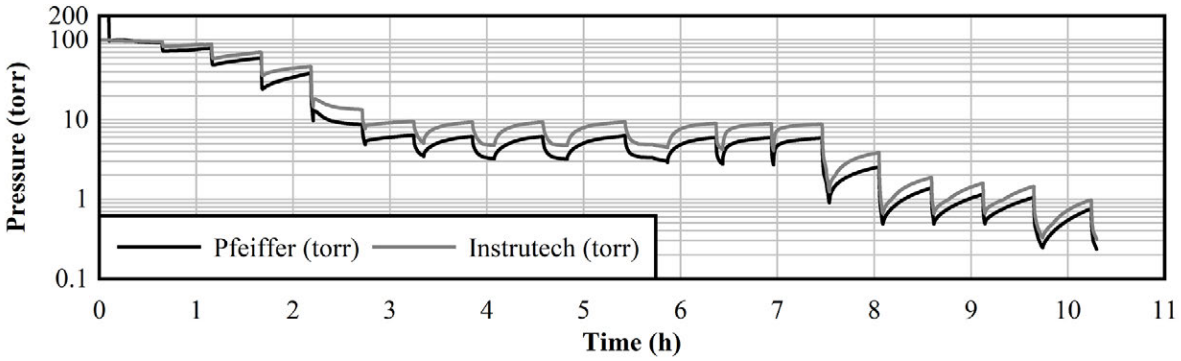

Figure 4-14 Pressure rebounds during the VT #6 (unheated, 0.123 in. hole ampoule).

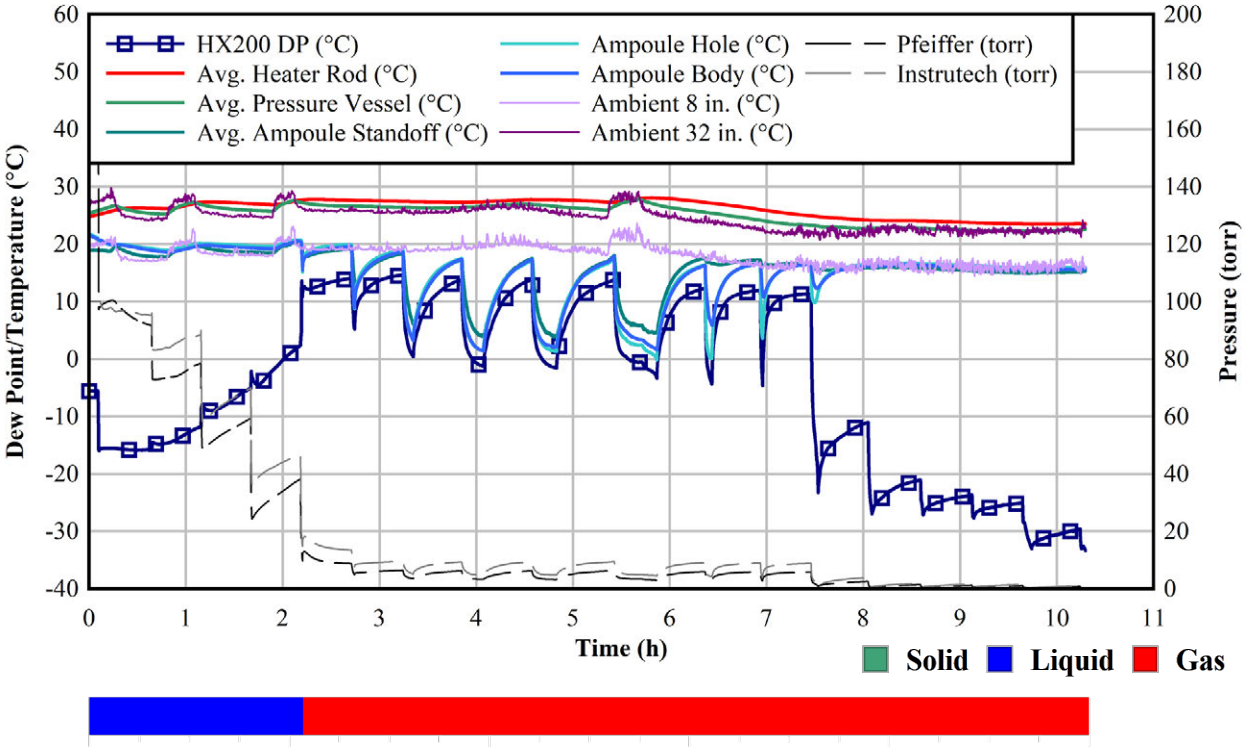

Figure 4-15 Dew point and ampoule temperatures during VT #6 (unheated, 0.123 in. OD ampoule). Indicator shows when water may enter gas phase based on minimum ampoule temperatures.

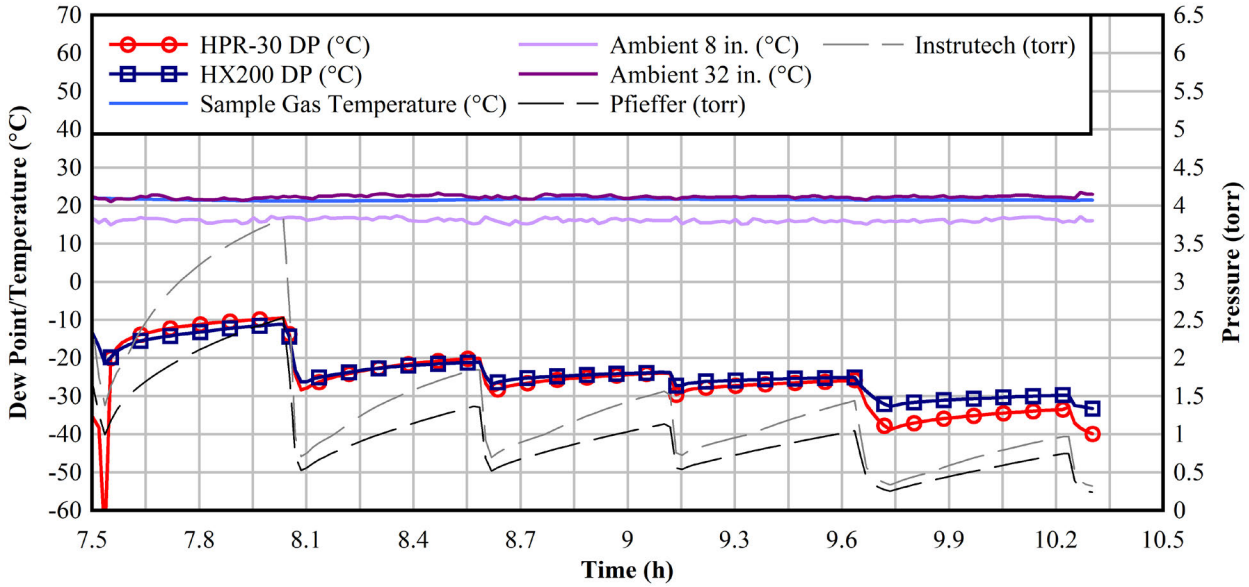

Figure 4-16 Mass spectrometer dew point data during VT #6 (unheated, 0.123 in. OD ampoule).

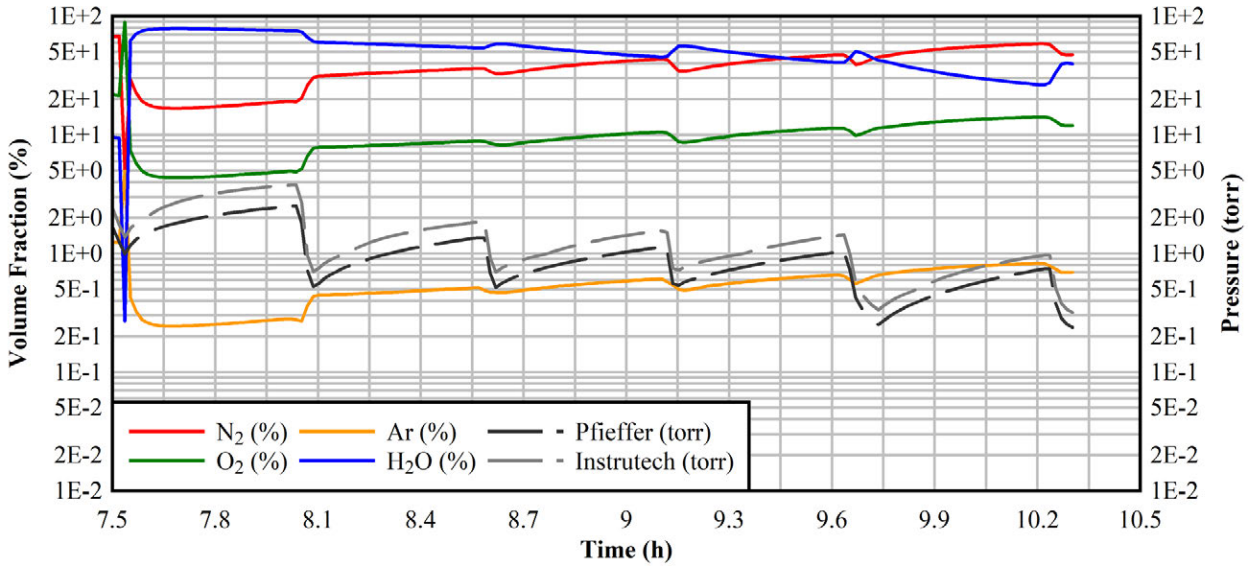

Figure 4-17 Mass spectrometer composition data from VT #6 (unheated, 0.123 in. OD ampoule).

4.2.3 Heated Tests

The vacuum drying test was conducted with the heater energized to 150 W as a demonstration of heated annulus effects on both water removal overall and water content measurement. In these tests, the ampoule was installed prior to energization and the hold procedure did not commence until the heater temperatures had reasonably steadied (see Section C.2.2 for transient temperature plots). Since the dew point and water content are measured at the top of the pressure vessel while the water source in on the bottom, the heated test will demonstrate the effects of axial convection in the void space relative to the unheated test, where such an effect is minimized. Axial temperature plots of the heater rod and pressure vessel are provided in Section C.2.3. Ideally, the temperature of water in the ampoule should also be affected, but the cold pin lengths of the heater rod may prove to be a limiting factor in effective heat transfer to the standoffs.

Furthermore, since no pressure vessel components were insulated for vacuum drying, heat transfer to the standoffs may have been impeded through fin effects.

4.2.3.1 Ampoule with 0.021 in. OD Hole, Heated (VT #7)

The pressure holds during the heated vacuum drying test with the 0.021 in. OD ampoule are shown in Figure 4-18 on a log-linear scale, with associated hold point data in Table C-5. In this test, rebounds in pressure occurred very suddenly when isolating at 3 torr, but suction capacity was not hindered when evacuating to this pressure. This suggests that while the rate of evaporation did not overwhelm the vacuum flow rate during evacuation, it was substantial enough to affect the pressure during isolation. Therefore, this hold point was skipped in favor of holding at 1 torr instead. This target hold pressure demonstrated reduced suction from the vacuum as water from the ampoule vaporized. Rebounds were still very strong after isolation, causing this hold to be repeated eight times. The final hold at 0.25 torr exhibits behavior on par with that observed for the unheated test.

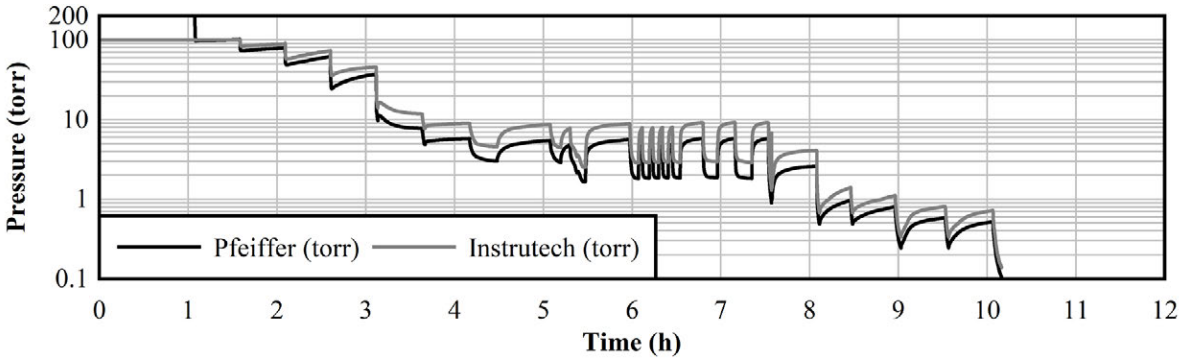

Figure 4-18 Pressure rebounds during VT #7 (150 W, 0.021 in. OD ampoule).

The dew point data is plotted in Figure 4-19, along with additional MS data points for a subset of pressures in Figure 4-20. The maximum dew points are larger compared to those of the unheated test. The ampoule temperature appears to respond in concert with the pressure rebounds, indicating that phase changes are indeed taking place at a rapid pace.

By the final hold at 1 torr, the maximum dew point begins to be suppressed, and the ampoule exhibits its final significant change in temperature before falling in line with ambient temperature. The HPR-30 composition data is shown Figure 4-21, which confirms that water content has been reduced by the end of the procedure.

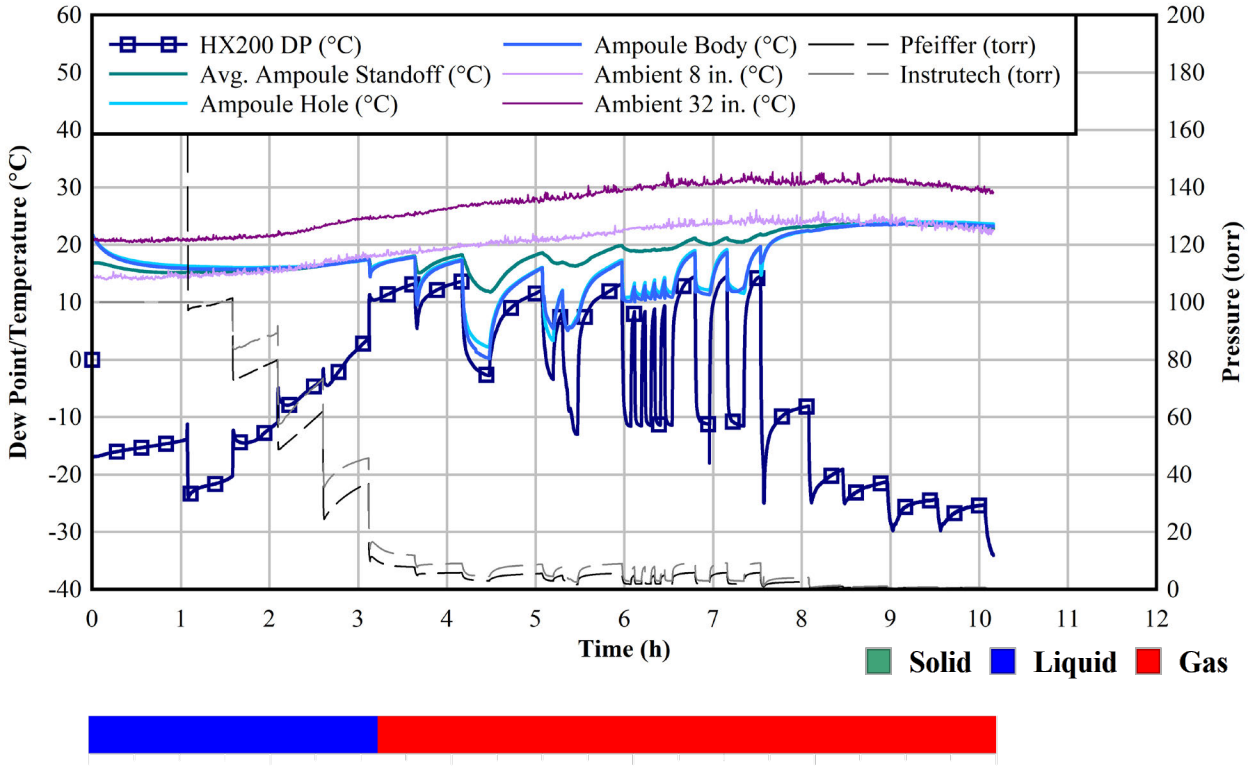

Figure 4-19 Dew point and ampoule temperatures during VT #7 (150 W, 0.021 in. OD ampoule). Indicator shows when water may enter the gas phase based on minimum ampoule temperatures.

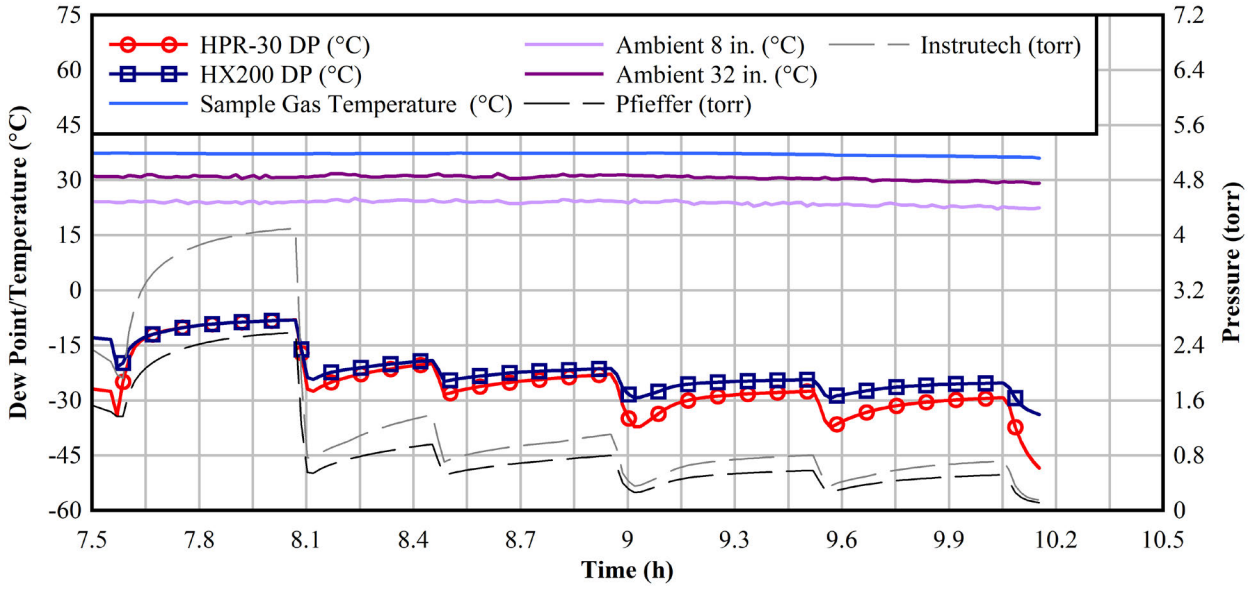

Figure 4-20 Mass spectrometer dew point data during VT #7 (150 W, 0.021 in. OD ampoule).

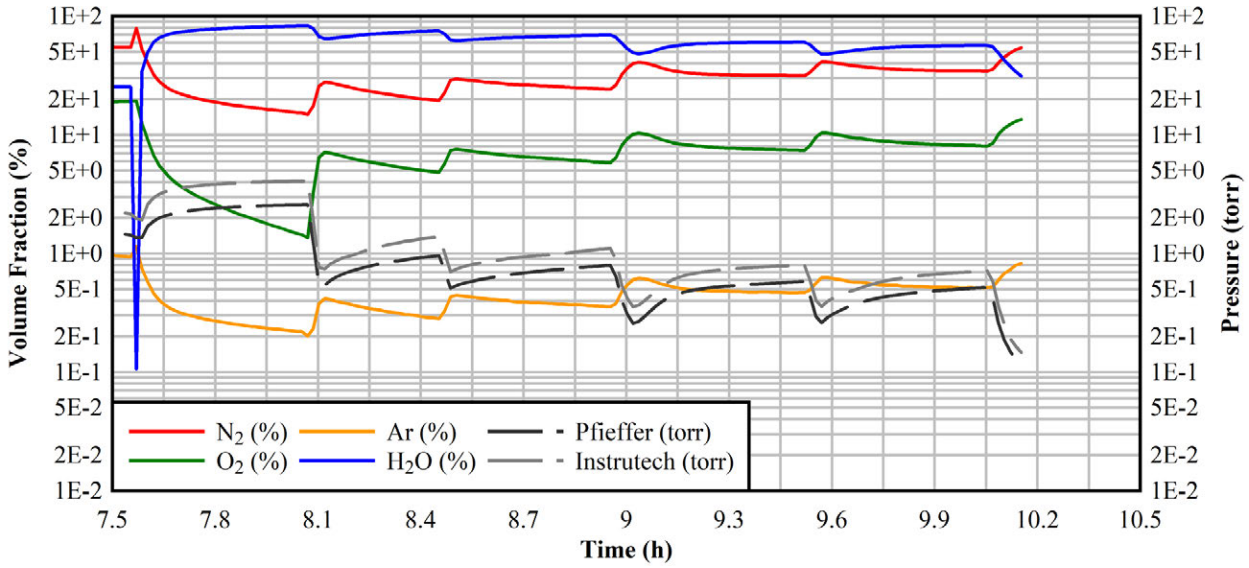

Figure 4-21 Mass spectrometer composition data from VT #7 (150 W, 0.021 in. OD ampoule).

4.2.3.2 Ampoule with 0.123 in. OD Hole, Heated (VT #8)

The pressure holds during the heated vacuum drying test with the 0.123 in. OD ampoule are shown in Figure 4-22 on a log-linear scale, with associated hold point data in Table C-6. The rebound data for the final hold at 0.5 torr is only slightly higher than that for the unheated test. The test was stopped at this hold due to time constraints since the 3 torr rebound criterion was already attained. Altogether, the pressure rebounds for the 0.123 in. OD ampoule (both heated and unheated) appear to be less drastic than their counterparts with the 0.021 in. OD ampoule. This suggests that the smaller orifice introduces a bottleneck effect during the phase change, such that after isolation from the vacuum flow rate, the rate of vaporization is able to substantially affect the pressure. Furthermore, the pressure rebound in heated tests appears to be elevated relative to the test at ambient, indicating that more vaporization is occurring upon isolation from condensed water.

The dew point data is plotted in Figure 4-23 along with additional MS data for a subset of pressures in Figure 4-24. The dew point magnitudes were not as high as those from the unheated test, indicating a minimal role of the heater rod. This may be due to the distance between the ampoule and the heater and the cold pin lengths. After the 3 torr holds, the dew points begin to be suppressed. However, the ampoule temperature change does not decrease until after the first 1 torr hold.

In this test, the ampoule was brought below 0 °C four times during the 3 torr holds. Figure 4-25 shows the minimum ampoule temperature (i.e. the minimum between TCs #15 and #16) color-coded with the phase deduced from the InstruTech gauge. The InstruTech is chosen as a conservative measure since it overestimated pressures compared to the Pfeiffer. Solid phase deposition is shown for the first three reductions to sub-zero temperatures. In a commercial operation, such ice formation would result in residual water being retained in the canister without continued drying operations. Within the 1 second sampling period of the DAQ, the first deposition around 7.25 h is extensive enough to allow for intermediate melting before reentering the vapor phase. The next two solidification events are very brief and appear to proceed directly to the vapor phase via sublimation. The last drop below 0 °C does not involve a phase change, and the water remains vaporized. The data confirms that solid deposition does occur during the 3 torr evacuation. This was not observed in the unheated test simply because the vacuum operators isolated the PV when reaching 0 °C due to time constraints.

The dew point begins to be suppressed after the 3 torr holds. Pressure rebound and ampoule temperature data indicate significant water removal by the end of the first 1 torr hold. Composition data from the mass spectrometer confirms a reduction in water content, as shown in Figure 4-26.

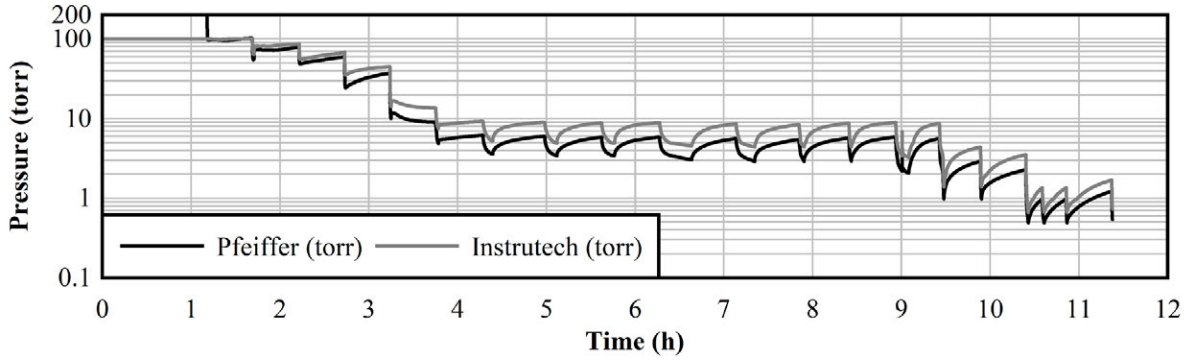

Figure 4-22 Pressure rebounds during VT #8 (150 W, 0.123 in. OD ampoule).

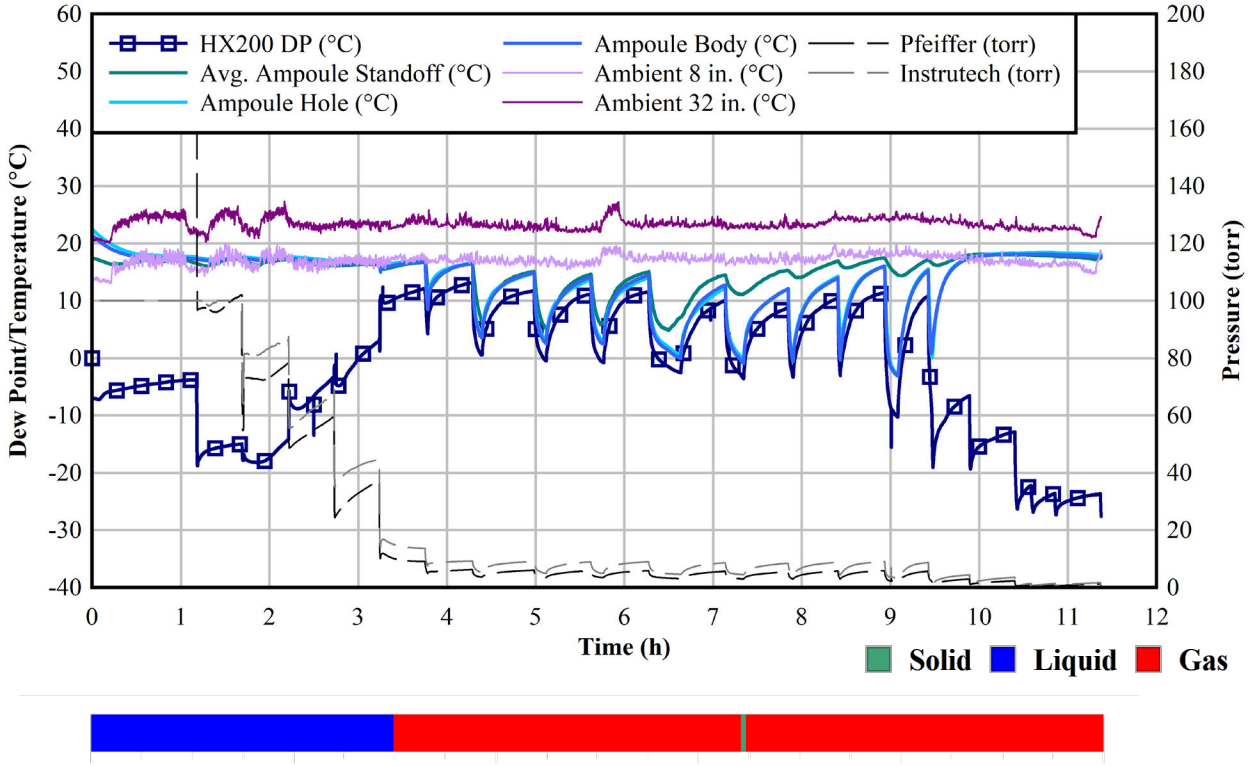

Figure 4-23 Dew point and ampoule temperatures during VT #8 (150 W, 0.123 in. OD ampoule). Indicator shows when water may enter gas or solid phase based on minimum ampoule temperatures.

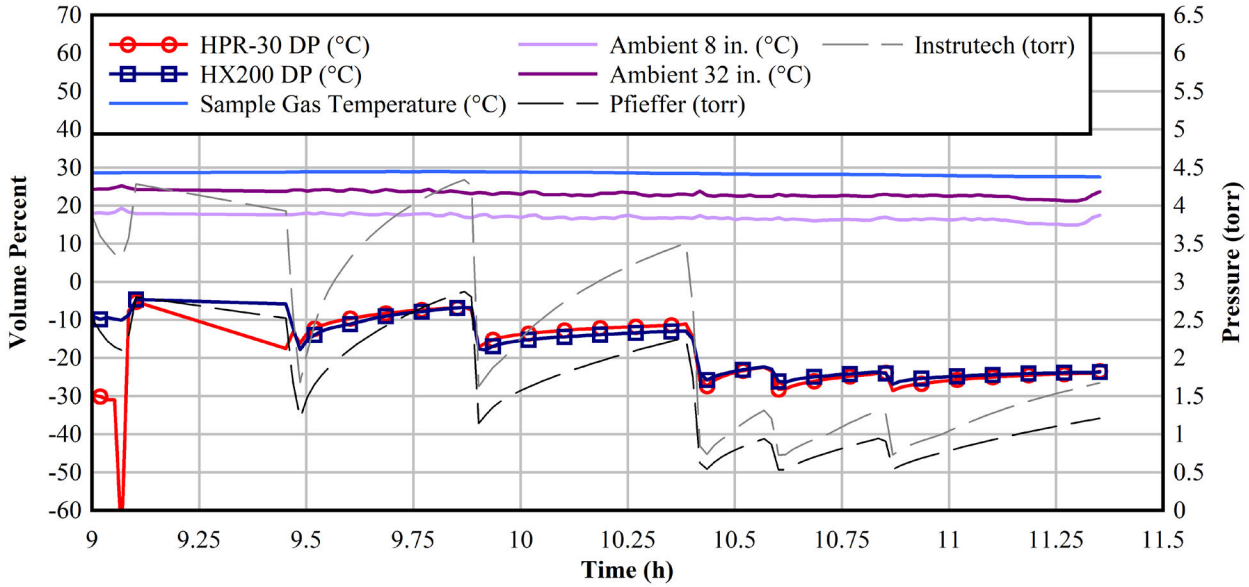

Figure 4-24 Mass spectrometer dew point data during VT #8 (150 W, 0.123 in. OD ampoule). At 9.13 h, the sample block was switched to the sample calibration line (with helium) as the pressure rose to the 3.75 torr limit. This was addressed by re-evacuating to 1 torr.

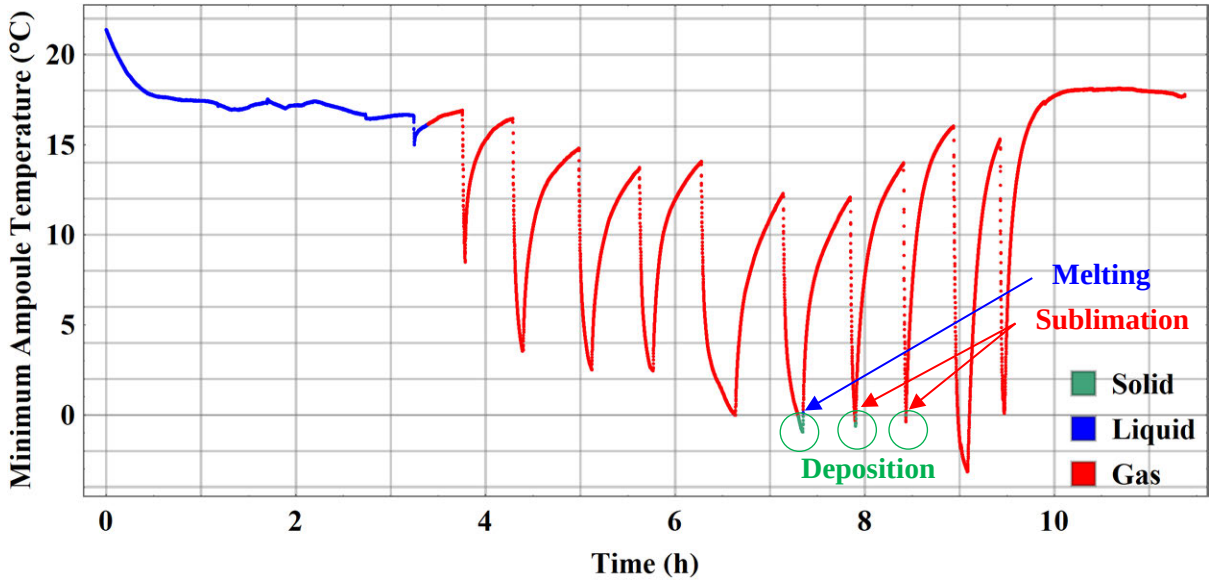

Figure 4-25 An inspection of potential water phases based on minimum ampoule temperatures and the InstruTech pressure of VT #8 (150 W, 0.123 in. OD ampoule).

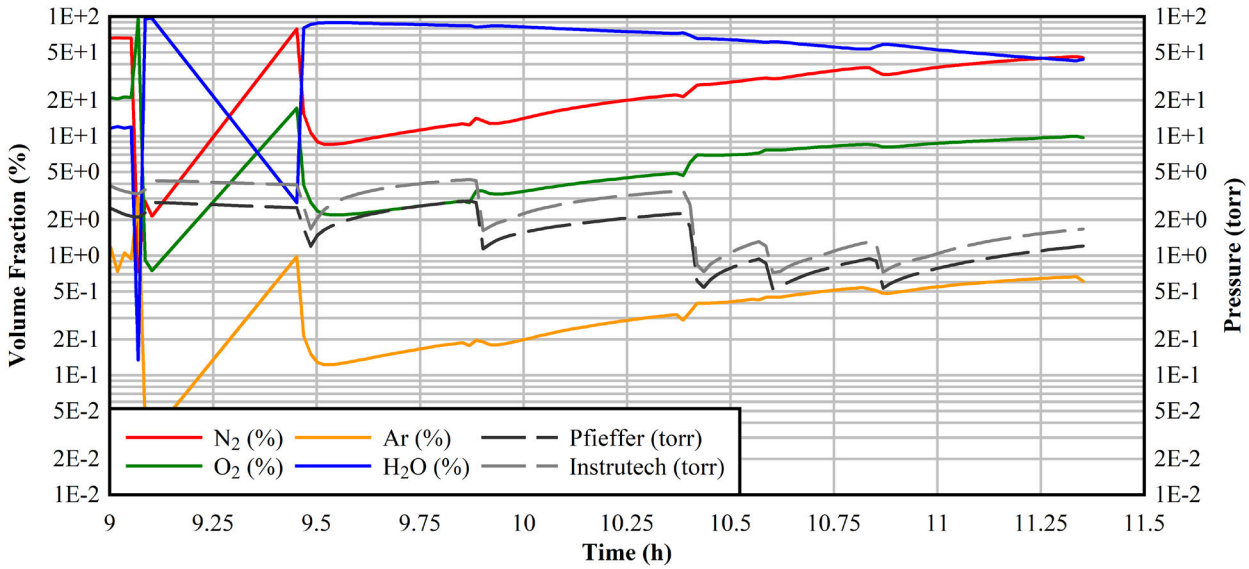

Figure 4-26 Mass spectrometer composition data from VT #8 (150 W, 0.123 in. OD ampoule).

4.2.3.3 Peak Cladding Temperature

The peak cladding temperature of the fuel rods during storage has implications on cladding integrity, and a limit of 400 °C is specified for short term loading operations including vacuum drying (NRC, 2003). A secondary objective of the heated vacuum drying tests was to evaluate how the PCT changes for the fuel rod surrogate during the vacuum drying procedure. This is intended to guide optimal heater power levels for future phases of testing at larger scales.

The PCTs of the two heated tests VT #7 and #8 are shown in Figure 4-27, while the associated temperature profiles are shown in Section C.2.3 and time-dependent data in Section C.2.1. For either test, the PCT on the heater occurred at TC #8 at z = 32 in., 0°. The peak surface temperature on the pressure vessel occurred at TC #21 at z = 24 in., 180°. This separation is likely due to conductive heat transfer to the stainless-steel middle and upper crosses. The behavior between both tests is comparable apart from the PCTs at 1 and 0.5 torr, which is due to differences in ambient temperature on the days of testing. At 0.5 torr, the PCT for VT#8 is 409 °C while that for VT #9 is 416 °C. The data confirm that as the pressure vessel is evacuated, the PCT is liable to increase to steady temperature until the water is evacuated. Afterwards, the PCT is liable to increase upon the lowest evacuation points imposed to ensure minimal pressure rebound. This data suggests that the additional hold points implemented after the majority of water removal must be minimized in time to reduce high-temperature effects on cladding integrity.

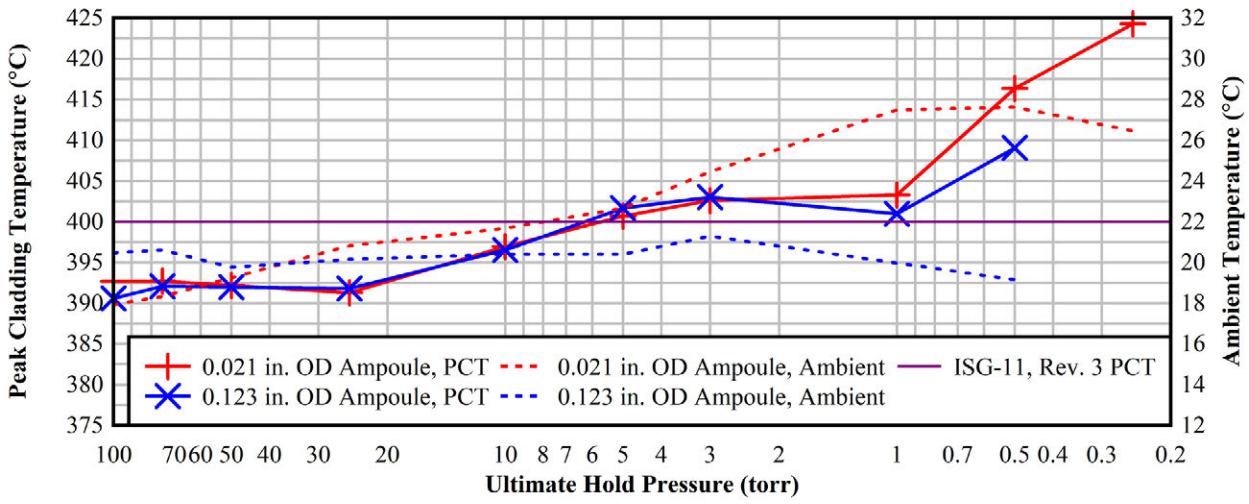

Figure 4-27 Peak cladding temperatures during the ultimate holds for VT #7 (red) and VT #8 (blue) at 150 W.

4.2.4 Use of Energy Balance to Estimate Water Removal

An inspection of the energy removed from the copper water ampoule and the stainless-steel standoff housing the ampoule allows can provide an estimate of the amount and timing of water removal during the vacuum drying tests. Tests with the 0.123 in. OD drill hole ampoule (VT #6 and 8) were chosen for evaluation. Figure 4-28 and Figure 4-29 show the system pressures and the temperatures of the copper water ampoule as well as the stainless-steel standoff housing it for the unheated test and the 150 W test, respectively.

For these two tests, the initial charge of water in the ampoule was 10.77 g and 10.74 g, respectively. The temperature of the water-filled ampoule started out at about 19 °C. At this temperature, water boils at 16.5 torr. As described earlier, the vacuum was applied in a stepwise fashion. At each step, the valve to the vacuum source was opened for sufficient time (up to several minutes) to lower the pressure and reach the target vacuum level. When evacuating to 5 torr, the temperature of the water ampoule and stainless-steel standoff housing dropped sharply, which is consistent with water inside the ampoule vaporizing rapidly. The pressure vessel was then isolated from the vacuum source and the pressure was allowed to rebound and the ampoule and standoff warmed 10 to 15 degrees. The process was then repeated nine times for VT #6 and eleven times for VT #8.

A simplistic energy balance was performed to estimate the water removal. During each cycle of evacuation, the step temperature change of the ampoule and the standoff housing were used to estimate the energy absorbed by the water vaporization. The mass of the dry copper ampoule was measured along with the mass of water charge placed inside. The heat capacity of the 56.6 g copper ampoule was taken as 0.385 J/g-K and water as 4.18 J/g-K. The stainless-steel housing weighed approximately 727 g. From the thermal mass and temperature change of the various components, the energy absorbed by the vaporizing water was estimated assuming adiabatic boundary conditions. The mass of water vaporized by each cycle was calculated using a heat of vaporization of 2,477 J/g of water at 10 °C. After each cycle the thermal mass of water in the ampoule was reduced for the next cycle calculation. For both of the tests considered here, most of the water was vaporized during the middle four cycles. The estimated water mass balance was within ±4 wt%.

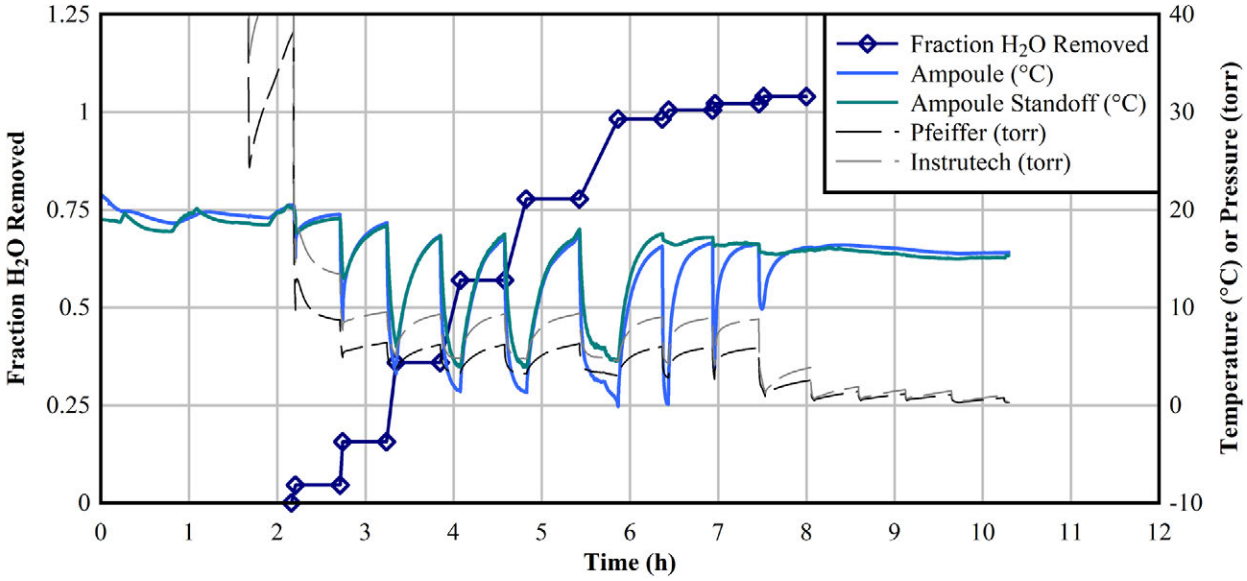

Figure 4-28 System pressure and water ampoule temperature swings indicating water removal for VT #6 (unheated, 0.123 in. OD ampoule).

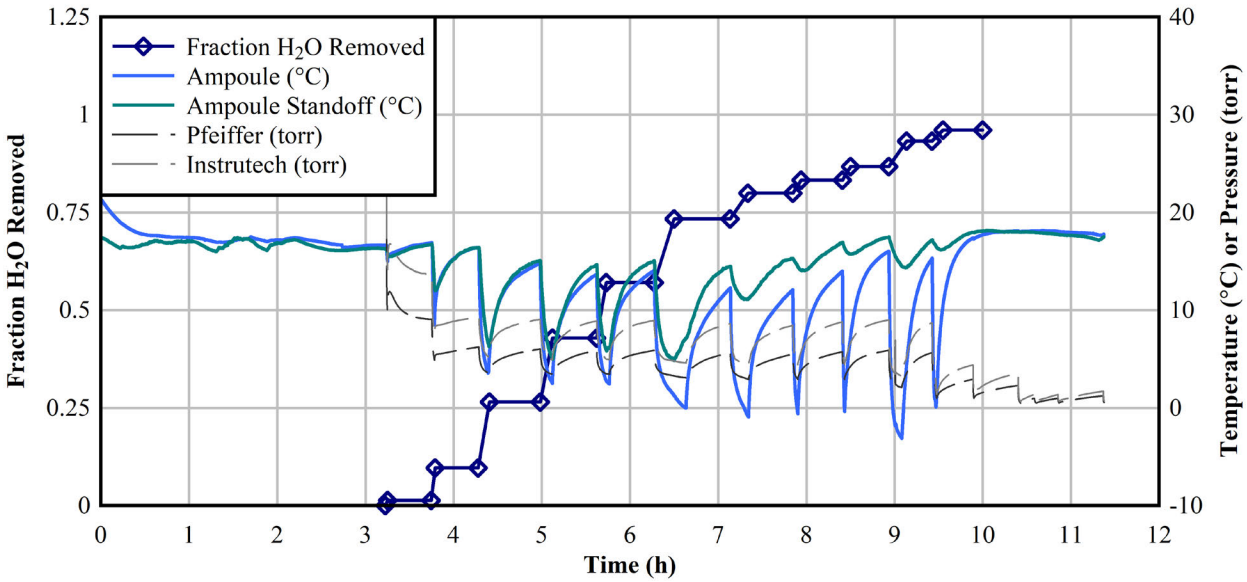

Figure 4-29 System pressure and water ampoule temperature swings indicating water removal for VT #8 (150 W, 0.123 in. OD ampoule).

This page is intentionally left blank.

5 FUTURE WORK

5.1 Improvements to Drying Procedures

The FHD results indicated that heat transfer to lateral standoffs in the pressure vessel, including the standoff containing the water ampoule, was both minimal and counteractive to the removal of water. This is due to the relative position of the cold pin lengths on the heater to the standoffs, along with the lack of insulation along the axial length of the pressure vessel directly surrounding the heater. Furthermore, natural convection was liable to occur primarily in the *z*-direction, while being negligible in the *y*-direction (see coordinates in Figure 2-6). This problem can be alleviated by devising a method of installing the ampoule vertically, or, as will be described later, using a dedicated fuel rod surrogate with a breach.

The first improvement to the FHD for the current setup is to fully insulate the pressure vessel. This will augment conductive heat transfer to the helium gas residing in the standoffs and the void space of the water ampoule. The next step would be to incorporate a parallel tube into the pressure vessel featuring an inline gas heater to drive a natural convection loop from the bottom of the heater to the ampoule and back to the top of the heater. This tube could be installed between the overflow and drainage valves in the PV (D2 and D3 in Figure 4-1, respectively). A recirculation pump could also be incorporated on this parallel line to impart forced convection. An additional measure would be including a gas drying unit, such as a steam separator or column of silica beads, to remove moisture as opposed to relying solely on venting.

Mass spectrometer measurements from FHD tests exhibited disproportionate dew point results for the high pressure (800 kPa) hold that did not compare well to the measurements from the Omega HX200 dew point sensor. It is recommended that in future testing, an additional HX200 be placed in the same sample stream as the mass spectrometer. This would allow for the assessment of sample flow rate and stagnation/mixing effects. There is also incentive to investigate the use of helium as a purge gas both before the vacuum drying procedure and between hold points to ensure thermal equilibration.

The mass spectrometer was unable to provide an intermediate range of sampling for vacuum drying pressures corresponding to the most significant pressure rebounds and potential phase changes. In this test, major fluctuations happened between 1 and 10 torr, but MS measurements could only be made when the PV pressure was 3.75 torr and below. The available measurements are fine, but they offer no insight on the phase transitions at higher pressures. In this test, the cold pin lengths on the heater rod and standoff lengths reduced heat transfer to the ampoule. In a future test at prototypic length, the source of water will likely be closer to the heated region. This will allow phase transitions to take place at higher hold points, which further necessitates expanding the range of measurement for the MS.

It was observed that the rate of evaporation from the water source can counteract the suction capacity of the vacuum pump. This is often the point in time where the temperature of the ampoule begins to drop most significantly. If the hold point pressure cannot be achieved, there is incentive to keep the pump running and not isolate the pressure vessel until the temperature of the ampoule noticeably drops or enters the solid phase regime. Otherwise, tests have shown that pressure rebounds and dew point behavior are very similar for repeated hold points.

The mass of water contained within the ampoule was proportionate to the amount of time required to completely evacuate it from the tube. However, as a tradeoff, it was also important to have a full ampoule to have more noticeable cooling effects, i.e. the tests with the 0.123 in. ampoule filled with 10 g was easier to cool than the smaller 0.021 in. ampoule filled with 5-6 g. The smaller orifice ampoule introduced bottleneck effects on the exiting stream of water during evacuation, as the evacuation steps to 3 torr demonstrated intermittent spikes in pressure. This is indicative of either phase transitions occurring at the orifice or capillary effects of liquid water on the surface of the drill hole. This incentivizes future work to continue investigating breach areas as a parameter in the test matrix.

5.2 Mass Spectrometry Calibration and Operation

5.2.1 Expanded Pressure Range Operation

Currently, the HPR-30 mass spectrometer has a dual pressure range inlet, a high-pressure range of 100-1000 kPa (14.5-145 psia) and a vacuum range of 0.05-0.5 kPa (0.375-3.75 torr). In addition, there is an independent calibration sample inlet that operates in the range of 20 kPa to 200 kPa (0.2 Bara to 2 Bara).

After conducting the present study, it is apparent that an analysis at a wider range of vacuums is required. Referring back to Figure 4-28 and Figure 4-29, most of the drying occurred in the pressure range of 0.4 to 1.3 kPa (3 to 10 torr) because the water was at an unrealistically low temperature of about 10 °C. In a more realistic system, the free water will be much hotter. At a water temperature of 50 °C, boiling starts at 12.4 kPa (93 torr). At 75 °C, boiling starts at 38.7 kPa (290 torr).

To accommodate the wide range of pressures, the three inlets of the HPR-30 will be reconfigured to cover the vacuum range from 0.05 kPa to 33 kPa (0.35 to 250 torr). The three ranges would be 0.05-0.5 kPa (0.35-3.5 torr), 0.40 to 4.0 kPa (3 – 30 torr) and 3.3 to 33 kPa (25 – 250 torr). Since the ambient pressure calibration inlet will be reconfigured to a vacuum sampling inlet, calibration will require a vacuum control system as shown in Figure 5-1 and described in the next section.

For the high-pressure range, a single inlet Hiden Analytical HPR-20 mass spectrometer will be upgraded to include a dual sample inlet. The HPR-20 is a larger, 19 mm quadrupole mass spectrometer with higher sensitivity for trace gas detection, where detection limits for krypton and xenon fall in the low part per billion range. Currently, the single inlet covers the pressure range of 20 kPa to 200 kPa (0.2 to 2 bara). Upgrading with an additional inlet will incorporate the pressure range from 85 kPa to 850 kPa (0.85 to 8.5 bara). The present inlet can sample gases at ambient pressure and can therefore be used to calibrate the HPR-20 in a similar means as the HPR-30 configured for use in this study and described in Section 3.3. After individual calibration of the newly reconfigured HPR-30 and HPR-20 systems, both instruments can be used to sample from the same pressure vessel using the same 3-port vacuum valve shown in Figure 5-1.

5.2.2 High Steam Calibration

Currently, the HPR-30 mass spectrometer has been calibrated for moisture in a background of air and for moisture in a background of helium. The calibration for moisture in a background of helium is used for the forced helium drying operations and for monitoring moisture after final pressurization with helium. The calibration for moisture in a background of air was used in this study for the vacuum drying operations, but the high fraction of steam suggests the true situation is nitrogen and oxygen in a background of steam. Proper calibration of nitrogen and oxygen in a background of steam is needed for future vacuum drying work.

Figure 5-1 shows a high steam content vacuum calibration system. The calibration gas is directed to the mass spectrometer sample inlet by a 3-way vacuum valve. Steam is sourced from water held in a sample bomb maintained at a constant controlled temperature. The water temperature will determine the pressure at which the system can operate - the higher the temperature, the higher the pressure. The vacuum level is set by a vacuum back-pressure controller. Two electronic vacuum flow controllers regulate the ratio of steam and air that flow through a chilled mirror hygrometer for dew point measurement before flowing past the 3-way valve inlet to the mass spectrometer. The controlled flow of steam and air provide the calibration points for H_2O, N_2, O_2 and Ar with a verification check by the dew point temperature measurement. The calibration is conducted at a range of different vacuum levels with the fraction of air varied from zero to 50% at each level of vacuum.

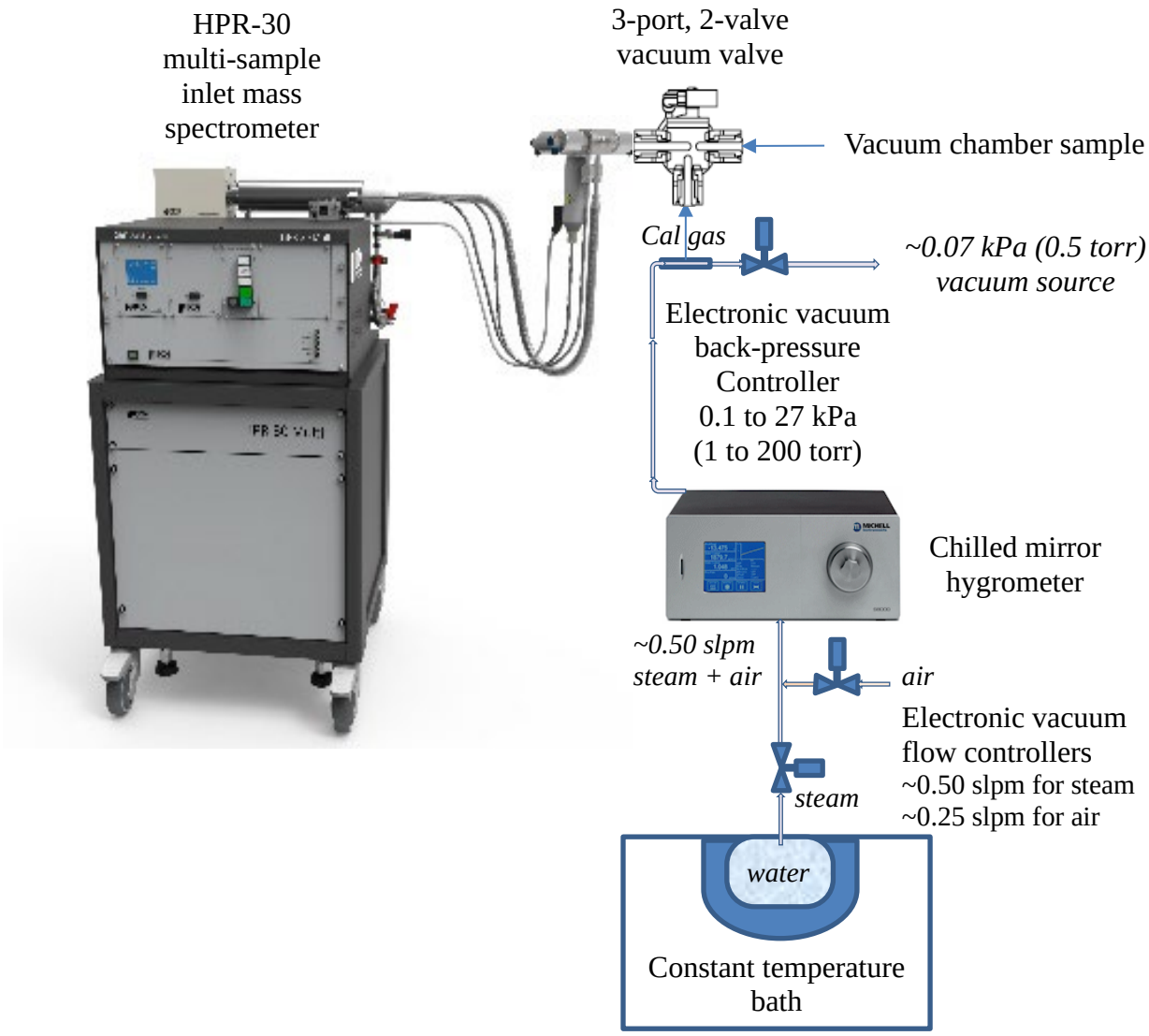

Figure 5-1 High steam content vacuum calibration system.

5.3 Expansion to Prototypic Length Scale and Assemblies

Although the vacuum drying tests for the single heater rod have been successful, a number of considerations prevent the scalability of results to a commercial dry cask system. The most important factor is the extent of water retention sites within the pressure vessel. While the pipe fittings, weld interfaces, standoffs, and instrumentation wires have served as retention sites for the small-scale test, these would not be representative of the numerous cavities in an actual internal canister volume. The use of an ampoule in a standoff presents a very wide gap between the heat source and retained water that is not representative of the water retained in a breached fuel rod. The temperature of the ampoule was also observed to remain near ambient temperature and below, which would not be the case for a breached fuel rod.

A multi-assembly test would bridge the prototypic complexity of the High Burnup Demo and the controlled environment of a lab-fielded apparatus that can build upon the successes of the Dry Cask Simulator (Durbin *et al.*, 2016) and its horizontal successor (Lindgren, Durbin, Pulido, & Salazar, 2019). Several concepts have been explored and are the subject of ongoing research. One promising concept would use prototypic PWR skeletons to harvest full-length “mini-assemblies” from a 17×17 commercial

skeleton as shown in Figure 5-2. They will be comprised of 1 guide tube, 24 fuel pins, and all other fundamental hardware (top and bottom nozzles, spacers, intermediate flow mixers, debris catcher).

A truncated assembly with labeled dimensions is shown in Figure 5-3. These mini-assemblies would retain prototypic geometric features but would be populated with waterproof, electrically resistive heaters, specialized rods, and instrumentation optimized for water content measurement. The fuel length would be prototypic and generate realistic temperature gradients, all while maintaining the intricate features of the guide tubes and grid spacers. The temperature measured at the water retention sites would also have a strong coupling to the thermal gradient of the assembly, as opposed to being in a separate, thermally isolated location.

Figure 5-4 shows a proposed arrangement of heater rods and diagnostic rods in the mini-assembly. Heaters comprise the majority of rod positions in the mini-skeleton with four diagnostic rods arranged in the middle. One diagnostic rod would be used for internal pressure monitoring, while the other three would be breached rods of varying breach geometries. Per given test, only one of the breached rods would feature a metered quantity of water while the other two would remain dry. Variability in the heated rod power is needed to emulate the power profile of a prototypic assembly. This can be done by configuring the bus plates to allow for two different power connections, or else by using two different types of heaters with different electrical resistances with a common power connection. A preliminary test can determine the optimal power level under vacuum to provide a PCT near the regulatory limit.

A pressure vessel concept for housing the mini-assembly is shown in Figure 5-5, along with proposed penetrants for fluids and instrumentation. It is comprised of two sections of nominal 4 in. pipes joined by welded flanges with ring-type joints. As opposed to using a tee, the lower penetrants are made at one flange to have better control over the total quantity of water introduced into the PV. All fluid lines entering the bottom flange would be united by valves in a single connection, providing more space for high-density TC feedthroughs. Saddle flanges are welded at a certain axial level to allow for the outflow of water below the assembly bus plates and to attach the neutral line to a grid spacer lying just above the water line. A heating and recirculation loop can be implemented between the bottom flange and a saddle flange for the PV gas during FHD tests. The mass spectrometer would have a direct sampling port near the top of the pressure vessel.

A further expansion of scaling would be the incorporation of several of these mini-assemblies into a scaled dry cask system. Although the lateral extent of each assembly would be truncated, configurations can be devised that would effectively incorporate heat transfer between assemblies as an improvement to the state of the art and offer a great deal of flexibility for future investigations. Further water-retaining features could be implemented such as spacer plates, siphon tubes, and a surrogate for a boral sheet.

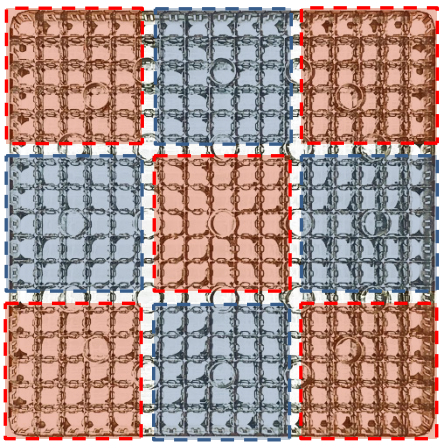

Figure 5-2 5×5 subassemblies taken from a 17×17 PWR skeleton.

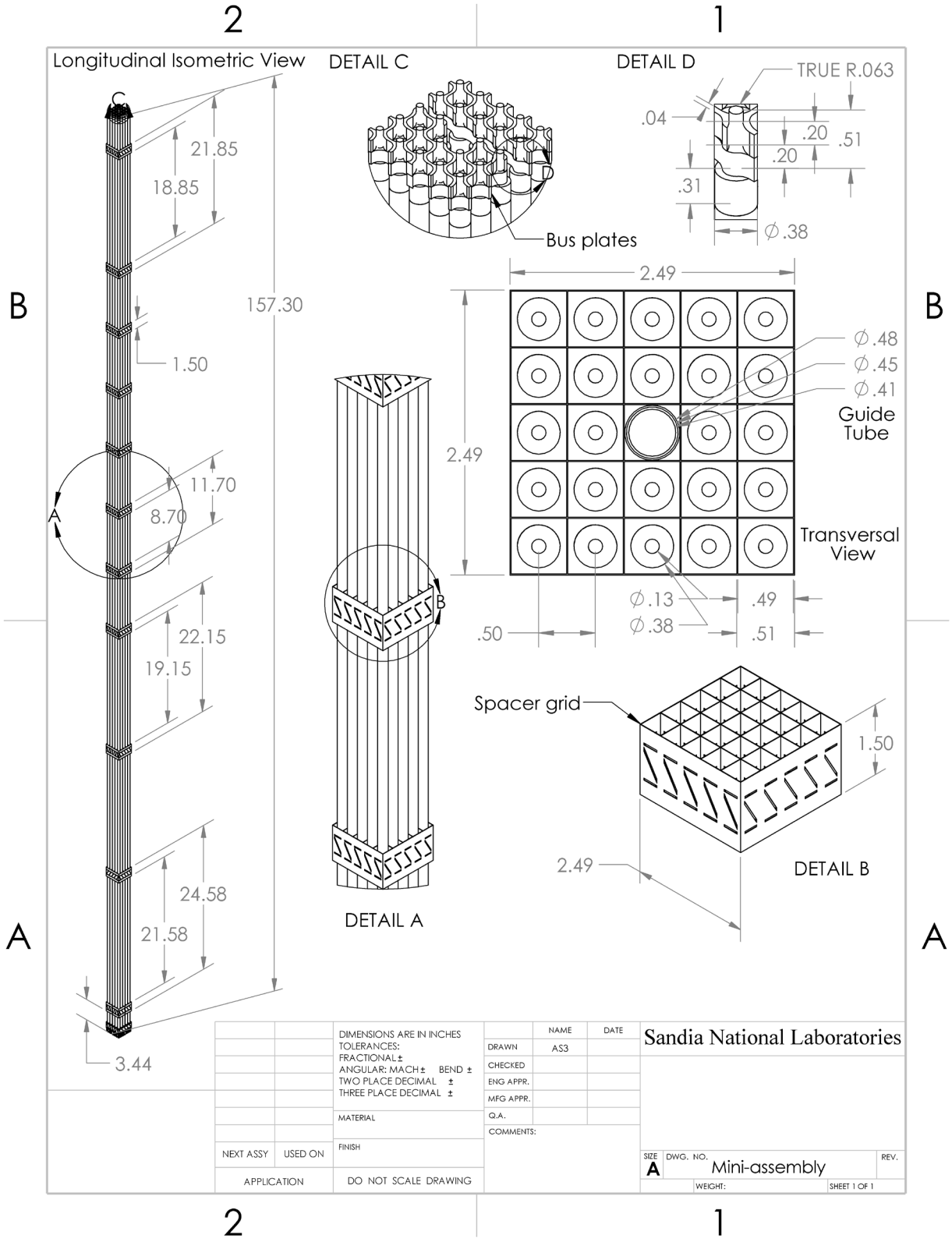

Figure 5-3 Schematic of mini-assembly.

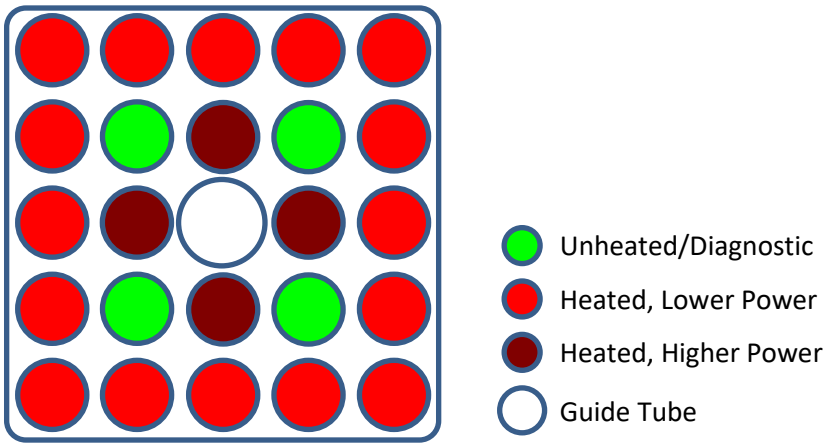

Figure 5-4 Proposed rod layout for a 5x5 mini-assembly.

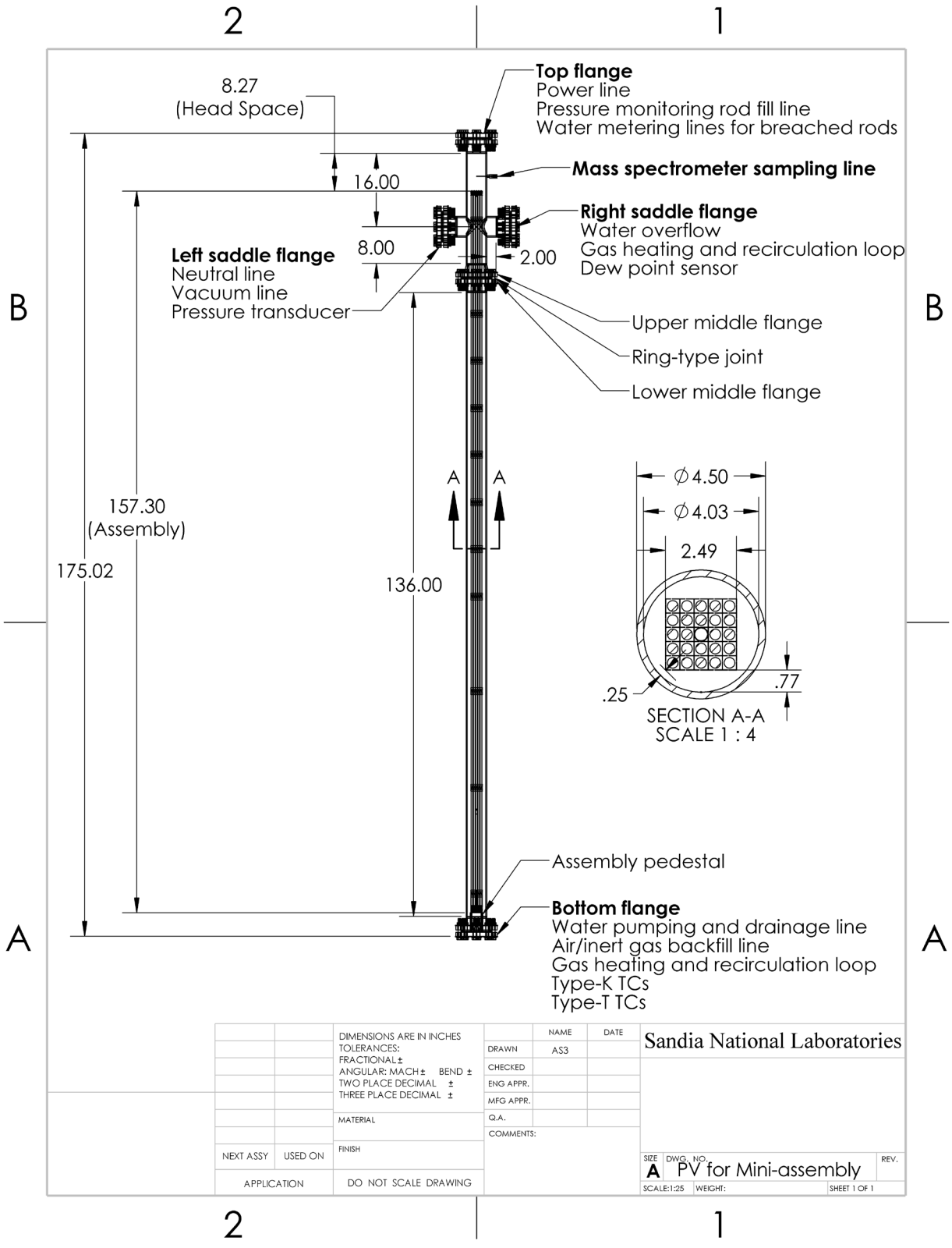

Figure 5-5 A pressure vessel design concept for the mini-assembly.

5.4 Internal Pressure Monitoring Rod

Internal rod pressure measurement is a slated objective for advanced testing. Such measurements are expected to vastly improve the current understanding of cladding stresses during storage operations by providing scaled data dependent on time, temperature, and pressure. Such versatility will allow for investigations of hoop stresses and zirconium hydride reorientation.

5.4.1 Preliminary Design

A scaled prototype of an internal pressure monitoring tube was tested for these efforts as described in Section 2.3. The tube was first placed concentrically in the test section of a vertically mounted tube furnace. At room temperature, the monitoring tube was pressurized to 7.47 MPa and isolated from the pressure system. This pressure is representative of the end-of-life pressures in a fuel rod with an integral fuel burnable absorber (IFBA) (NRC, 2018). Next, power was applied to the tube furnace to heat the pressure monitoring tube. Figure 5-6 shows the time history of the internal pressure, region temperatures, and moles of gas in each tube section during the test. The temperatures represent the integrated average value derived from the available cladding thermocouple data for each region. The moles in each tube section is shown in the lower part of Figure 5-6. These values were calculated using the measured pressure, integrated average temperatures, and the Ideal Gas Law.

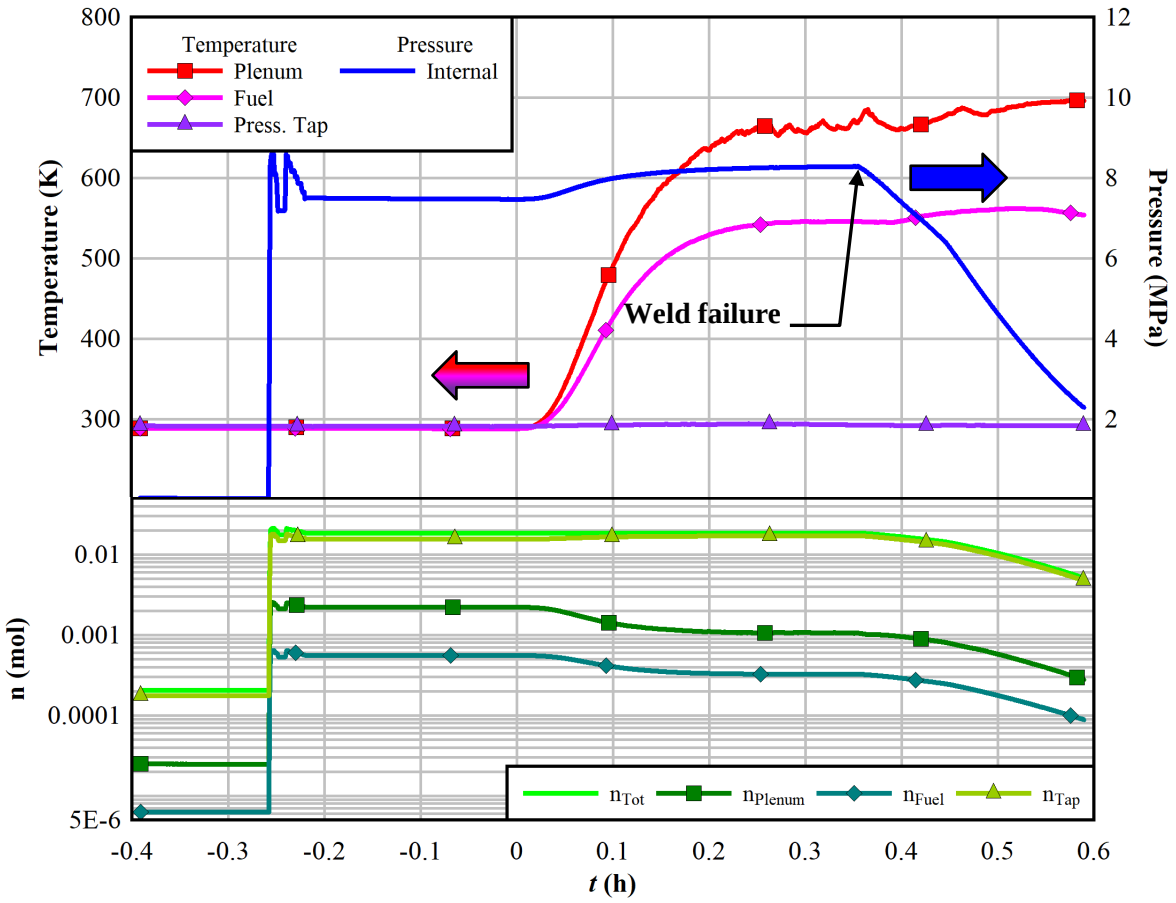

Figure 5-6 Pressure, temperature, and moles as a function of time for the pressure monitoring rod during the heated test.

The internal pressure increased as the tube temperatures increased. Figure 5-7 shows the axial temperature profiles of the pressure monitoring tube at different times during the test. The moles of gas in

the heated fuel and plenum regions decreased by the inverse of their respective temperatures. At t = 0.357 h, a pinhole failure in the weld between the plenum and transition collar occurred. The monitoring tube depressurized to approximately 2 MPa over a 14-minute period, and the test was concluded. While unintended for this test series, this pressure monitoring tube provided some initial data and insight for breached rod design in the future.

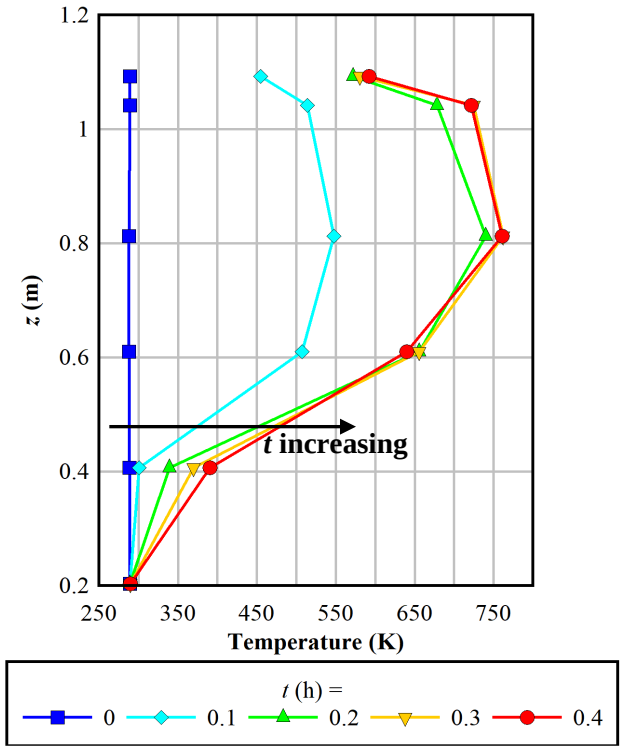

Figure 5-7 Temperature profiles of the pressure monitoring rod during heated testing.

5.4.2 Proposed Improvements

The pressure tube intended for this tests series was constructed to fit in the 0.2 in.-wide annulus of the pressure vessel. It was designed to simulate a representative plenum void volume using special tubing and wire diameters as opposed to fuel pellet surrogates. This introduced tight constraints on manufacturing, in particular the need for laser welding or brazing on thin-walled tube as opposed to orbital welds on more representative cladding thicknesses and diameters.

Figure 5-8 shows the diagnostic pressure monitoring rod proposed for implementation in the miniature assembly. The rod is expected to be manufactured on site and consists of a clad with a welded end plug similar to the one used for the waterproof heater rod. The clad is filled with magnesium oxide pellets of uniform geometry that are held in place with a spring. Considering the gap size between the cladding and the pellets and the spring volume, the pellets can be stacked to impart both a prototypic plenum void volume and rod void volume in general.

The top of the rod features a welded endcap that itself contains a welded connection to thick-walled, small-diameter tubing. This tubing is meant to be fed through the top of the pressure vessel and connected to an external tree featuring a pressure transducer, a pressure relief valve, and a valve to interface with a helium fill line (see Figure B-7). The rod would be pressurized to a representative end-of-life pressure and then isolated. The transducer would monitor internal pressure during drying operations, and a relief valve is installed since the initial pressure is liable to rise with increasing temperature. The rod can then be relieved upon conclusion of testing.

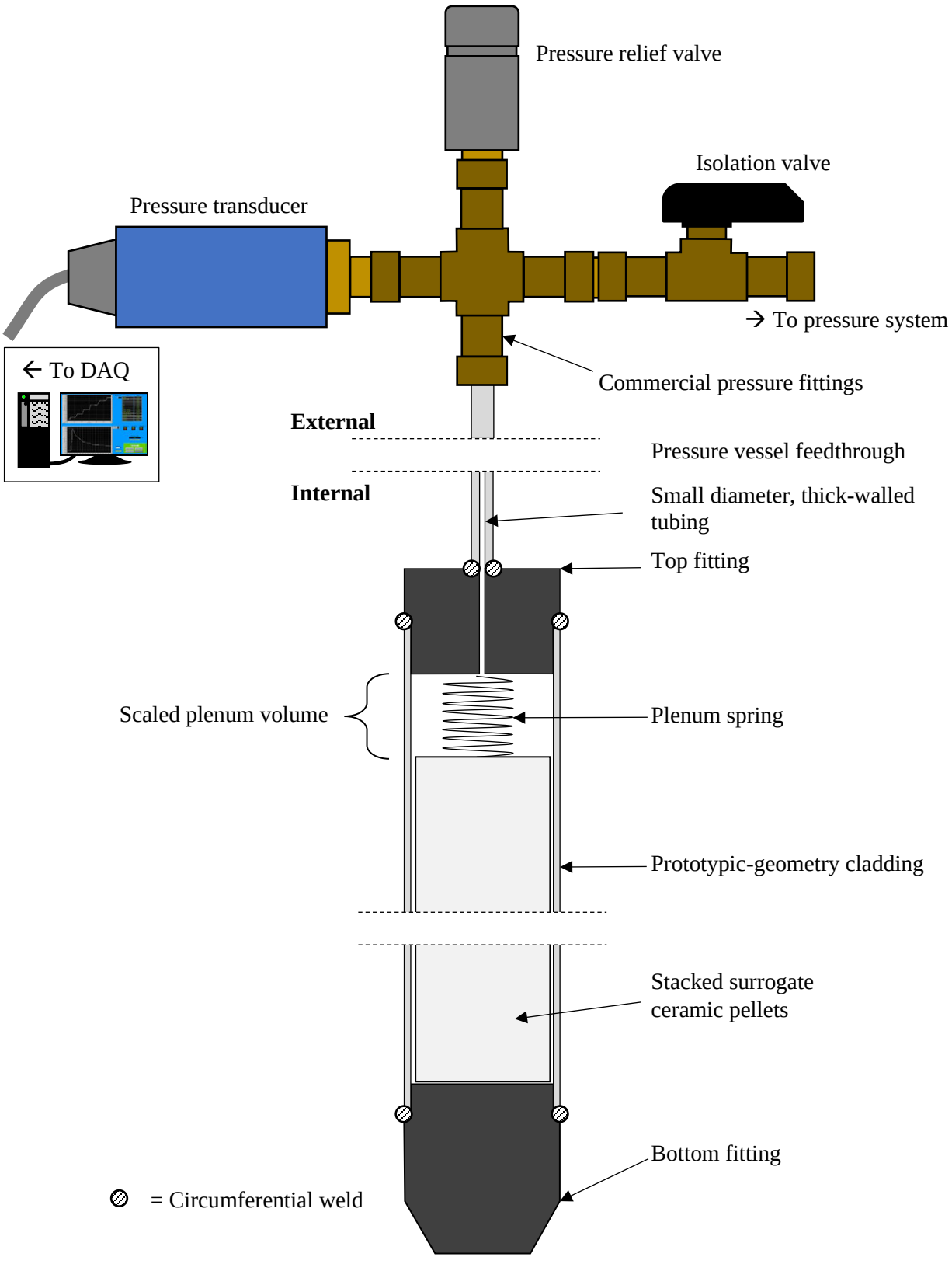

Figure 5-8 Cross-sectional view of a pressure monitoring rod.

5.5 Breached Rods

Figure 5-9 shows the proposed implementation of an unheated diagnostic rod that will simulate a breached clad filled with water. It will fulfill a more integrated role than the water ampoule featured in this report and allow for investigations of water removal under prototypic thermal boundaries and readily scalable geometries.

The rod consists of a clad with a welded end plug similar to the one used for the waterproof heater rod. The clad is filled with the same quantity of magnesium oxide pellets as the pressure monitoring rod to provide the same plenum volume. The pellets are held in place with a plenum spring, and the top of the clad features a special endcap welded to thin-walled tubing. This tubing is fed through the top of the pressure vessel and connected to external pipe fittings likely comprised of VCR-type fittings for performance under vacuum. These fittings would feature a leak-tight isolation valve and a pressure transducer for the measurement of the pressure response within the breached rod.

A set quantity of deionized water can be metered into the plenum through the isolation valve by way of a mass flow controller. This same filling line can also be used to evacuate the cladding with a secondary vacuum system if the main vacuum system of the PV is incapable of removing the water.

The breach diameter of each of these three diagnostic rods will be unique and machined at a common axial level lying above the water line of the pressure vessel, within the plenum zone, and close to the hot lengths of the surrounding heaters. This will allow for experiments that control residual water in one or more breached rods, the PV void space, or any of the above.

5.6 Separate Effects Tests

The effects of cladding oxidation and crud on water retention in dry storage systems can be explored via separate effects tests (SETs). This would involve smaller-scale tests that would measure chemisorbed and physiosorbed water content on samples of cladding with existing oxidation and crud. Initial guidance regarding this data retrieval may be taken from the Sister Rod nondestructive examination efforts (Montgomery *et al*., 2018). With this information, a coordinated focus from SETs would be centered on incorporating these water retention properties either into cladding analogues or cladding with recreated oxidation and crud layers.

A series of small-scale, benchtop drying tests are underway that aim to investigate the amount of trapped and absorbed water on canister features (Poloski & Colburn, 2019). These tests have included the gravimetric evaluation of water loading on fuel cladding materials parametrized by tubing length and surface area. These cladding samples will be autoclaved to introduce an oxide layer, saturated in a water bath, and then held in a drying oven at incremental temperatures to verify changes in sample mass as a measure of drying. This will allow for an investigation of the number of hydrated compounds generated, the quantity of water remaining in the hydrated compounds, and the equilibrium water vapor pressure as a function of temperature, as recommended in drying standards (ASTM, 2016).

It may be possible to employ the results of the oxide layer tests to devise a special diagnostic rod with an engineered crud-simulant layer. A drying test series can then be conducted in the single-rod pressure vessel or using one of the diagnostic rod locations in the prototypic-length mini-assembly. Results can be compared with those for a normally cladded surrogate rod to highlight effects of chemisorbed water.

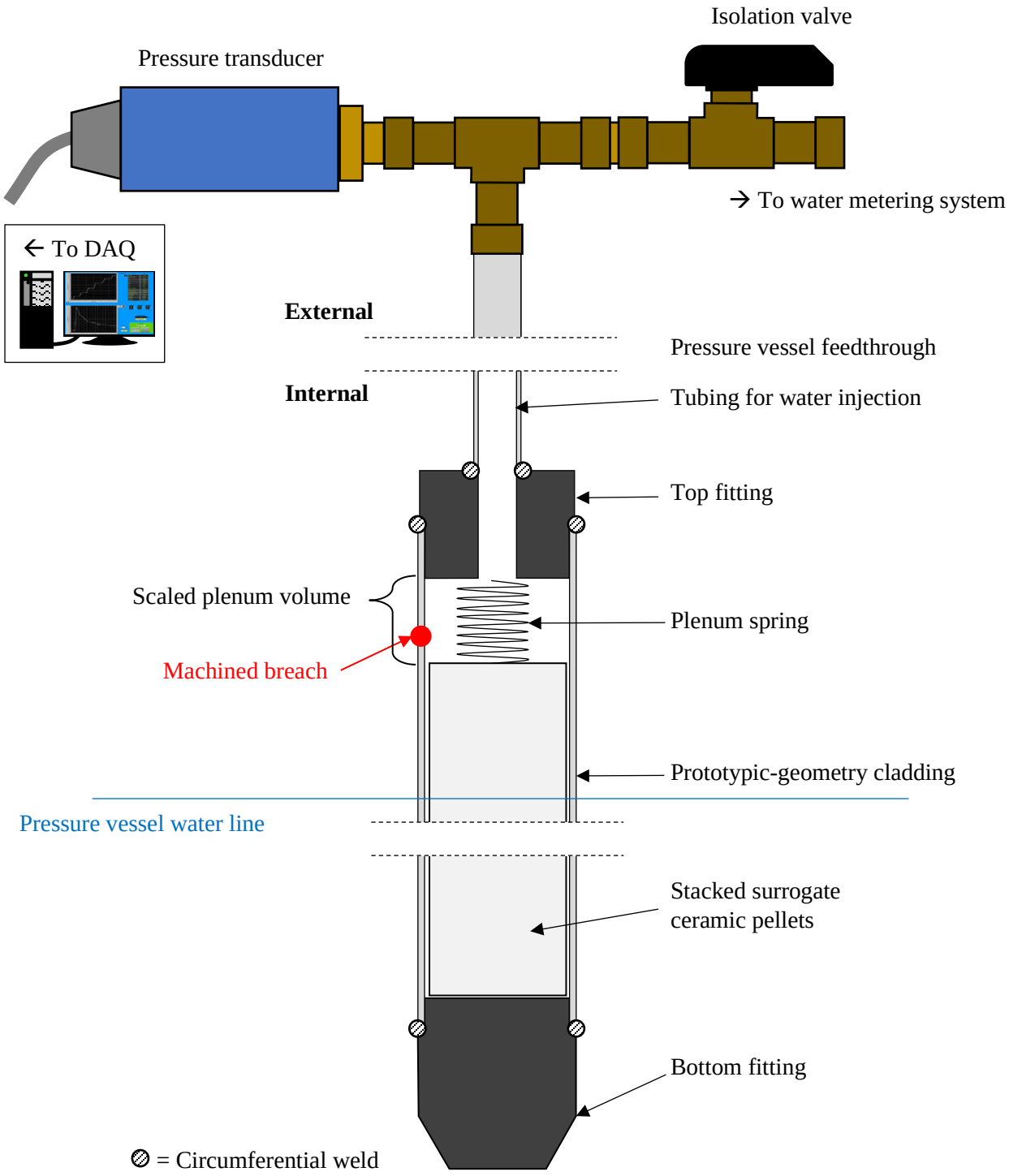

Figure 5-9 Cross-sectional view of a breached cladding rod.

6 SUMMARY

This report describes the development of experimental components, methodology, and instrumentation to examine spent fuel drying operations conducted by industry. Experiments with surrogate spent fuel and prototypic assemblies were conducted to represent vacuum drying and FHD.

The removal of water using sequential vacuum drying hold points has been demonstrated in a small-scale pressure vessel with a partially submersible heater rod. Time-dependent temperature and pressure data has been obtained along with confirmatory water content measurements from a mass spectrometer. Dew point data derived from the MS were confirmed to align with those from a second sensor, although this was only possible for the range of pressures below 3 torr (or above ambient pressure for the FHD tests). Results cumulatively verify the evacuation of water under both heated and unheated conditions for ampoules of two different orifice diameters.

In the near future, the MS will be reconfigured to analyze pressures between 3 and 200 torr, as significant phase transitions happen in this regime depending on the temperature of the water. Future tests will raise the temperature of the water source and require coverage of higher pressures to monitor phase transitions and nuanced behavior caused by breach orifices. The effects of employing a preliminary helium purge prior to testing for thermal equilibration purposes should be investigated to assess effects on the MS data analysis, along with the utilization of intermediate helium backfills between vacuum drying holds.

The removal of residual water via forced helium dehydration was simulated using two water filling methods. One involved wetting the internal surfaces of the pressure vessel using pumped water followed by drainage and a blowdown with helium. The second used an ampoule to install a fixed quantity of water like the vacuum drying tests. The boundary conditions of the pressure vessel could not be controlled to allow for sufficient heating of the pressure vessel standoffs and/or ampoule for significant water removal in those regions. The small quantity of water in the ampoule test was apparent in its disparate dew point behavior. While sufficient mixing of water vapor was observed for the bulk filling test, the test with the ampoule exhibited poor mixing and condensation effects near the MS sample inlet. Water content measurements nonetheless were generally in good agreement and confirmed that some quantity of water was evacuated from the pressure vessel in either test.

A scaled prototype of a pressure-monitoring tube was created and tested externally to the main drying tests. This tube demonstrated the viability of such a tube to directly measure internal pressure during simulated drying cycles. Although unscheduled, a weld in this tube failed during this preliminary testing providing further insight for breached rod surrogates.

The data and operational experience from these tests will guide the next evolution of experiments on a prototypic-length scale with multiple surrogate rods in an assembly. These assemblies will feature partially submersible heater rods and specialized diagnostic rods to introduce cladding breach effects and internal rod pressure monitoring. The use of multiple heaters will provide more representative power profiles for PCT evaluations, and the breached rods will act as directly integrated water ampoules directly affected by the heat source. The pressure monitoring rods will have prototypic plenum volumes and cladding geometries that can be directly scaled to dramatically enhance existing data from the field. Diagnostic rods with engineered oxide layers can also be implemented to address the separate effects of chemisorbed water. Altogether, the assembly components will provide a more representative array of water retention sites that would be expected in commercial operations with SNF, and drying effects will be observable in the water content of internal gas samples over a wide dynamic range of pressures.

Instrumentation and procedures were developed for this test series to verify their accuracy and resilience in quantifying conditions similar to commercial drying operations. These techniques and hardware provide the basic tools for more prototypic testing in the future including actual canister loadings if needed. The insight gained through these investigations is expected to support the technical basis for the continued safe storage of SNF into long term operations.

This page is intentionally left blank.

7 REFERENCES

ASTM International (2016). Standard Guide for Drying Behavior of Spent Nuclear Fuel (C1553-16). ASTM Book of Standards Volume 12.01. West Conshohocken, PA.

ASTM International (2017). Standard Specification for Temperature-Electromotive Force (emf) Tables for Standardized Thermocouples (E230/E230M-17). ASTM Book of Standards Volume 14.03. West Conshohocken, PA.

Billone, M. C., Burtseva, T. A., & Han, Z. (2013). Embrittlement and DBTT of High-Burnup PWR Fuel Cladding Alloys (FCRD-UFD-2013-000401, ANL-13/16). Argonne National Laboratory. Lemont, IL.

Bryan, C. R., Jarek, R. L., Flores, C., & Leonard, E. (2019). Analysis of Gas Samples Taken from the High Burnup Demonstration Cask (SAND2019-2281). Sandia National Laboratories. Albuquerque, NM.

Hanson, B. D., & Alsaed, H. A. (2019). Gap Analysis to Support Extended Storage and Transportation of Spent Nuclear Fuel: Five-Year Delta (SFWD-SFWST-2017-000005, Rev 1; PNNL-28711). Pacific Northwest National Laboratory. Richland, WA.

Hiden Analytical Limited (2018). TWN QIC Dual Stage Sampling Head manual (HA-085-850). Warrington, United Kingdom.

Hiden Analytical Limited (2008). Relative Sensitivity RS Measurements of Gases. Hiden Analytical (Application Note 282). Warrington, United Kingdom.

Hoffmann E., & Stroobant V. (2007). Mass Spectrometry Principles and Applications. John Wiley & Sons Inc. Hoboken, NJ.

Knight, T. W. (2019). Experimental Determination and Modeling of Used Fuel Drying by Vacuum and Gas Circulation for Dry Cask Storage (NEUP 14-7730). University of South Carolina. Columbia, SC.

Knoll, R., & Gilbert, E. (1987). Evaluation of Cover Gas Impurities and their Effects on the Dry Storage of LWR (Light-Water Reactor) Spent Fuel (PNL-6365). Pacific Northwest National Laboratory. Richland, WA.

Leck, J. H. (1989). Total and Partial Pressure Measurement in Vacuum Systems. Glasgow, United Kingdom.

Lindgren, E. R., & Durbin, S. G. (2007). Characterization of Thermal-Hydraulic and Ignition Phenomena in Prototypic, Full-Length Boiling Water Reactor Spent Fuel Pool Assemblies after a Complete Loss-of-Coolant Accident (SAND2007-2270). Sandia National Laboratories. Albuquerque, NM.

Lindgren, E. R., Durbin, S. G., Pulido, R. J. M., & Salazar, A. (2019). Update to the Thermal-Hydraulic Investigations of a Horizontal Dry Cask Simulator (SAND2019-11688 R). Sandia National Laboratories. Albuquerque, NM.

Lindgren, E. R., Salazar, A., & Durbin, S. G. (2019). Component Concepts for Advanced Dry Storage Investigations (SAND2019-3587 R). Sandia National Laboratories. Albuquerque, NM.

List, R. J. (1951) Smithsonian Meteorological Tables, 6th ed., vol. 114, p 1-527. Smithsonian Instituition. Washington, D.C.

Mackenzie F. T., & Mackenzie J.A. (1995). Our Changing Planet. Prentice-Hall. Upper Saddle River, NJ.

Mass Spectrometry Data Centre (1991). Eight Peak Index of Mass Spectra. Royal Society of Chemistry. Cambridge, United Kingdom.

Michell Instruments, (2019). S8000 Precision Chilled Mirror Hygrometer. Michell Instruments. Cambridgeshire, United Kingdom.

Miller, L., Walter, G., Mintz, T., Wilt, T., & Oberson, G. (2013). Vacuum Drying Test Plan (NRC-02-07-C-006). CNWRA. San Antonio, TX.

Montgomery, R., Bevard, B., Morris, R. N., Goddard Jr., J., Smith, S. K., Hu, J., Beale, J., & Yoon, B. (2018). Sister Rod Nondestructive Examination Final Report (SWFD-SFWST-2017-000003 Rev. 1). Oak Ridge National Laboratory. Oak Ridge, TN.

Nuclear Regulatory Commission (2001). A New Comparative Analysis of LWR Fuel Designs (NUREG-1754). Washington, D.C.

Nuclear Regulatory Commission (2002). Westinghouse Technology Manual (ML023040131). Washington, D.C.

Nuclear Regulatory Commission (2003). Spent Fuel Project Office Interim Staff Guidance-11, Revision 3. Washington, D.C.

Nuclear Regulatory Commission (2010). Standard Review Plan for Spent Fuel Dry Storage Systems at a General License Facility (NUREG-1536). Washington, D.C.

Nuclear Regulatory Commission (2018). Dry Storage and Transportation of High Burnup Spent Nuclear Fuel (NUREG-2224). Washington, D.C.

Parish O., & Putnam T. (1977). Equations for the Determination of Humidity from Dewpoint and Psychrometric Data. National Aeronautics and Space Administration, Dryden Flight Research Center. Edwards, California.

Poloski, A., & Colburn, H. (2019). Small-Scale Drying: FY2019 Interim Report (PNNL-29046 Rev. A). Pacific Northwest National Laboratory. Richland, WA.

Salazar, A., Pulido, R. J. M., Lindgren, E. R., & Durbin, S. G. (2019). Advanced Concepts for Dry Storage Cask Thermal-Hydraulic Testing (SAND2019-11281 R). Sandia National Laboratories. Albuquerque, NM.

Salazar, A., Pulido, R. J. M., Lindgren, E. R., & Durbin, S. G. (2020). Analysis of Water Retention in Isothermal Vacuum Drying Test (SAND2020-1449 C, ICONE28-POWER2020-16599). To be published in Proceedings of the 2020 28th Conference on Nuclear Engineering (ICONE28). August 2-6, 2020. Anaheim, CA.

APPENDIX A MECHANICAL DRAWINGS

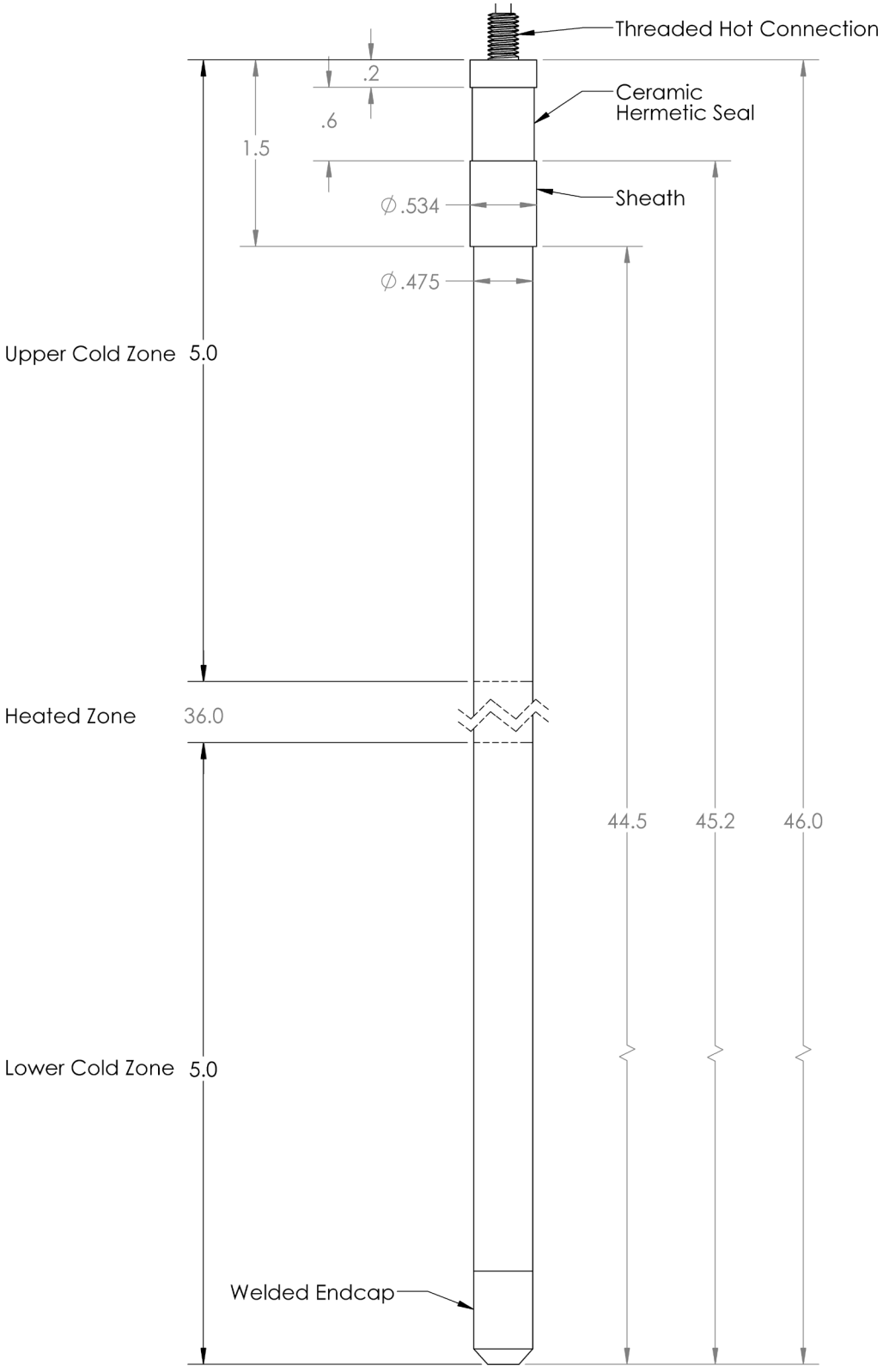

Figure A-1 Schematic of heater rod.

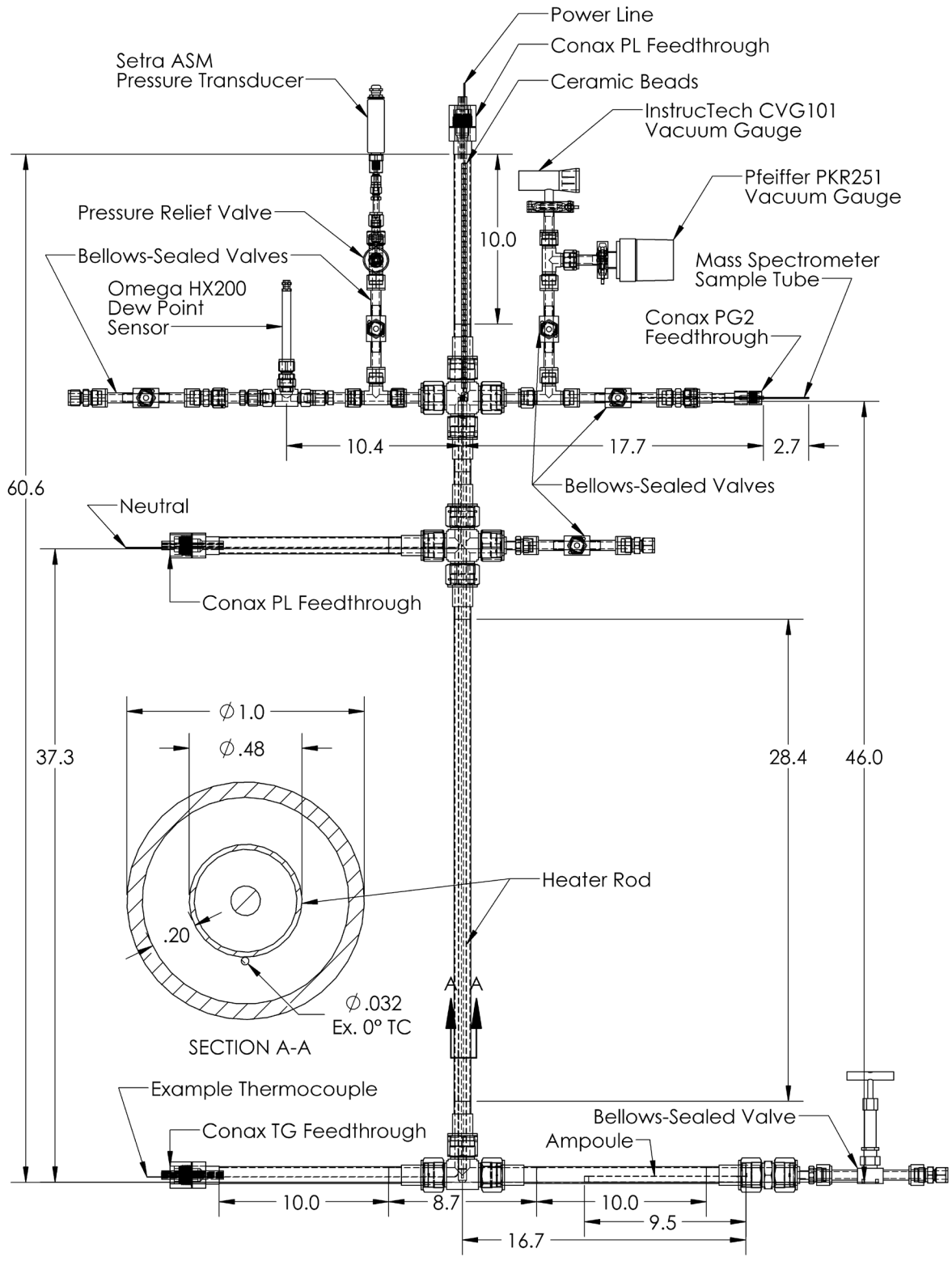

Figure A-2 Schematic of pressure vessel, where section A-A is scaled 12:1.

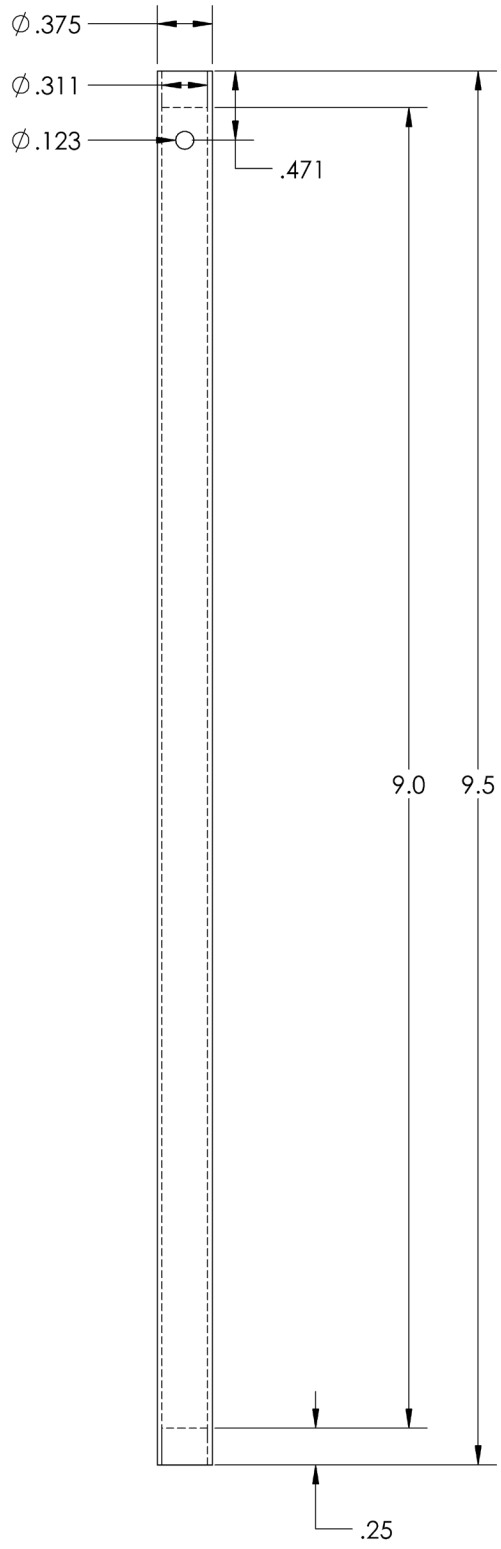

Figure A-3 Schematic of ampoule with 0.123 in. drill hole.

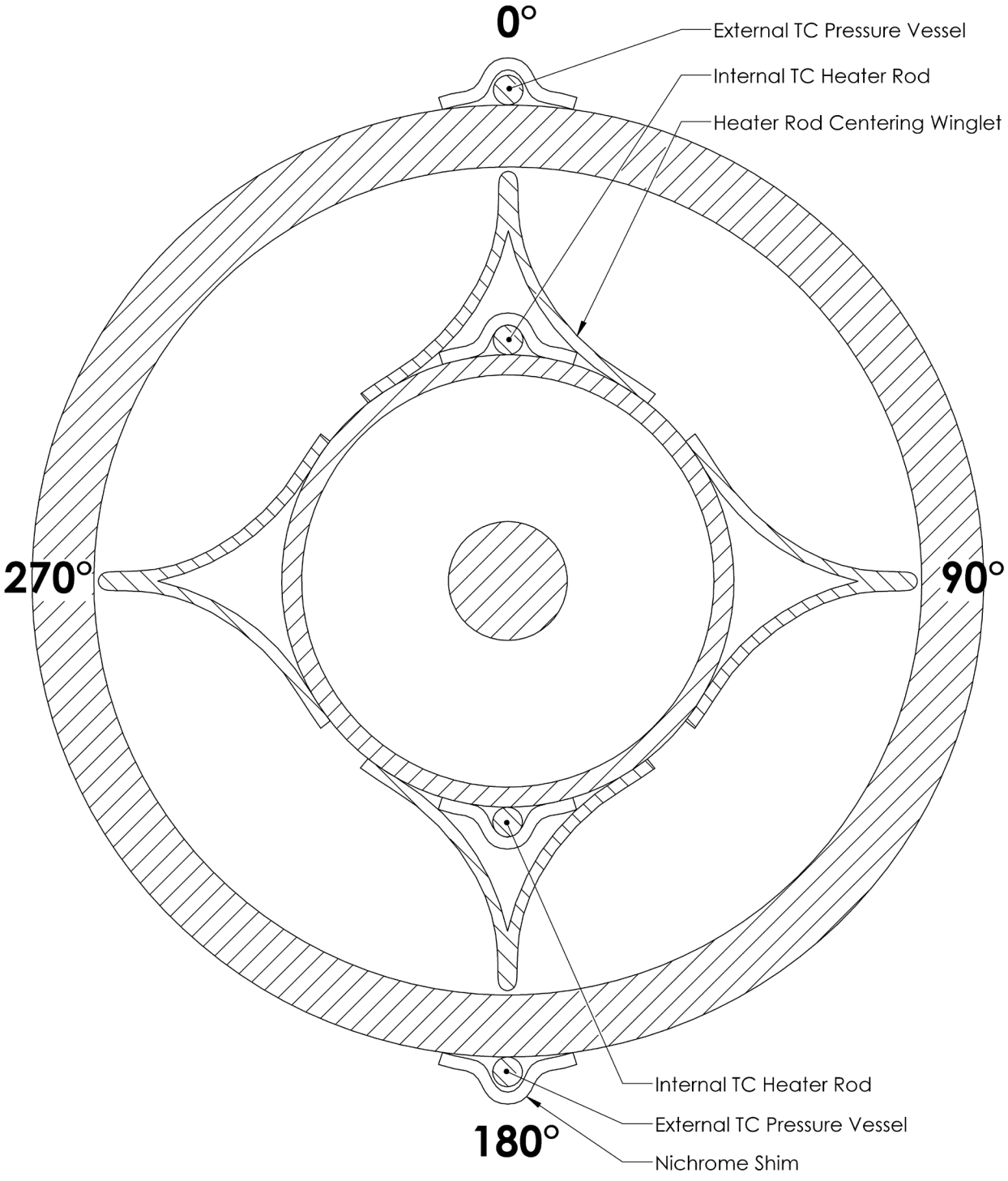

Figure A-4 Alignment of thermocouples in the radial direction.

APPENDIX B PRESSURE SYSTEM

This appendix includes comprehensive schematics of the pressure vessel and the pressure systems interfacing with the pressure vessel. The color codes and abbreviations for the system lines are described in Figure B-1.

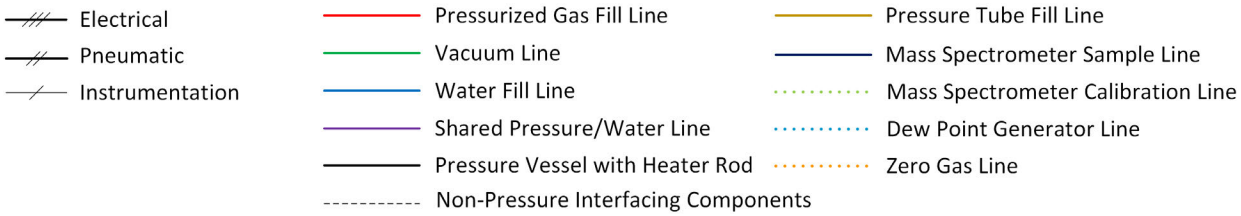

HP	High pressure	QIC	Quartz inert capillary
LP	Low pressure	QP	Quadrupole
CAL	Calibration	AMP	Amplifier
DAQ	Data acquisition system	PRV	Pressure relief valve
DP	Dew point	PT	Pressure transducer
L	Power line	PV	Pressure vessel
N	Neutral line		

Figure B-1 Legend and nomenclature for pressure system lines.

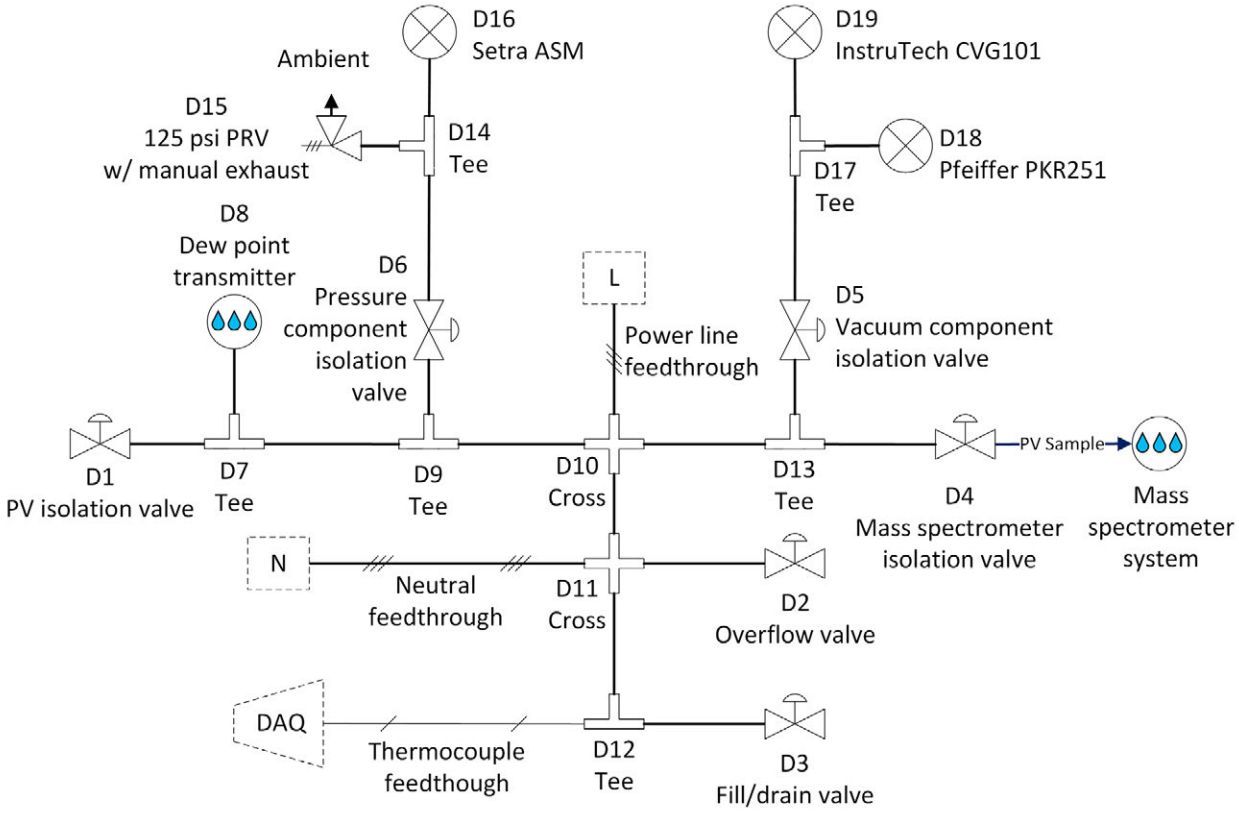

Figure B-2 Pressure vessel components. Valves D10 or D14 were sometimes removed and replaced with caps if the connected gauges were not needed. Valve D2 and D3 were also capped for the vacuum drying tests since no water pumping was needed.

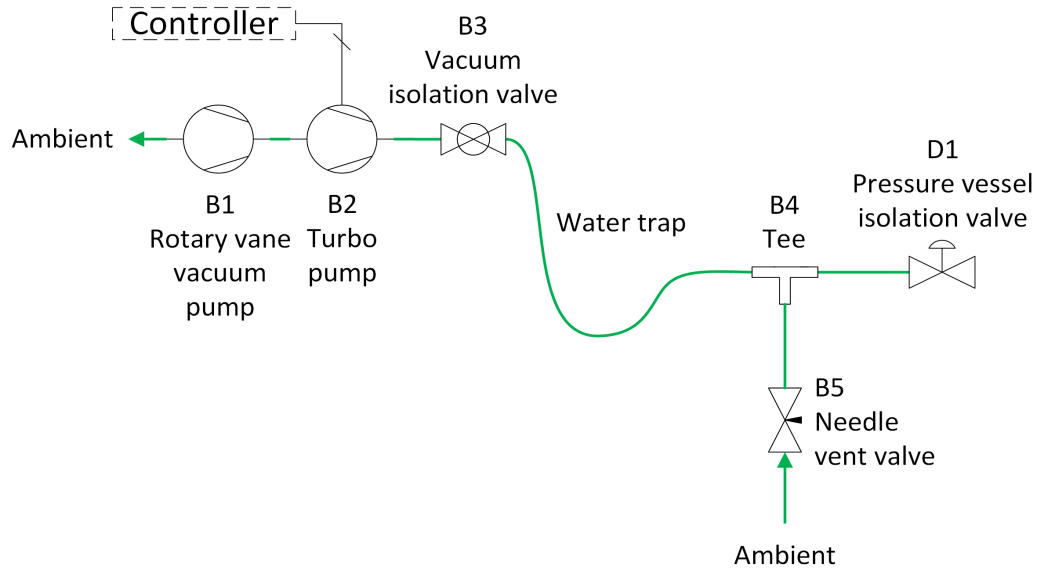

Figure B-3 Vacuum line components. The water trap is comprised of specially bent tubing. Valve B3 was later removed due to excessive flow restriction and since adequate pressure control was feasible via B5 and D1.

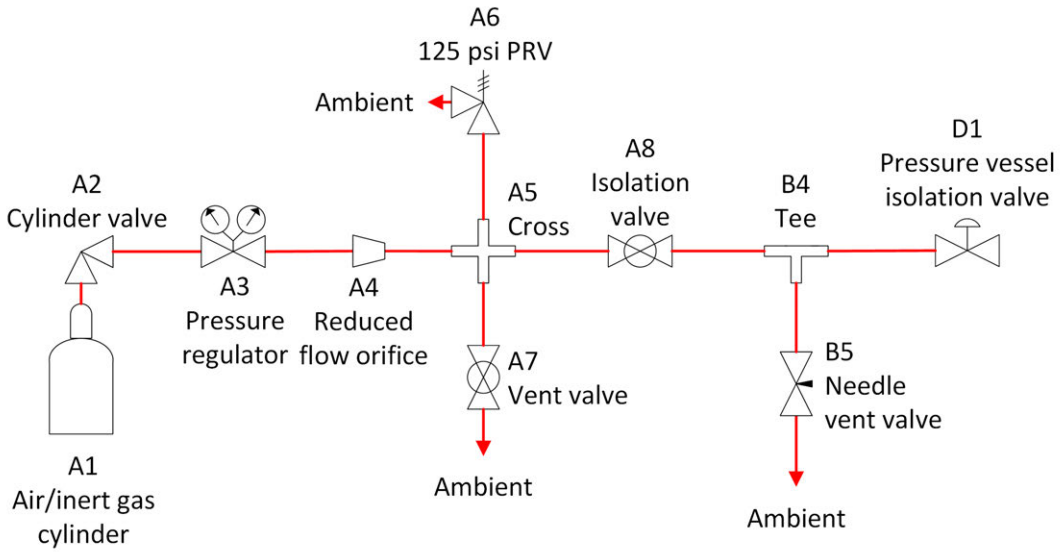

Figure B-4 Pressure line components, where B5 from the vacuum line is retained to allow for venting of pressurized gas through the top of the pressure vessel in FHD #11.

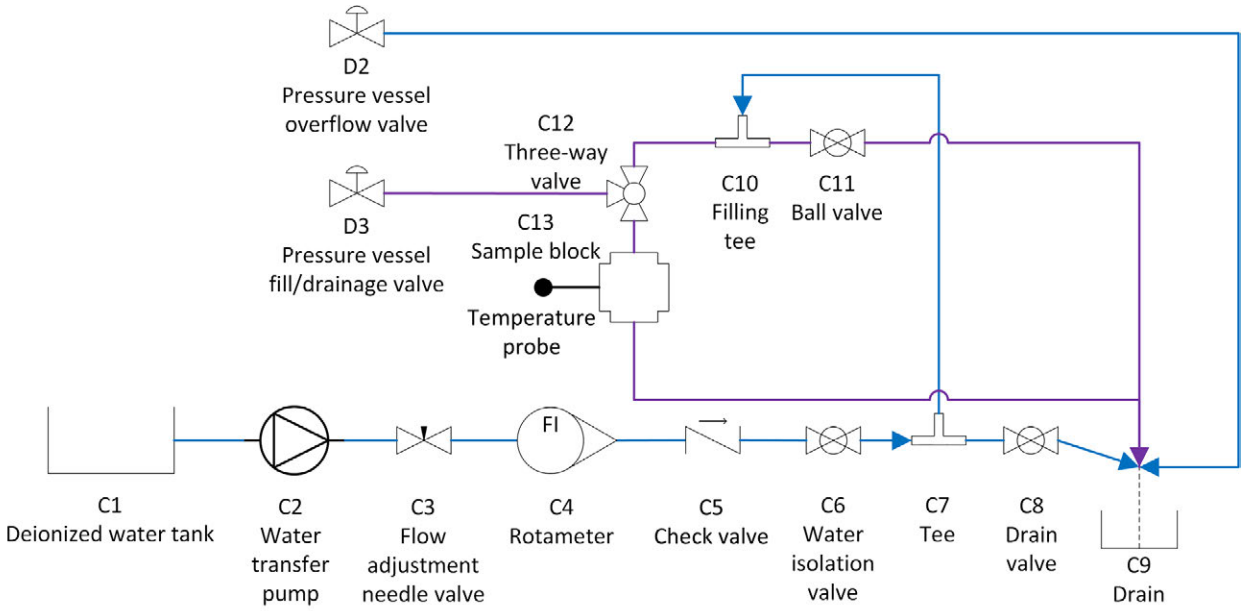

Figure B-5 Water line components.

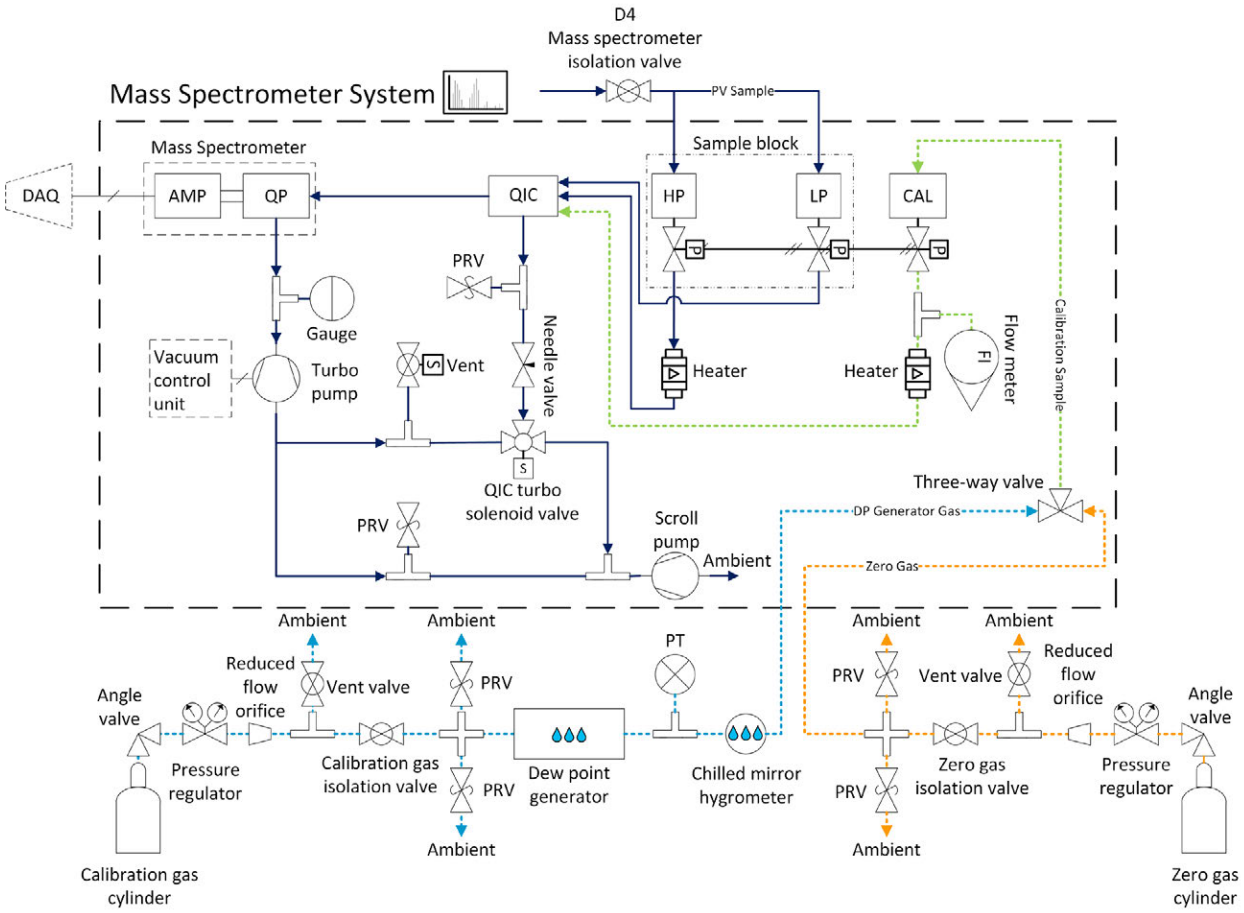

Figure B-6 Mass spectrometer and related calibration line components.

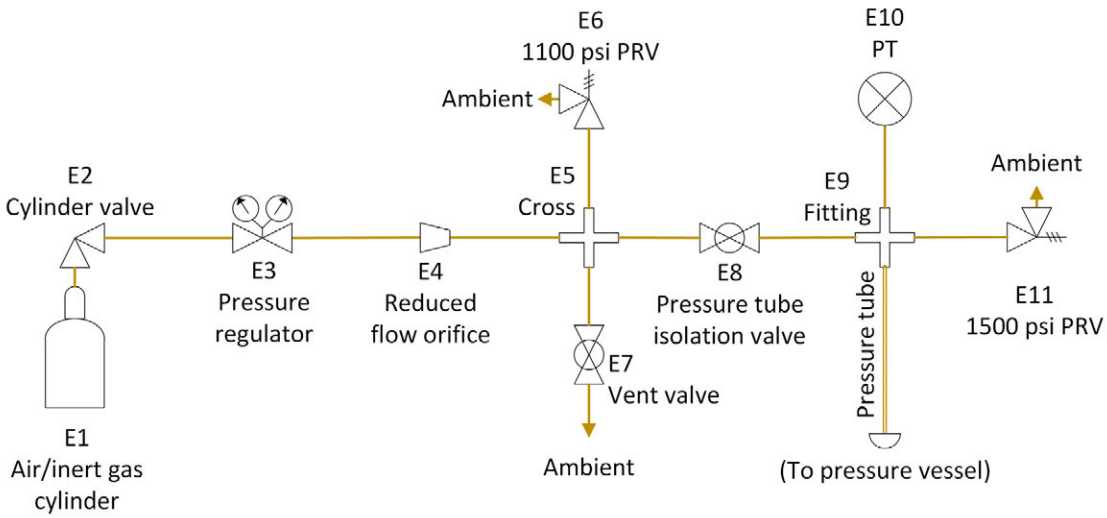

Figure B-7 Pressure tube fill line components. The pressure tube was meant to be fed out of the top of the pressure vessel using the same feedthrough as the hot connection.

APPENDIX C AUXILIARY TEST DATA

C.1 Pressure

C.1.1 Forced Helium Dehydration Hold Points

The pressure, dew point, and temperature data are included here for hold points in the FHD tests, where T_{PV} is the average temperature of the pressure vessel, T_H is the average temperature of the heater, and T_W is the ampoule temperature (average of TCs #15-16) within the hold period. The error in pressure is propagated from random error and instrument error from Setra ASM measurements during the hold. T_H and T_{PV} are presented to deduce an average void space temperature along the axial length of the pressure vessel. The maximum change in T_W for FHD #2 serves as an indicator of heat transferred to the water.

Table C-1 Pressure, temperature, and dew point figures for holds in FHD #1 at 150 W with bulk filling and draining of water. Dew point data from the HX200 obtained during venting steps.

Hold (kPa)	Time (h)	Pressure (kPa)	HX200 DP (°C)	T_{PV} (°C)	T_H (°C)
800	0.6-1.3	819.83±15.01	9.2 → 12.5	92.0	165.5
200	1.3-1.8	206.18±7.42	12.4 → 13.5	122.9	221.3
150	1.8-2.3	146.51±7.14	-	127.4	230.8
800	2.3-2.6	789.21±11.58	9.9 → 15.2	131.5	220.6
200	2.6-3.1	202.31±7.16	12.6 → 14.7	130.4	226.1
150	3.1-3.7	150.93±7.17	-	133.9	235.6
800	3.7-3.9	790.32±11.91	4.7 → 12.4	136.7	227.8
200	3.9-4.6	201.74±7.19	13.1 → 15.3	129.6	226.9
150	4.6-5.1	148.75±7.15	-	124.1	224.4
800	5.1-5.4	785.94±14.10	13.2 → 17.0	127.8	216.0
200	5.4-5.9	203.21±7.15	10.0 → 18.7	123.8	218.7
150	5.9-6.4	152.53±7.14	-	125.1	223.0
800	6.4-6.7	787.07±11.05	9.0 → 17.9	133.5	222.5
200	6.7-7.3	201.43±7.18	14.8 → 15.7	131.2	228.0
150	7.3-7.8	151.01±7.15	-	126.4	227.6
800	7.8-8.1	785.14±12.00	9.7 → 17.4	129.7	217.7
200	8.1-8.6	197.54±7.14	16.4 → 17.2	129.2	224.7
150	8.6-9.1	150.21±7.16	-	131.8	233.4

Table C-2 Pressure, temperature, and dew point figures for holds in FHD #2 at 150 W with the 0.123 in. OD ampoule. HX200 data was available continuously.

Hold (kPa)	Time (h)	Pressure (kPa)	HX200 DP (°C)	T_{PV} (°C)	T_H (°C)	ΔT_W (°C)
800	0.2-0.4	821.11±7.61	-33.2 → -25.3	85.1	146.2	0.7
200	0.5-1.0	201.58±7.15	-27.3 → -5.0	132.0	214.7	1.3
150	1.0-1.5	146.32±7.13	-7.9 → 1.6	144.0	230.7	1.3
800	1.6-1.8	791.59±11.25	-21.4 → -14.0	146.6	232.6	1.1
200	1.9-2.4	201.80±7.17	-25.8 → -1.1	146.7	232.1	1.8
150	2.5-3.0	150.15±7.14	-3.1 → 5.2	148.9	234.5	1.5
800	3.0-3.3	783.47±11.63	-20.6 → -14.4	149.0	233.4	1.0
200	3.3-3.8	197.44±7.20	-23.1 → 1.0	149.1	233.5	1.4
150	3.9-4.4	149.26±7.14	0.4 → 7.2	149.3	233.8	1.6
800	4.4-4.7	780.56±12.55	-17.6 → -11.4	149.1	233.3	1.5
200	4.7-5.2	197.63±7.24	-21.0 → 2.9	148.4	232.8	1.5
150	5.2-5.7	150.01±7.17	0.3 → 7.1	147.9	232.2	1.1
800	5.7-6.0	785.65±13.36	-19.6 → -12.4	147.6	231.5	1.4
200	6.0-6.5	199.37±7.27	-21.7 → 0.7	147.9	232.2	1.2
150	6.5-7.0	149.24±7.17	-2.3 → 4.7	146.7	230.7	1.2

C.1.2 Vacuum Drying Hold Points

The pressure rebounds observed in the vacuum drying tests are shown in tables. The pressure measured upon isolation is P_0, the change in pressure during the hold is ΔP. The maximum change in ampoule temperature (ΔT_W) is shown as an indirect measure of the total heat transferred from the ampoule, which was used in the water removal analysis of Section 4.2.4. The pressure error is propagated from random error and instrument error from either gauge reading within the hold period. The dew point is presented in terms of minima and maxima, as both the magnitude and total change in DP are relevant. An asterisk (*) indicates when the hold point was truncated due to the rebound threshold being exceeded.

Table C-3 Pressure changes upon isolation for holds in VT #5 (unheated, 0.021 in. OD ampoule).

Hold (torr)	Time (h)	Pfeiffer (torr)		Instrutech (torr)		30 min ΔP (torr)	DP (°C)	ΔT_W (°C)
		P_0	ΔP	P_0	ΔP			
100	0.3-0.8	97.21	6.56	-	-	-	-22.4 → -20.7	0.8
75	0.8-1.3	73.03	5.15	82.00	2.93	4.04±3.68	-18.2 → -15.9	1.1
50	1.3-1.8	48.65	10.05	52.71	12.14	11.09±2.29	-11.8 → -7.6	0.9
25	1.8-2.3	24.36	8.90	34.61	7.62	8.26±5.84	-6.5 → -1.6	0.7
10	2.3-2.8	8.61	2.90	12.64	3.56	3.23±2.71	8.4 → 10.2	1.1
5	2.9-3.4	5.05	0.66	7.50	1.13	0.90±1.69	4.1 → 11.0	4.6
3*	3.6-3.8	3.18	1.70	4.63	2.92	2.31±1.30	-2.5 → 7.5	8.8
3*	4.0-4.3	2.92	1.95	4.37	3.17	2.56±1.31	-3.8 → 7.3	9.4
3*	4.4-4.6	2.92	1.95	4.37	3.18	2.56±1.31	-3.6 → 7.4	6.2
3	4.6-5.3	2.91	2.59	4.36	4.06	3.33±1.37	-2.9 → 10.3	6.0
3*	5.3-5.4	3.03	1.85	4.38	3.20	2.52±1.28	-2.3 → 7.4	1.4
3	5.4-5.4	3.32	1.53	4.66	2.88	2.21±1.27	-1.1 → 7.6	0.9
1	5.5-6.0	1.65	3.96	2.40	6.16	5.06±1.17	-14.0 → 11.2	8.4
1	6.2-6.8	1.55	3.73	2.18	5.97	4.85±1.11	-14.9 → 9.2	10.5
1	7.1-7.6	1.55	3.87	2.19	6.16	5.02±1.13	-14.9 → 10.4	11.4
1	7.7-8.2	0.99	1.27	1.35	2.14	1.71±0.50	-25.1 → -13.0	4.8
0.5	8.3-8.8	0.51	0.58	0.68	0.84	0.71±0.19	-26.1 → -21.4	0.6
0.5	8.8-9.3	0.49	0.43	0.66	0.61	0.52±0.16	-26.6 → -23.5	0.7
0.25	9.4-9.9	0.25	0.39	0.33	0.53	0.46±0.09	-31.5 → -27.5	0.6

Table C-4 Pressure changes upon isolation for holds in VT #6 (unheated, 0.123 in. OD ampoule).

Hold (torr)	Time (h)	Pfeiffer (torr)		Instrutech (torr)		30 min ΔP (torr)	DP (°C)	ΔT_W (°C)
		P_0	ΔP	P_0	ΔP			
100	0.1-0.6	91.63	28.17	-	-	-	-16.0 → -13.8	1.9
75	0.7-1.2	72.79	5.87	83.00	5.43	5.62±7.03	-14.9 → -11.7	1.6
50	1.2-1.7	48.65	10.69	58.20	11.52	11.10±7.04	-9.0 → -5.1	0.8
25	1.7-2.2	24.30	13.89	35.67	10.62	12.27±6.90	-4.5 → 2.4	1.6
10	2.2-2.7	8.72	4.22	13.41	4.72	4.46±3.49	10.9 → 14.0	4.2
5	2.7-3.2	4.87	1.52	7.67	1.85	1.68±2.10	5.2 → 14.6	10.2
3	3.3-3.8	3.48	2.70	5.07	4.23	3.46±1.67	0.4 → 13.8	14.3
3	4.1-4.6	3.24	2.94	4.77	4.54	3.73±1.65	-1.3 → 13.8	16.0
3	4.8-5.4	3.31	3.02	4.81	4.63	3.21±1.37	-1.4 → 13.9	16.1
3	5.9-6.4	2.92	3.05	4.43	4.59	3.83±1.62	-3.4 → 12.3	16.6
3	6.4-6.9	2.97	2.97	4.37	4.57	3.76±1.55	-4.2 → 11.9	16.2
3	7.0-7.5	2.86	3.02	4.15	4.67	3.84±1.49	-4.6 → 11.4	12.9
1	7.5-8.0	1.13	1.42	1.58	2.28	1.85±0.62	-20.4 → -11.0	4.0
0.5	8.1-8.6	0.50	0.90	0.66	1.22	1.05±0.23	-27.0 → -21.0	0.6
0.5	8.6-9.1	0.50	0.65	0.66	0.92	0.78±0.21	-27.2 → -23.7	0.6
0.5	9.1-9.6	0.50	0.56	0.66	0.80	0.68±0.20	-59.9 → -25.0	0.7
0.25	9.7-10.2	0.24	0.52	0.33	0.66	0.59±0.11	-33.0 → -29.6	0.4

Table C-5 Pressure changes upon isolation for holds in VT #7 (150 W, 0.021 in. OD ampoule).

Hold (torr)	Time (h)	Pfeiffer (torr)		Instrutech (torr)		30 min ΔP (torr)	DP (°C)	ΔT_W (°C)
		P_0	ΔP	P_0	ΔP			
100	1.1-1.6	97.141	4.334	-	-	2.16±2.13	-24.2 → -20.2	0.5
75	1.6-2.1	72.973	6.968	83.597	5.733	6.34±7.06	-14.5 → -10.9	0.5
50	2.1-2.6	48.716	13.360	57.524	15.602	14.51±7.03	-7.9 → -3.4	0.6
25	2.6-3.1	24.357	12.771	35.426	10.281	11.45±6.90	-4.5 → 3.7	1.1
10	3.1-3.6	7.736	3.627	11.826	4.700	4.16±3.27	10.2 → 13.2	3.5
5	3.7-4.2	4.864	0.927	7.728	1.306	1.12±2.16	6.1 → 13.6	7.9
3	4.5-5.1	3.014	2.496	4.571	4.166	2.79±1.42	-2.8 → 12.1	15.8
3	5.2-5.3	3.268	1.586	4.806	3.016	11.31±7.83	-2.3 → 8.2	8.5
1	5.5-6.0	1.661	3.976	2.520	6.423	5.20±1.47	-13.0 → 13.2	10.4
1*	6.1-6.1	1.818	3.024	2.859	5.041	47.44±17.05	-11.6 → 8.3	3.1
1*	6.2-6.2	1.829	3.014	2.880	5.028	51.11±18.50	-11.5 → 8.4	3.0
1*	6.3-6.3	1.853	3.017	2.910	5.048	51.70±18.78	-11.5 → 8.5	3.0
1*	6.4-6.5	1.845	3.158	2.924	5.229	44.46±15.85	-11.4 → 9.3	3.6
1*	6.5-6.8	1.842	3.970	2.918	6.253	9.92±3.04	-11.4 → 14.5	8.2
1*	7.0-7.2	1.857	3.955	2.966	6.265	12.86±4.03	-18.1 → 14.5	7.9
1*	7.3-7.5	1.819	3.994	2.890	6.312	13.56±4.15	-11.5 → 14.6	8.2
1	7.6-8.1	0.984	1.606	1.390	2.714	2.15±0.68	-24.8 → -8.1	4.4
0.5	8.1-8.5	0.485	0.478	0.672	0.719	0.87±0.32	-25.0 → -19.1	0.9
0.5	8.5-9.0	0.486	0.317	0.673	0.445	0.39±0.18	-25.1 → -21.2	0.7
0.25	9.0-9.5	0.245	0.338	0.334	0.473	0.41±0.11	-29.7 → -24.3	0.5
0.25	9.6-10.1	0.248	0.271	0.336	0.383	0.33±0.10	-29.8 → -25.3	0.6

Table C-6 Pressure changes upon isolation for holds in VT #8 (150 W, 0.123 in. OD ampoule).

Hold (torr)	Time (h)	Pfeiffer (torr)		Instrutech (torr)		30 min ΔP (torr)	DP (°C)	ΔT_W (°C)
		P_0	ΔP	P_0	ΔP			
100	1.2-1.7	92.82	9.23	-	-	-	-18.8 → -14.9	0.6
75	1.7-2.2	72.28	6.03	80.92	5.47	5.74±5.90	-18.2 → -14.1	0.6
50	2.2-2.7	48.64	11.12	55.60	12.51	11.72±5.37	-13.5 → -3.3	1.0
25	2.7-3.2	24.37	12.73	35.04	9.71	11.18±6.46	-4.8 → 3.0	0.6
10	3.3-3.8	9.05	2.85	13.61	3.18	3.00±3.33	9.6 → 12.4	2.1
5	3.8-4.3	5.16	1.06	7.80	1.46	1.25±2.00	4.4 → 13.1	7.6
3	4.4-5.0	3.62	2.41	5.25	3.78	2.65±1.41	0.6 → 11.7	11.3
3	5.1-5.6	3.59	2.25	4.99	3.90	3.06±1.56	-0.5 → 11.2	11.3
3	5.8-6.3	3.55	2.33	4.95	4.00	3.12±1.55	-0.8 → 11.6	11.9
3	6.6-7.1	3.07	2.57	4.58	4.04	3.30±1.58	-2.6 → 10.1	12.7
3	7.3-7.8	2.92	2.59	4.41	4.03	3.30±1.56	-3.6 → 8.9	13.1
3	7.9-8.4	2.92	2.82	4.41	4.40	3.57±1.59	-3.3 → 10.5	14.9
3	8.4-8.9	3.04	2.83	4.42	4.58	3.71±1.59	-3.1 → 11.4	16.5
3*	9.1-9.4	2.08	3.57	3.25	5.44	6.55±2.18	-10.3 → 10.8	18.7
1*	9.5-9.9	1.01	1.90	1.38	3.00	2.98±0.79	-19.1 → -6.5	16.2
1	9.9-10.4	0.97	1.31	1.38	2.15	1.73±0.58	-19.4 → -12.9	1.1
0.5*	10.4-10.6	0.49	0.48	0.66	0.70	1.90±0.63	-26.3 → -22.2	0.4
0.5*	10.6-10.9	0.49	0.49	0.66	0.69	1.19±0.40	-60.0 → -23.5	0.4
0.5	10.9-11.4	0.51	0.72	0.68	1.02	0.87±0.23	-27.4 → -23.6	0.7

C.2 Temperature

C.2.1 Time-Dependent Temperature for Forced Helium Dehydration

The time-dependent temperatures measured during the forced helium dehydration tests are shown in Figure C-1 and Figure C-2 for FHD #1 (bulk filling/draining) and FHD #2 (water ampoule) tests, respectively. Unsteady behavior is apparent in both tests for the initial pressurization to 800 kPa.

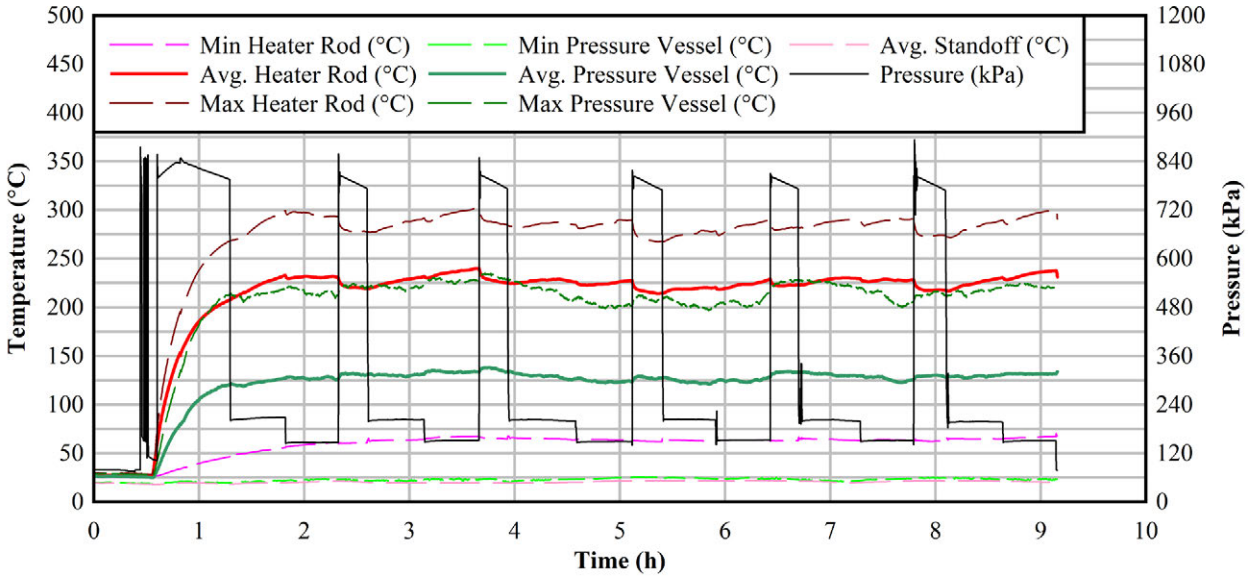

Figure C-1 Temperature boundaries during FHD #1 at 150 W after the bulk filling and drainage of water.

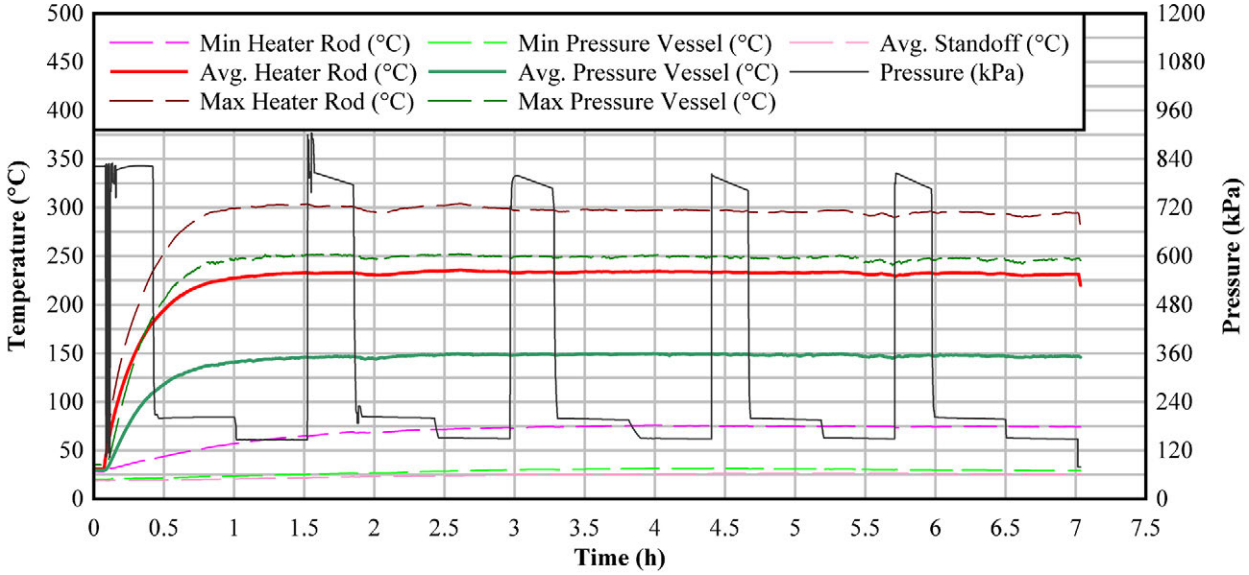

Figure C-2 Temperature boundaries during FHD #2 at 150 W with the 0.123 in. OD ampoule.

C.2.2 Time-Dependent Temperature for Vacuum Drying

The temperatures measured during the heated vacuum drying tests are shown in Figure C-3 and Figure C-4 for VT #7 (ampoule OD 0.021 in.) and VT #8 (ampoule OD 0.123 in.), respectively. These plots show the PCT and peak pressure vessel temperature over time. The minimum PV temperature occurs at the upper standoff and is thus very close to the ambient temperature.

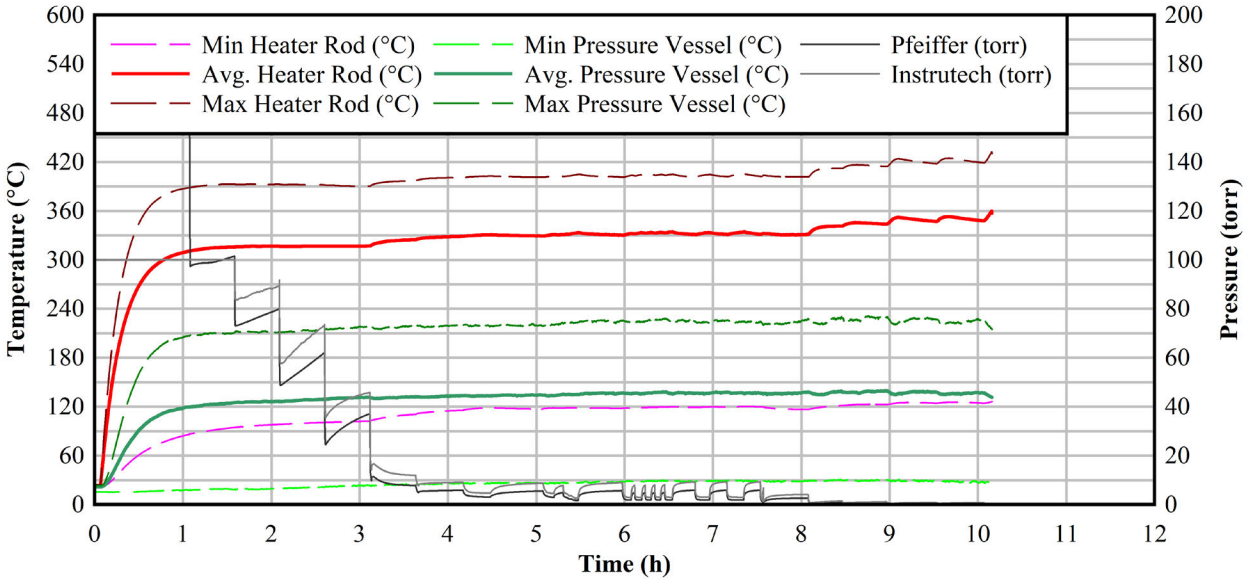

Figure C-3 Temperature boundaries over time during VT #7 (150 W, 0.021 in. OD ampoule).

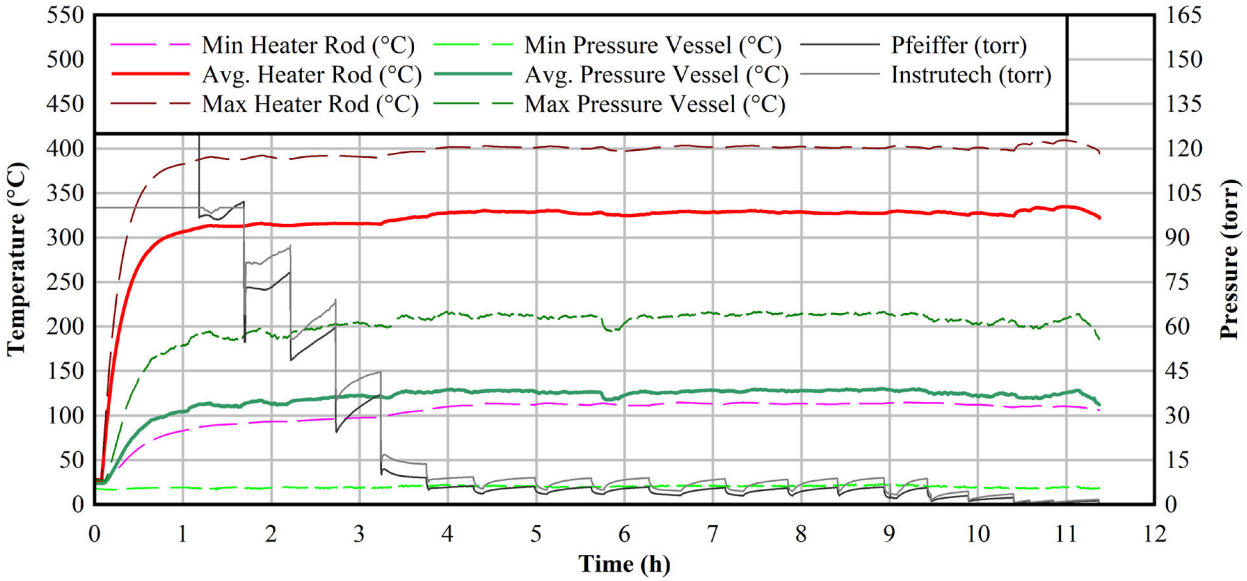

Figure C-4 Temperature boundaries over time during VT #8 (150 W, 0.123 in. OD ampoule).

C.2.3 Axial Temperature Profiles for Vacuum Drying

The axial temperature profiles for the heater rod and main axial length of the pressure vessel from the heated vacuum drying tests are shown in Figure C-5 and Figure C-6 for VT #7 and #8 (ampoule orifice ODs 0.021 in. and 0.123 in.), respectively. The plots are similar, although VT #8 features a higher PCT for the 0.25 torr hold point. Also, the 0.5 torr hold in VT #8 is observed to be relatively unsteady.

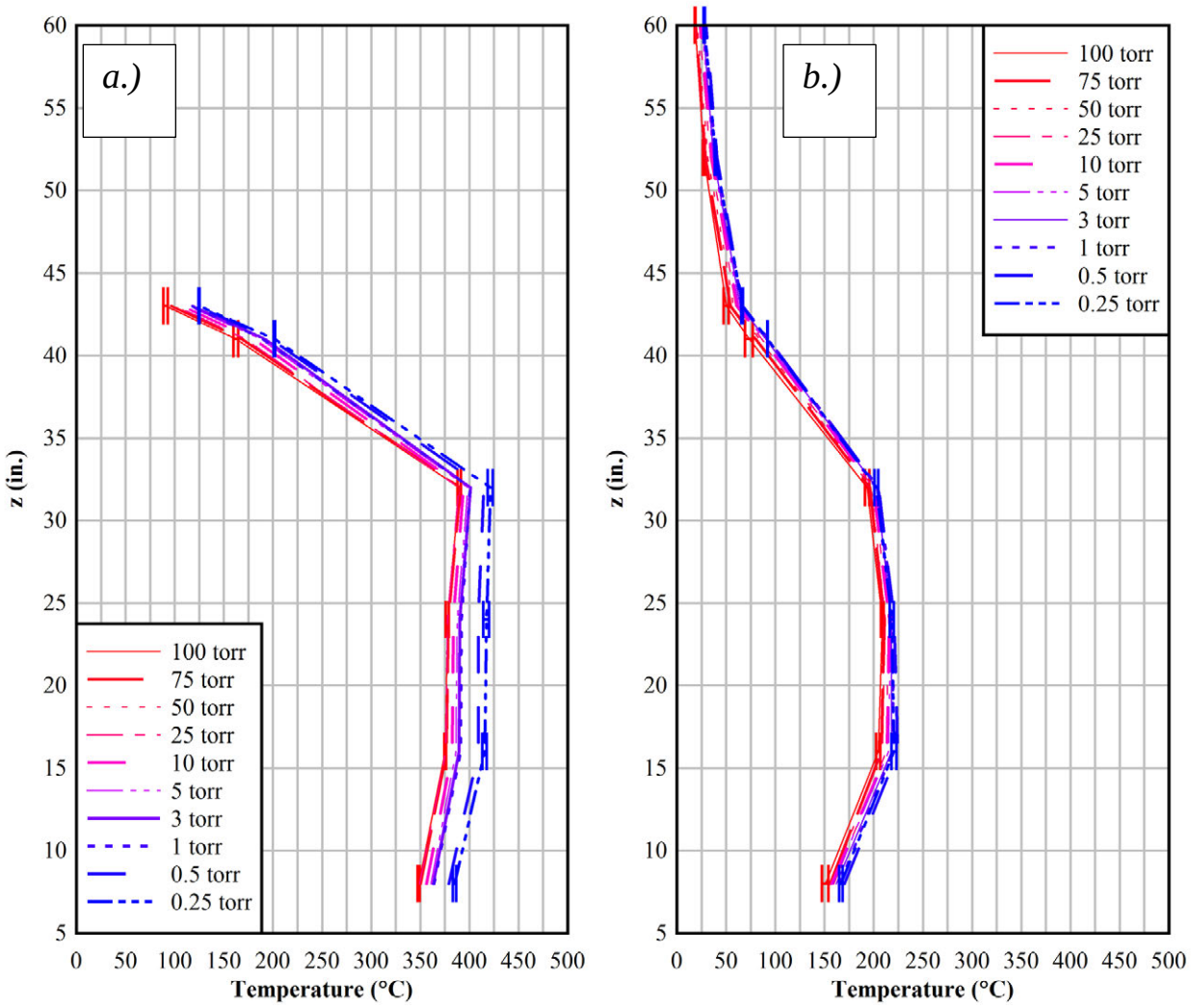

Figure C-5 Temperature profiles of the *a.)* heater and *b.)* pressure vessel for ultimate holds during VT #7 (150 W, 0.021 in. OD ampoule). Error bars shown for the first and last hold point.

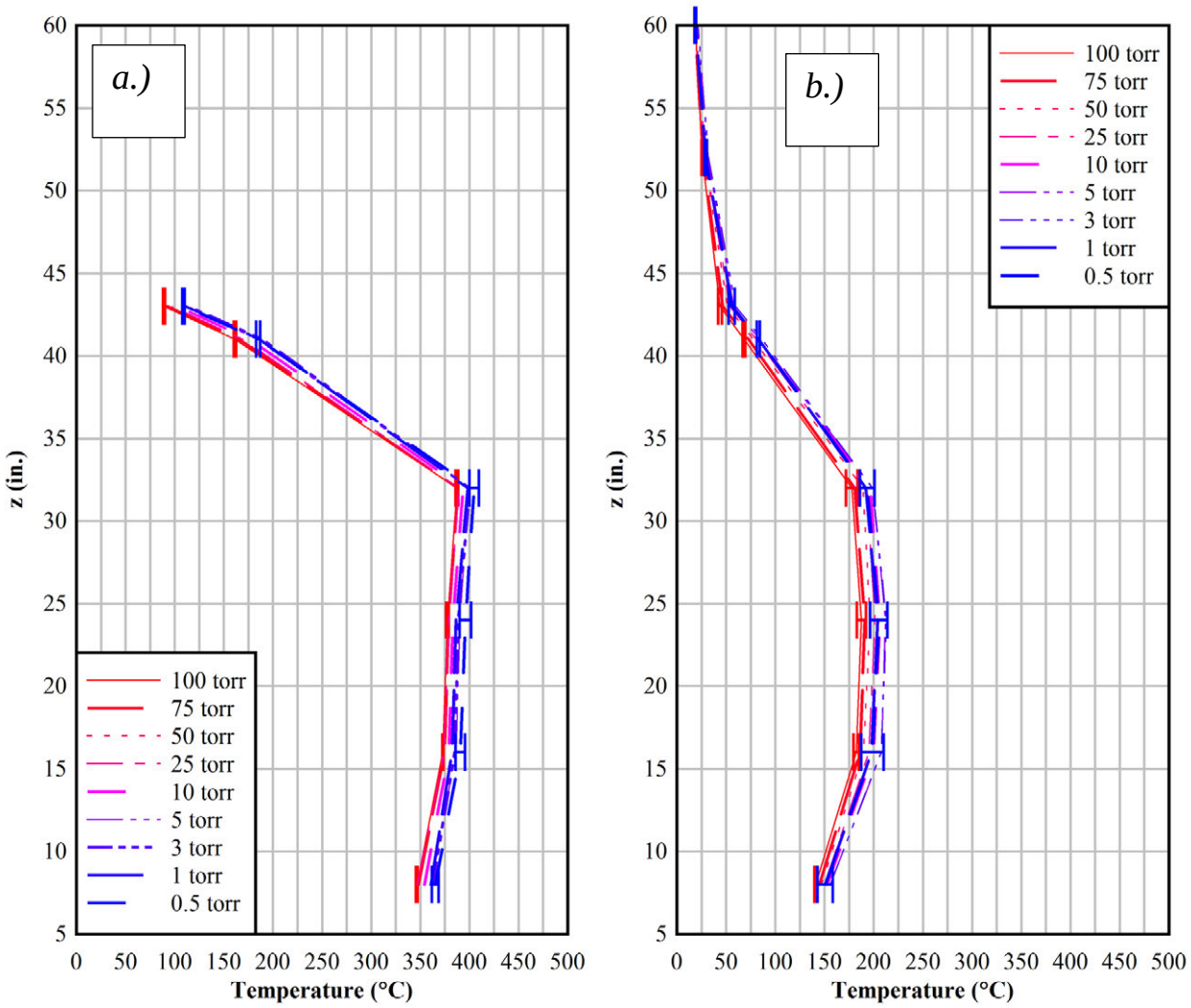

Figure C-6 Temperature profiles of the *a.)* heater and *b.)* pressure vessel for ultimate holds during VT #8 (150 W, 0.123 in. OD ampoule). Error bars shown for the first and last hold.

C.3 Phase Transitions during Vacuum Drying

This section shows plots for the phase transitions of the vacuum drying tests based on the InstruTech gauge pressure and the minimum ampoule temperature (i.e. the lowest temperature recorded for either TC #15 or #16). A general transition to the vapor phase is observed during the 10 torr hold. Afterwards, during the 5 and 3 torr holds, pressure and temperature approach the triple point of water. The overlapping lines indicate multiple attempts to hold at the nominal 3 torr hold point as the vacuum suction is hindered by the rate of evaporation. Only VD #8 exhibits solid deposition, as circled in the plot. After the 3 torr hold, water is conclusively in the vapor phase.

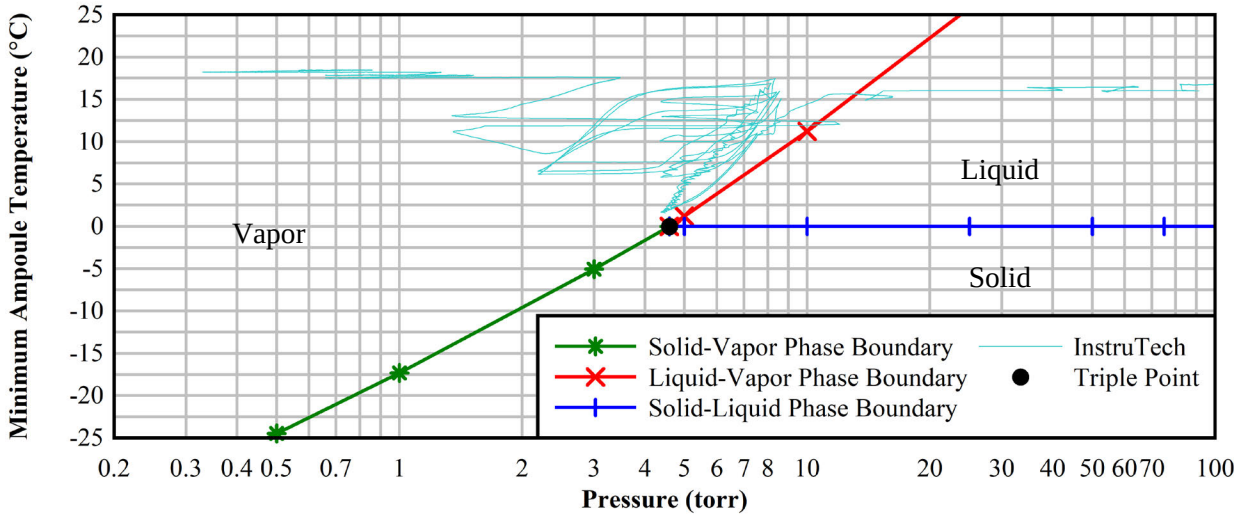

Figure C-7 Overlay of phase diagram with minimum ampoule temperatures for the InstruTech pressure during VT #5 (unheated, 0.021 in. OD ampoule).

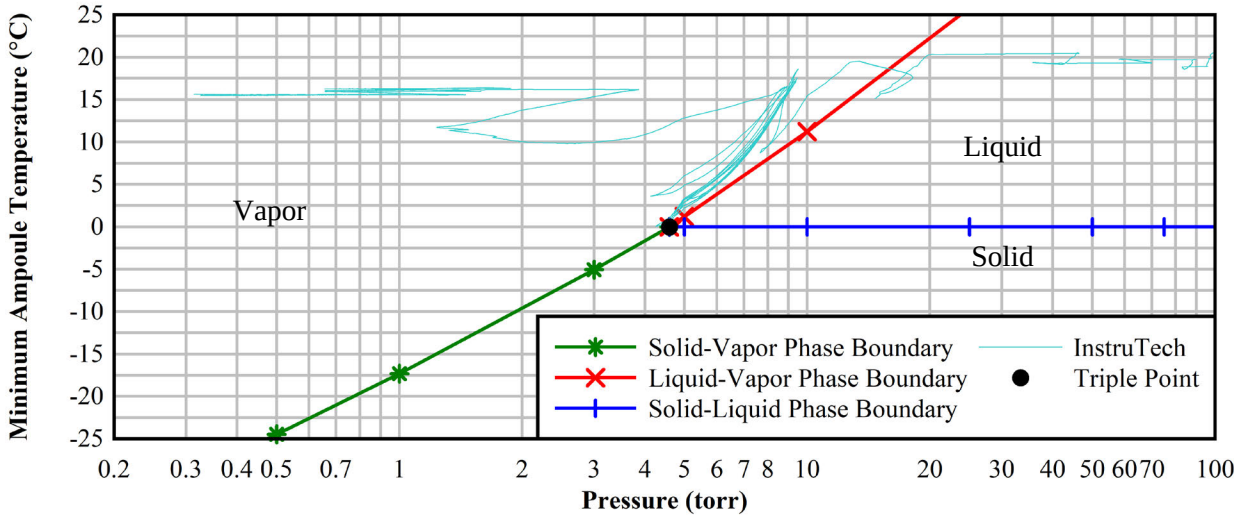

Figure C-8 Overlay of phase diagram with minimum ampoule temperatures for the InstruTech pressure during VT #6 (unheated, 0.123 in. OD ampoule).

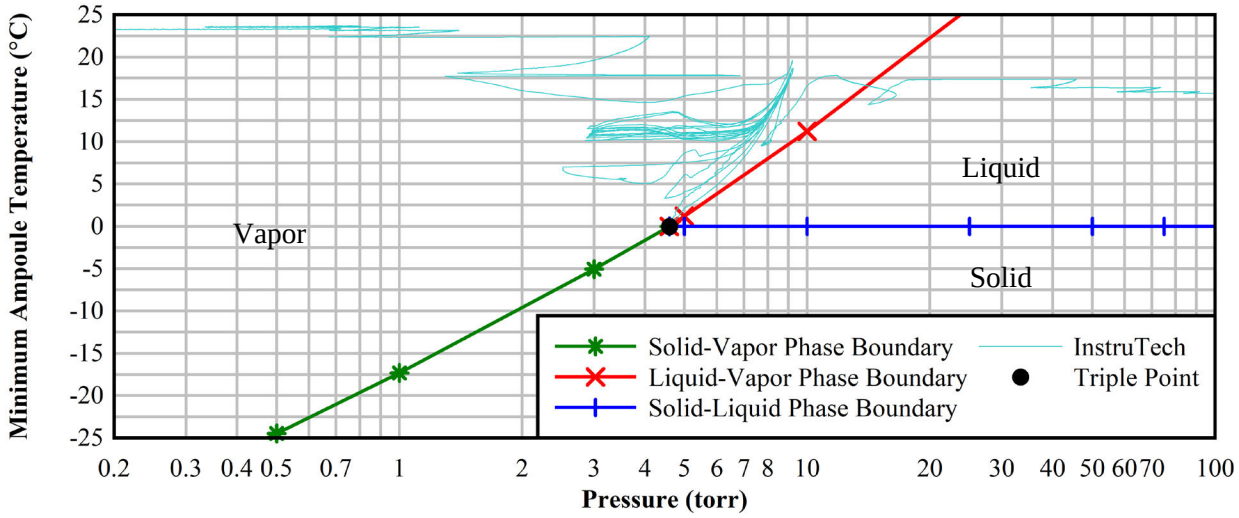

Figure C-9 Overlay of phase diagram with minimum ampoule temperatures for the InstruTech pressure during VT #7 (150 W, 0.021 in. OD ampoule).

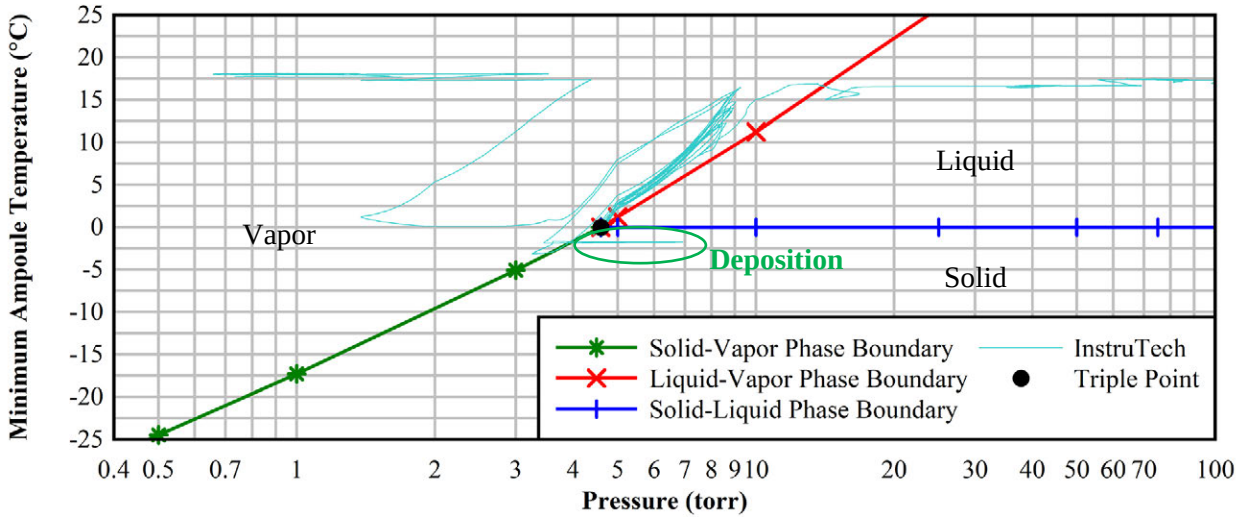

Figure C-10 **Overlay of phase diagram with minimum ampoule temperatures for the InstruTech pressure during VT #8 (150 W, 0.123 in. OD ampoule)**

Sandia National Laboratories